



# Targeted Training Activity (TTA) 2017- Monsoons in a Changing Climate



## Tibetan Forcing and the onset and Evolution of Asian Summer Monsoon

**Guoxiong WU,**

Yimin LIU, Bian HE,

Anmin DUAN, Qing BAO, Boqi LIU

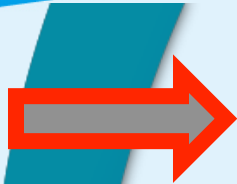
LASG, Institute of Atmospheric Physics (IAP), CAS, China

Trieste, Italy, 31 Jul- 4 Aug





# Outline



**Introduction- general circulation**



**Dynamics of ASM onset**



**Evolution of the ASM onset**



**Maintenance of the ASM**



**Variability of the ASM**



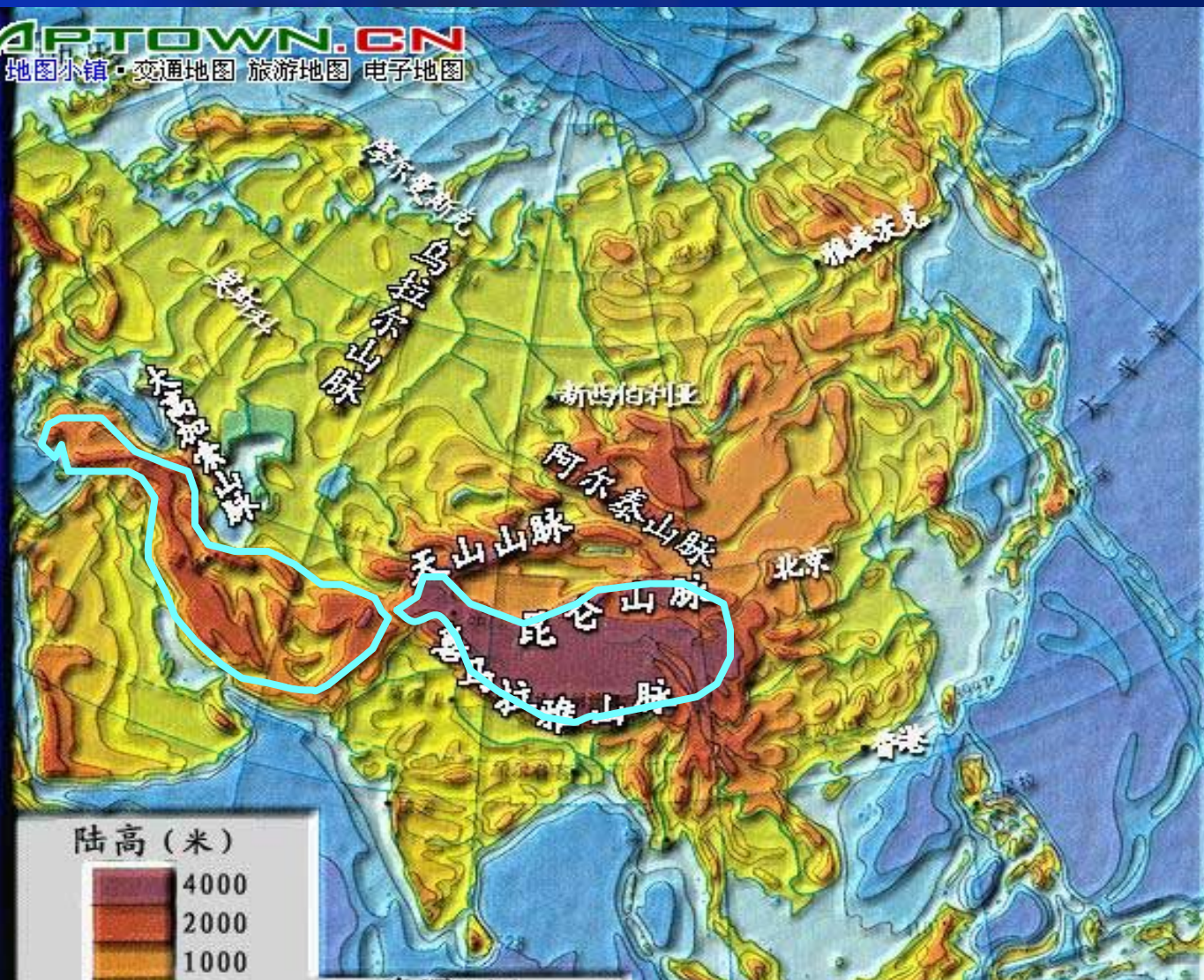
**Conclusion**



# 尺度一横跨欧亚大陆、占1/4中国国土



MAPTOWN.CN  
地图小镇·交通地图 旅游地图 电子地图



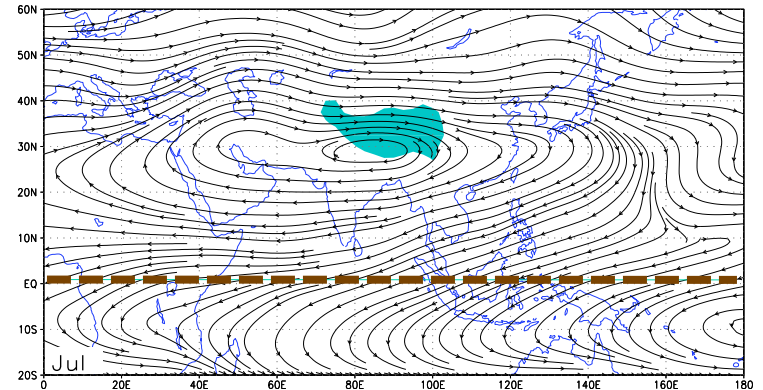
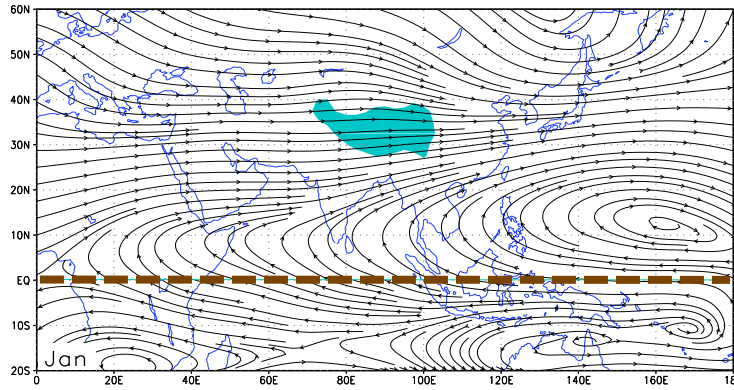
亚洲地形图

➤ 产生巨大的大陆尺度定常波型

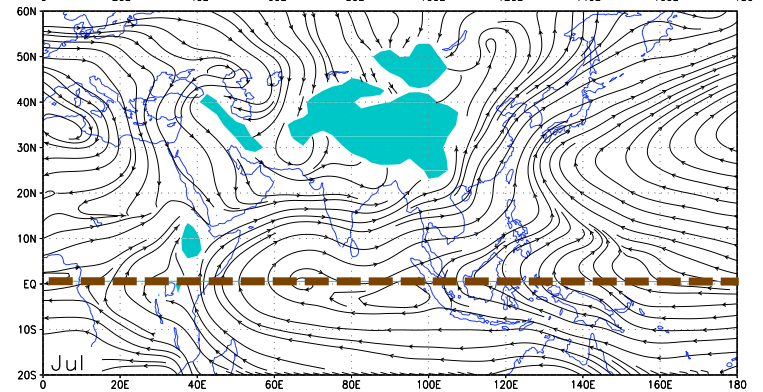
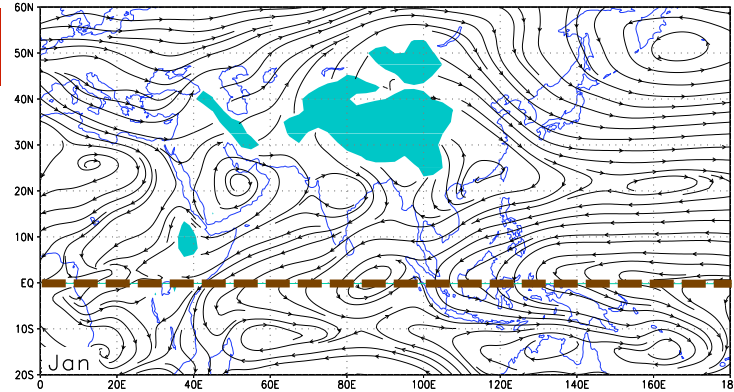
January

July

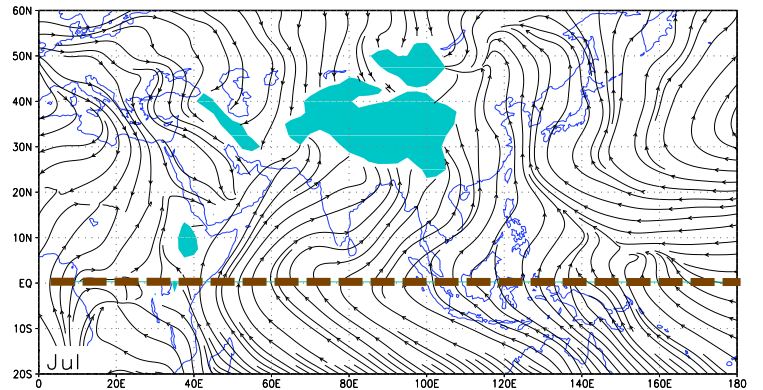
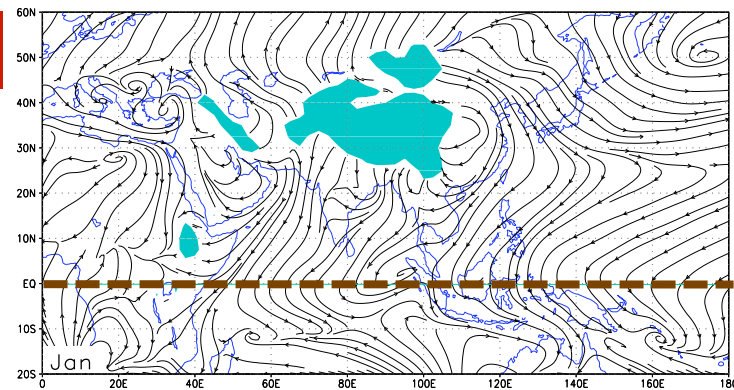
200 hPa



850 hPa



1000 hPa



Streamline at pressure levels in January and July

# Zonal Wind

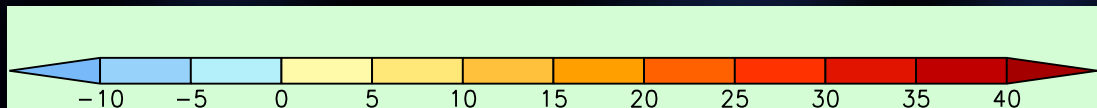
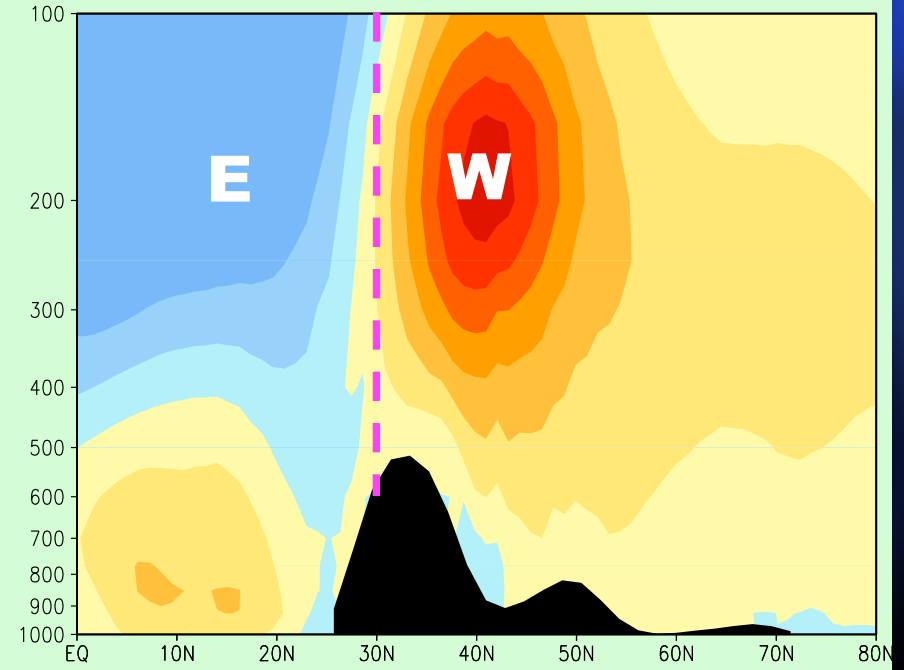
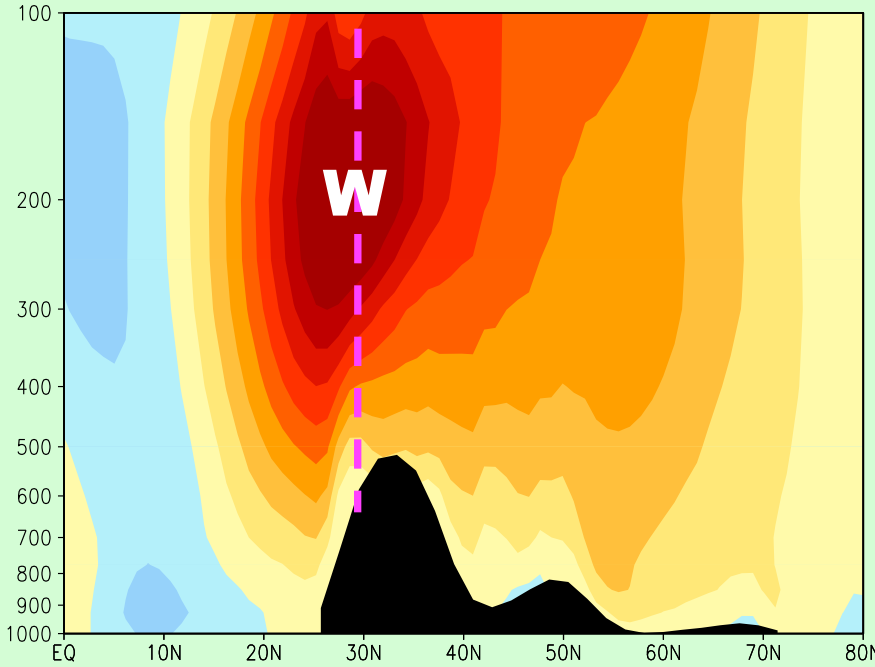


## Winter

## Summer

U at 90E in DJF

U at 90E in JJA



TP locates below westerly jet  
horizontal advection is strong

TP locates in the boundary of westerly and easterly  
horizontal advection is small

# Linearized QG thermodynamic equation:

(Held, I., 1983)

$$[u] \frac{\partial}{\partial x} \frac{\partial \psi^*}{\partial z} - \frac{\partial \psi^*}{\partial x} \frac{\partial [u]}{\partial z} + \frac{N^2}{f_0} W^* = \frac{\kappa Q^*}{f_0 H} \equiv R^*$$

## 2. If Convection dominates

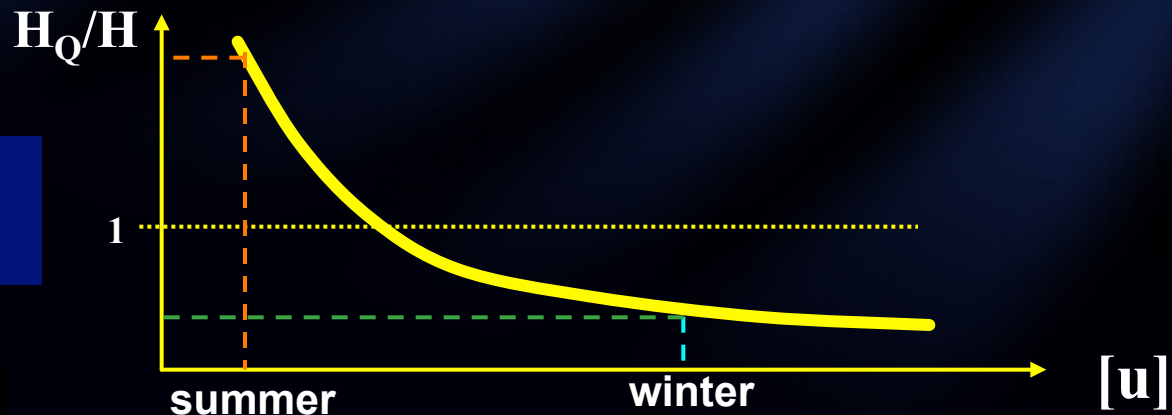
$$\tilde{\psi}_p = \frac{-if_0^2}{k\rho_0[u](K_s^2 - K^2)} \frac{\partial}{\partial z} \left( \frac{\rho_0 R}{N^2} \right)$$

“Equivalent topography”

$$\tilde{h}_T = \frac{if_0}{N^2 k [u]} \tilde{R}(0)$$



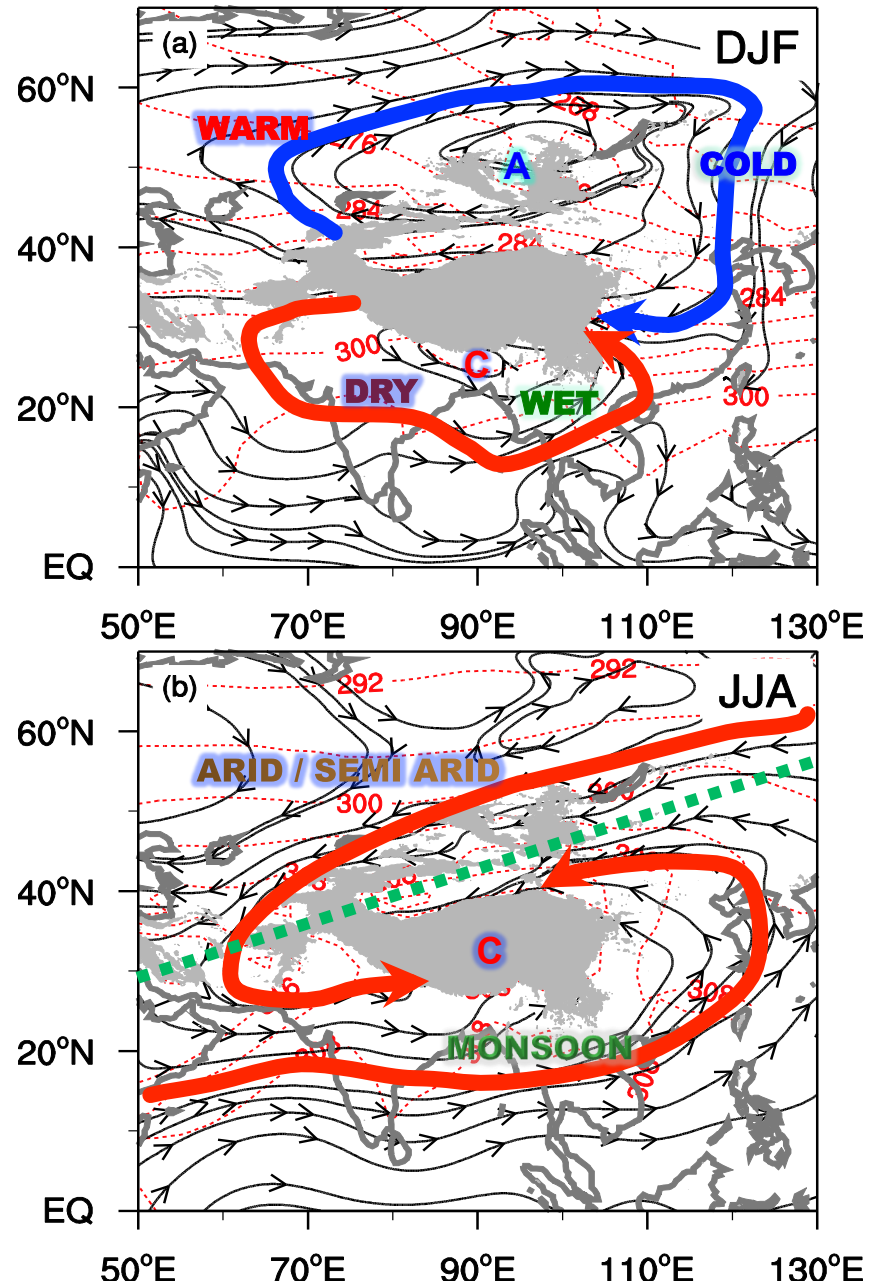
Schematic  
Diagram



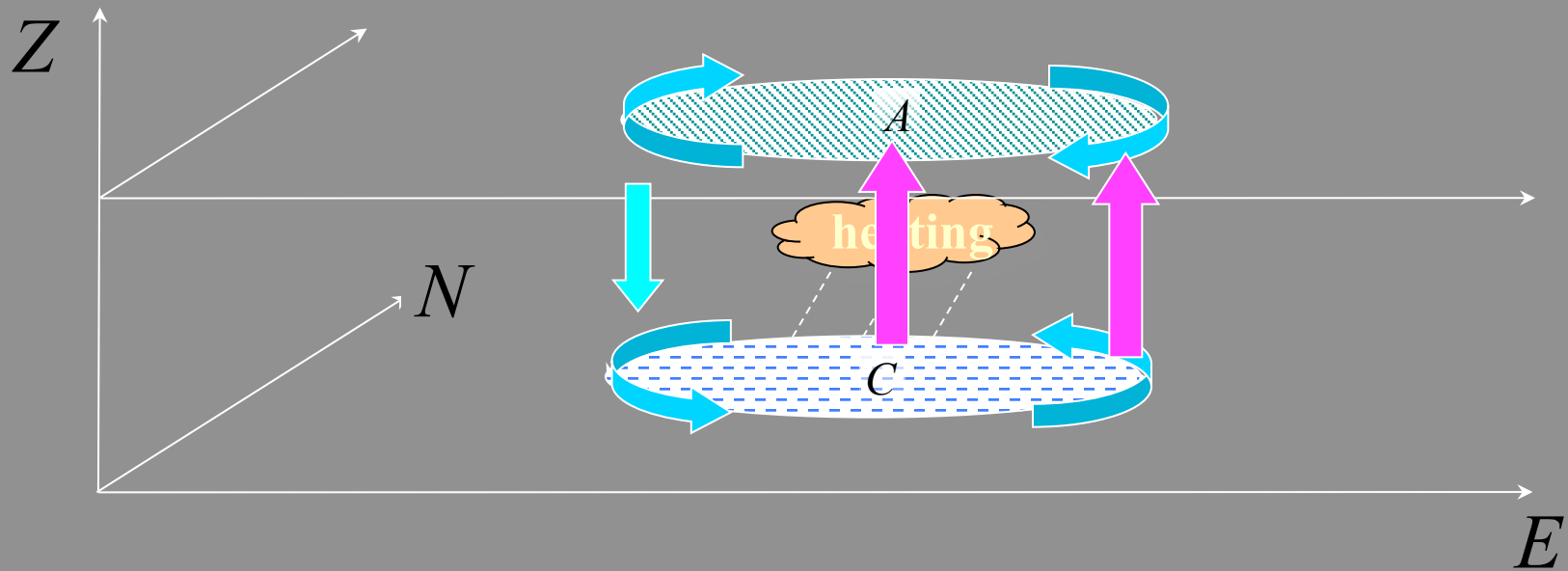


**Winter:** impinging westerly generates negative mountain torque and an asymmetric stationary wave circulation pattern, influencing temperature and moisture advection

**Summer:** thermal pumping of the TP generates convergence spiral stationary wave pattern, influencing moisture advection

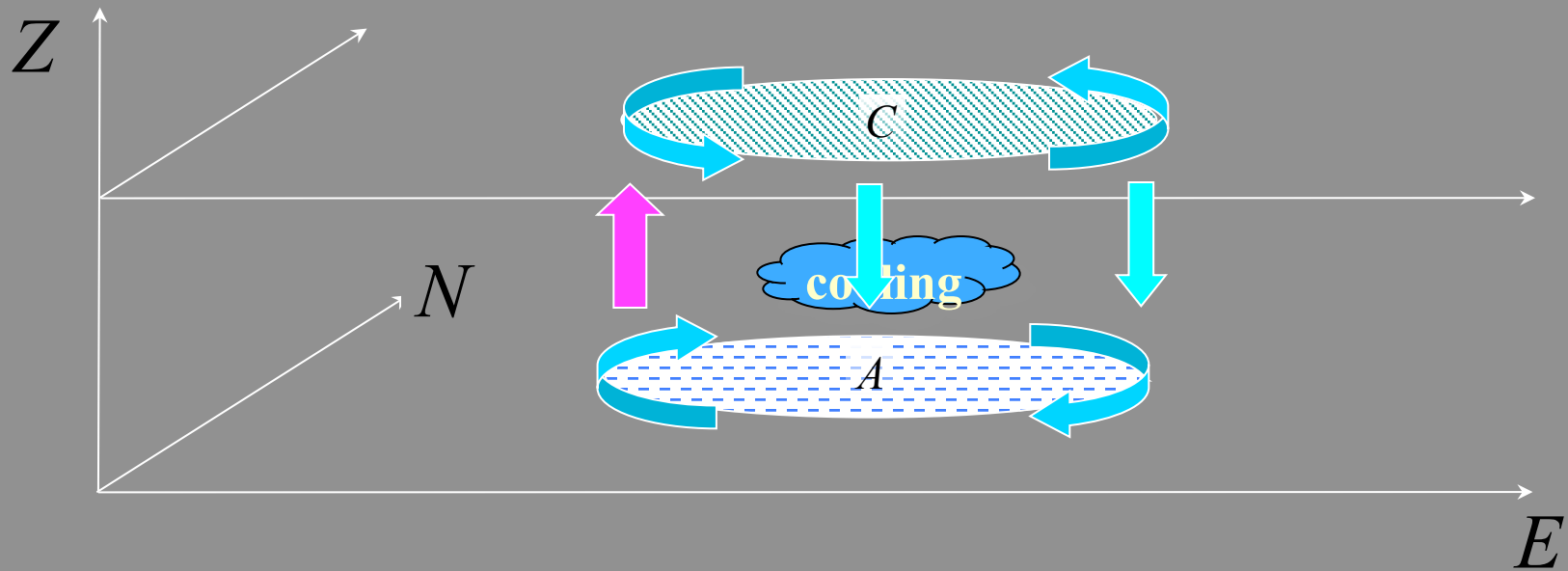


# Thermal Adaptation- heating



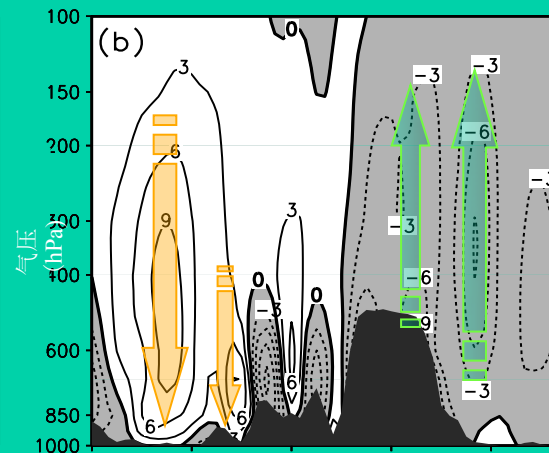
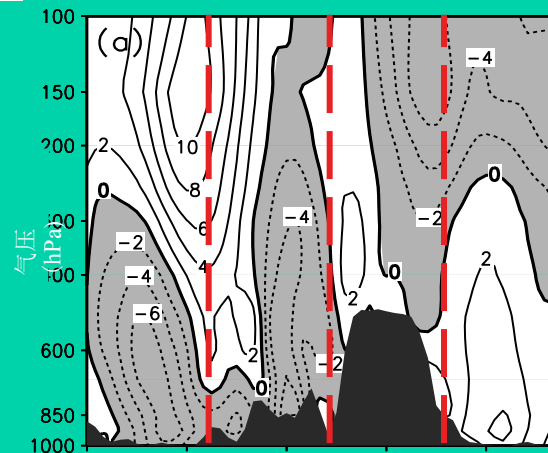
$$w \propto -\beta \frac{\partial v}{\partial z}$$

# Thermal Adaptation-cooling



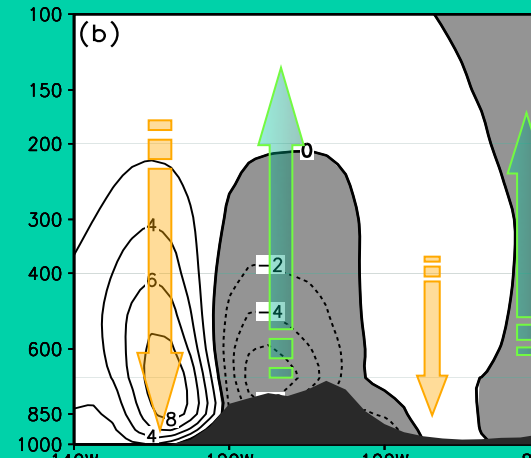
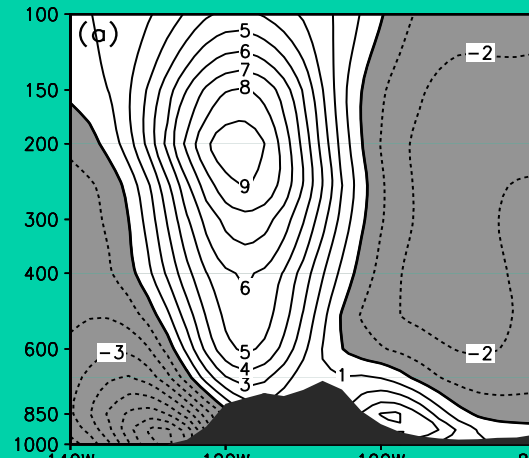
$$w \propto -\beta \frac{\partial \mathbf{v}}{\partial \mathbf{z}}$$

# Tibetan July



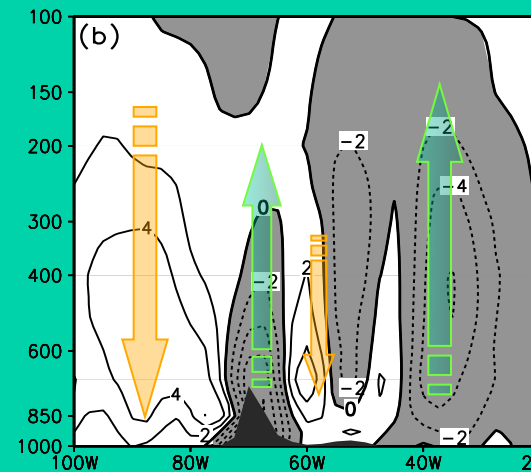
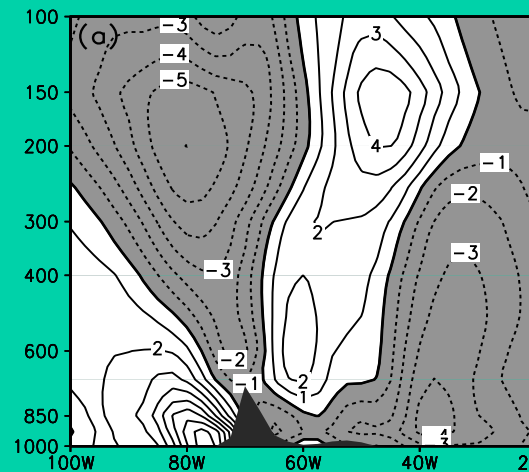
# Rockies July

V



$\omega$

# Andes January



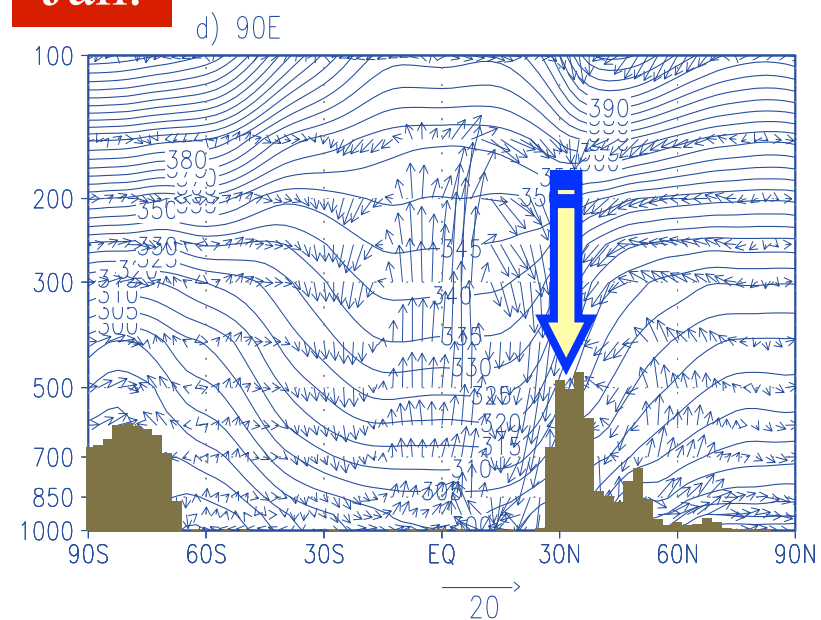
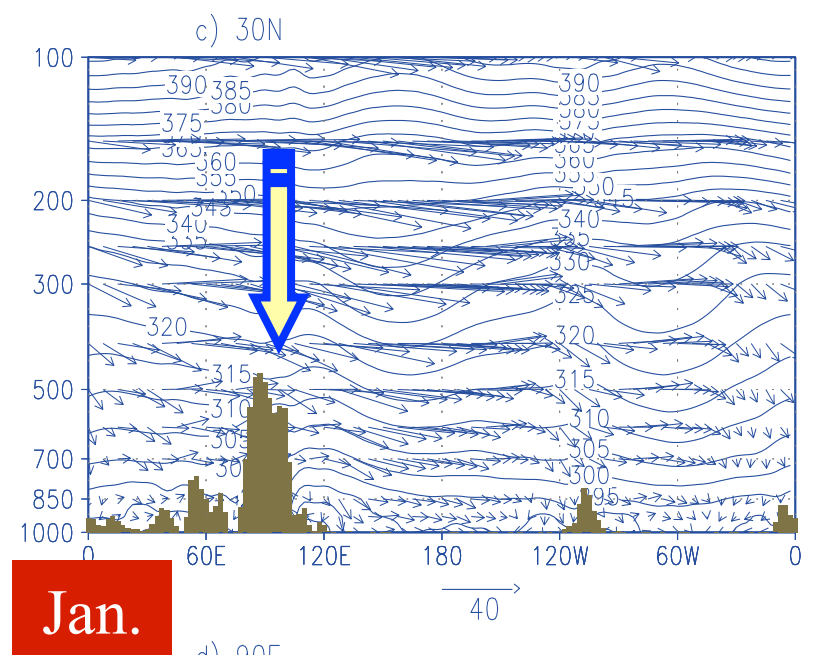
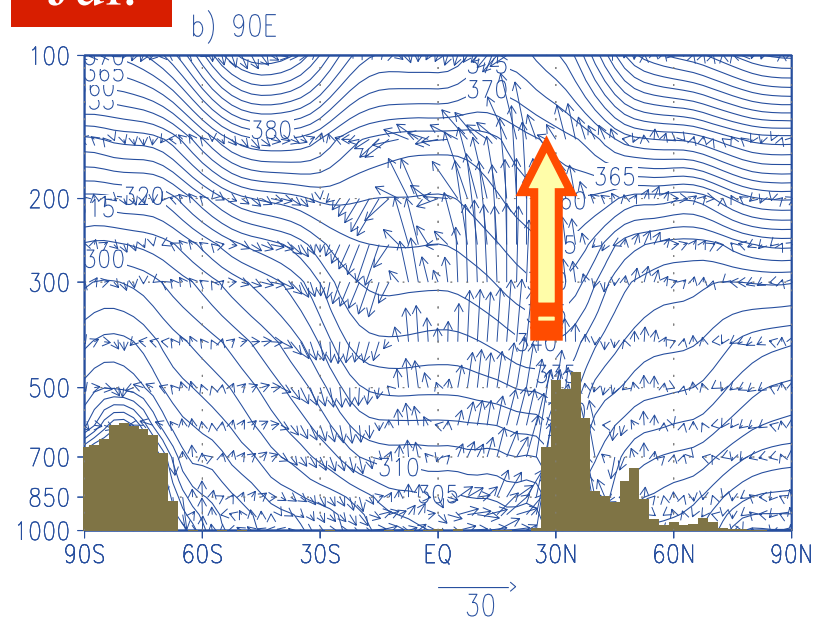
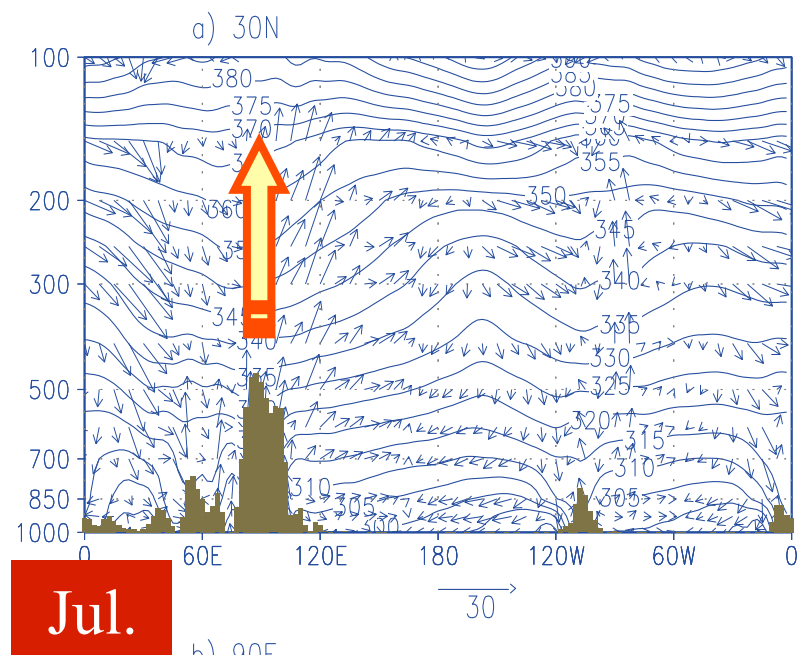
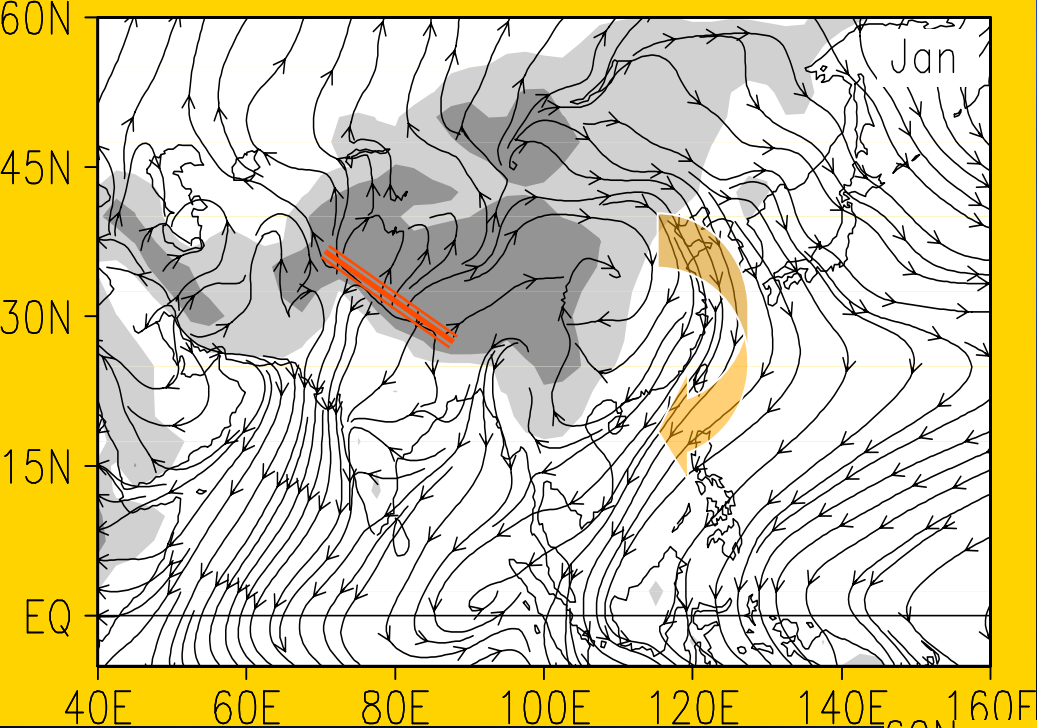


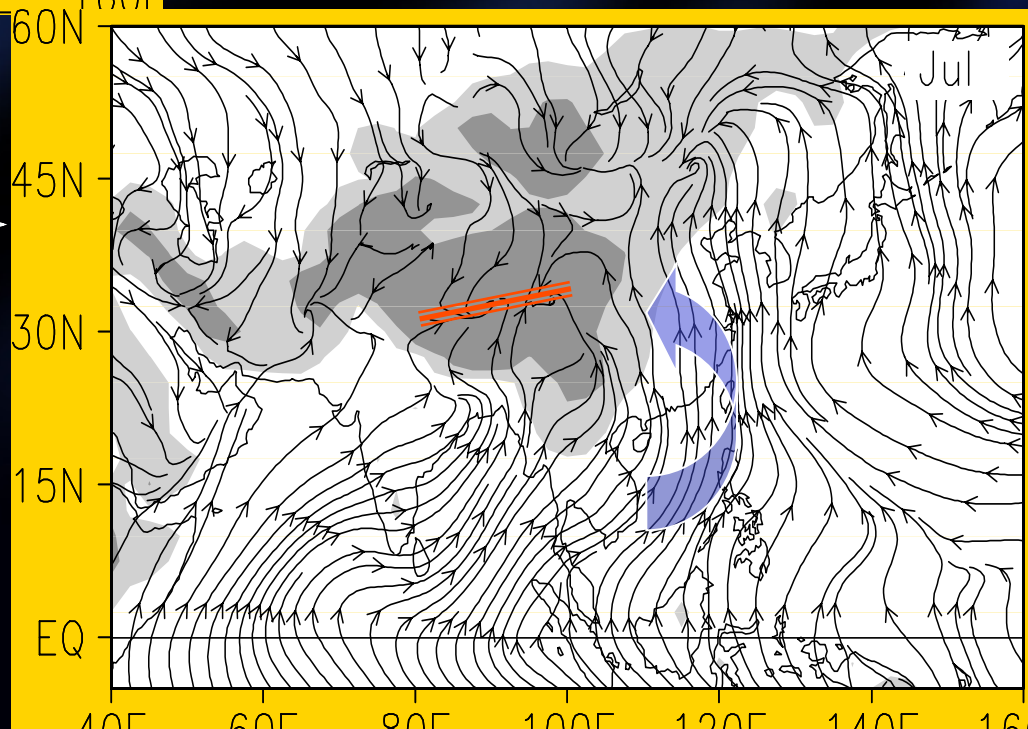
fig. 4; 1986–1995 10 years mean Jul. potential temperature and wind vector cross-section; theta(K) Wind(m/s)

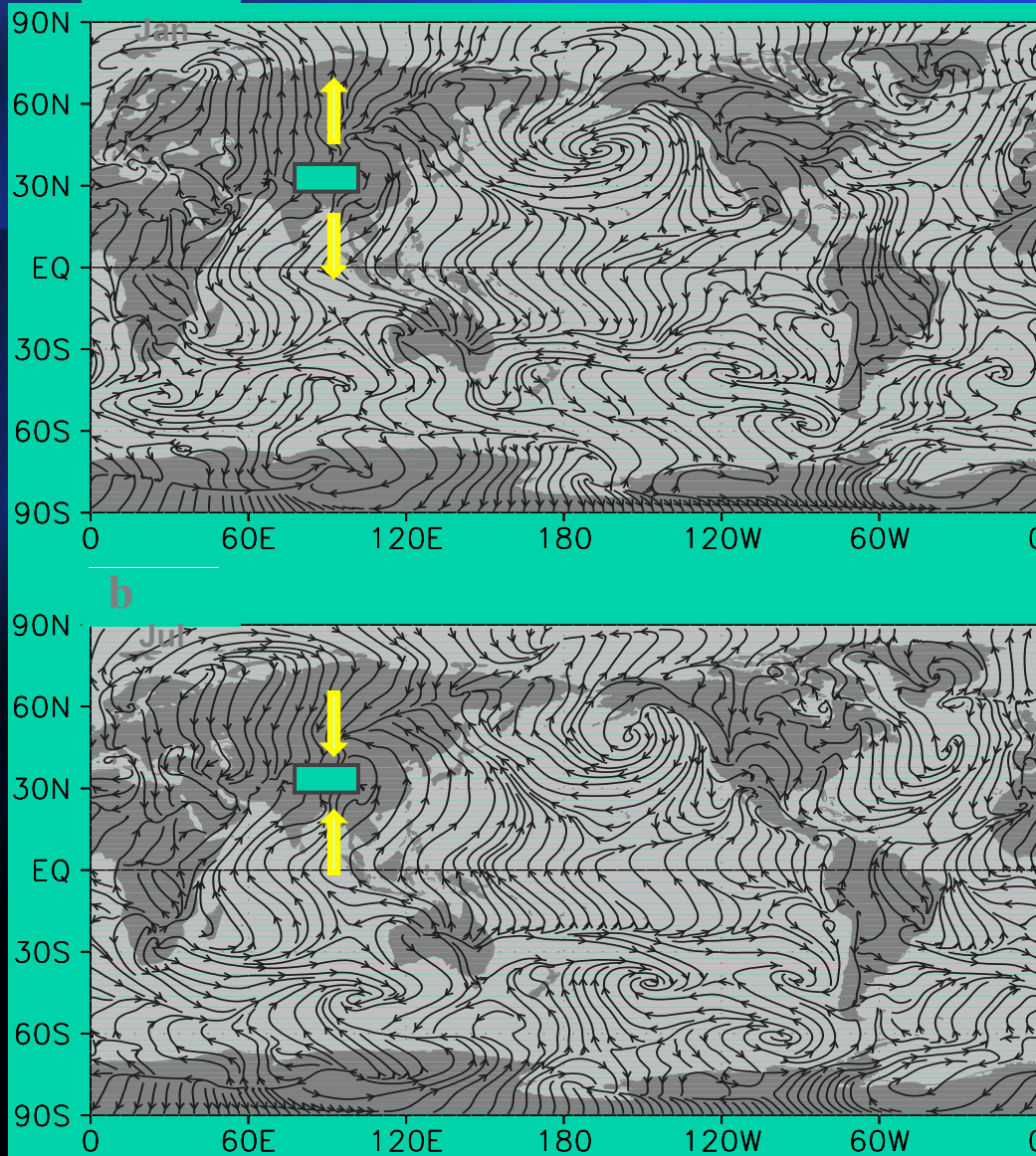
1986–1995 10 years mean Jan. potential temperature and wind vector cross-section; theta(K) Wind(m/s)



10 m wind– Jan.

10 m wind– Jul.





**Distributions of the monthly mean stream field composed of horizontal wind deviations at 10m from the corresponding annual means of 1979-1998 NCEP/NCAR reanalysis. (a) January; (b) July. Dark shadings highlight elevations higher than 3000 m. Rectangle indicates the Tibetan Plateau area as defined in the text.**



# Outline

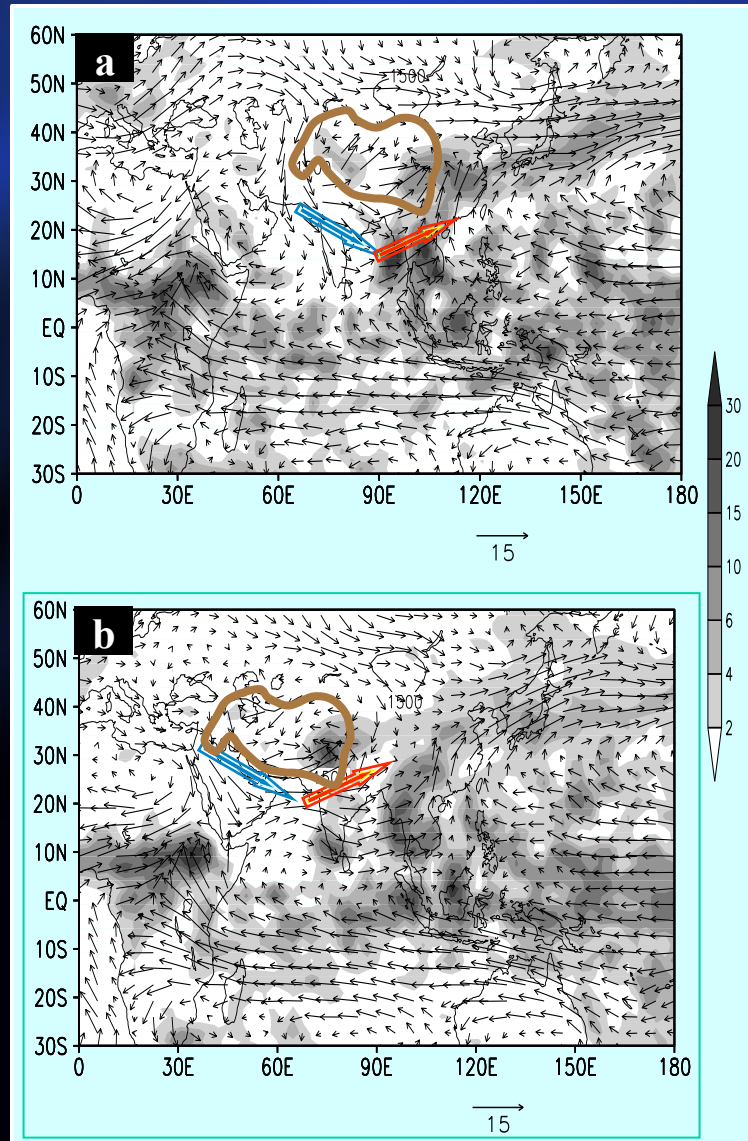


- 1 **Introduction- general circulation**
- 2 **Dynamics of ASM onset**
- 3 **Evolution of the ASM onset**
- 4 **Maintenance of the ASM**
- 5 **Variability of the ASM**
- 6 **Conclusion**



# TP- anchoring of the ASM onset

## GCM Experiment of the ASM onset

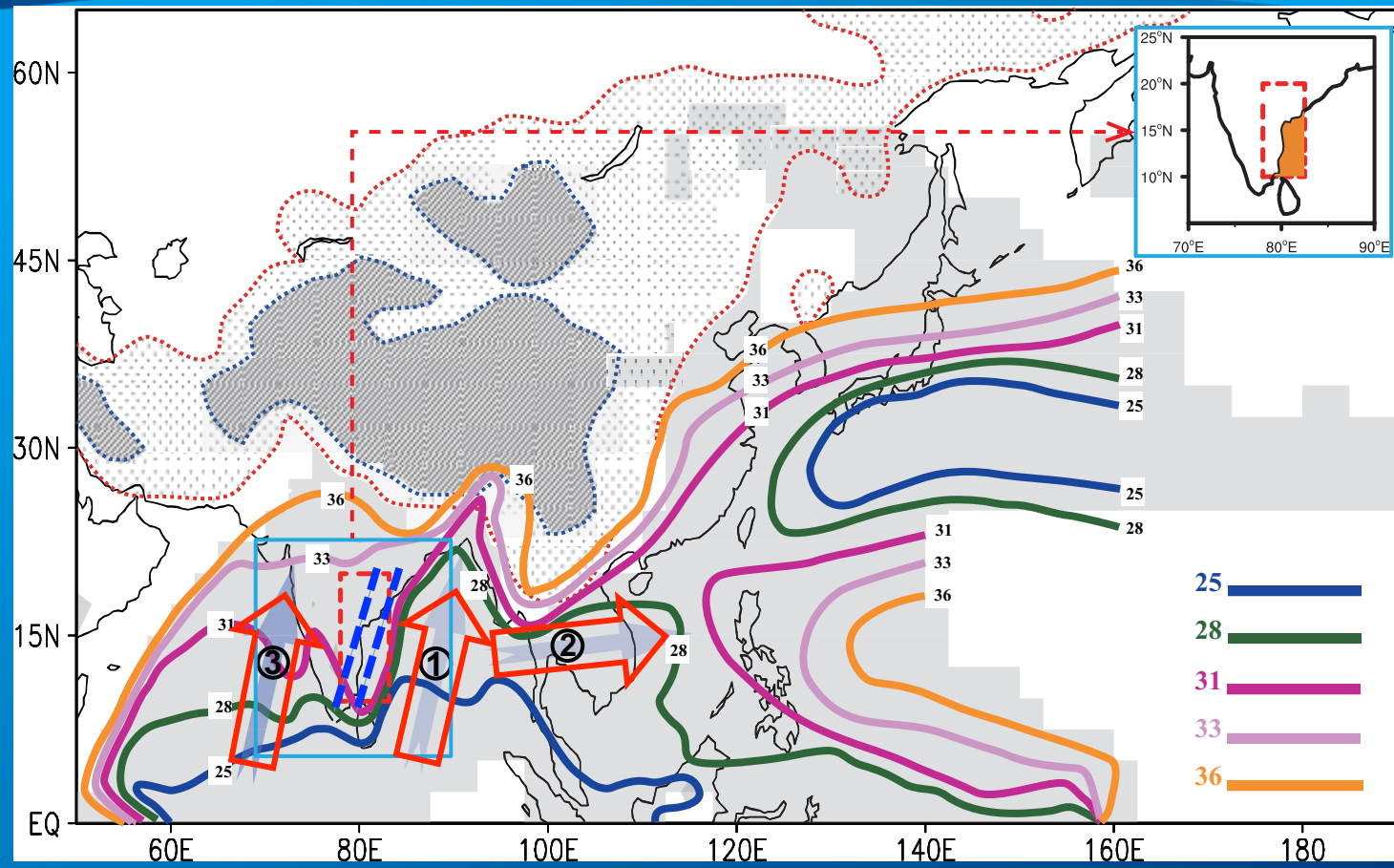


TP at 90E

TP at 60E



# ASM onset isochrones (unit: pentad)



3. IND (MOB) 1. BOB => 2. SCS => NWP



# Upper-lower troposphere coupling



**Upper  
troposphere**

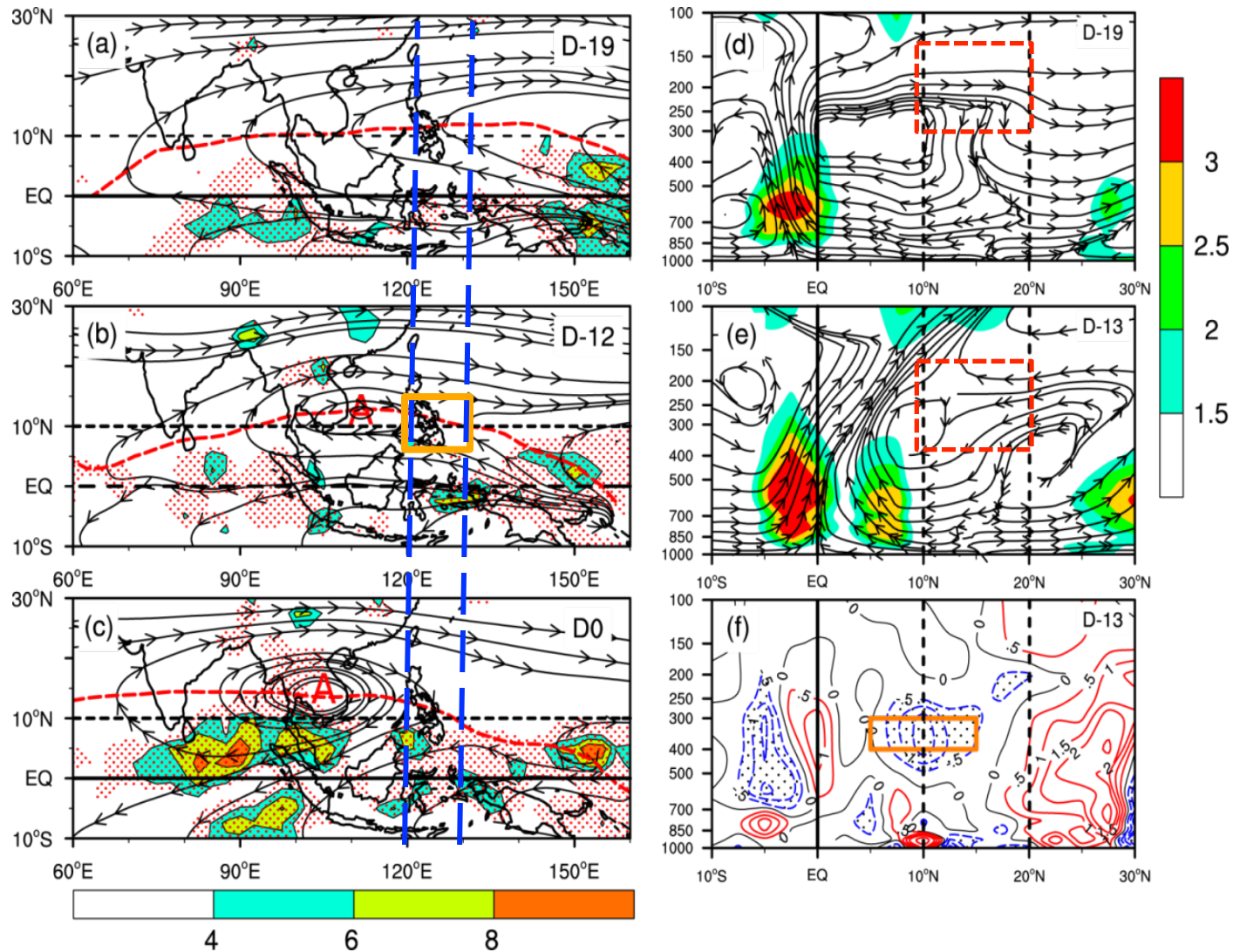


Fig. 8 Streamline and divergent field (shaded, units:  $10^{-6} \text{ s}^{-1}$ ) at 150hPa, and the diabatic heating averaged from 500hPa to 200hPa (red stipple denotes greater than  $1.5 \text{ K day}^{-1}$ ) during the BOB summer monsoon onset period on (a): D-19, (b): D-12, c: (D0); the Pressure–latitude cross section (averaged over  $120^{\circ}$ – $130^{\circ}\text{E}$ ) of  $Q_1$  (shading, units:  $\text{K day}^{-1}$ ) and meridional circulation on (d) D-19 and (e) D-13; and (f) vorticity source  $S$  on D-13 (interval is  $0.5 \times 10^{-11} \text{ s}^{-2}$ , values greater than  $-0.5$  are stippled). “A” and the red dash line in (a) to (c) denote, respectively the anticyclone center and the ridgeline. The orange boxes in (f) denotes the area of maximum  $S$  over Philippines. (reproduced from Liu et al., 2012)

## Original Gill model:

$$\left\{ \begin{array}{l} \varepsilon u - \frac{y}{2} v = -\frac{\partial p}{\partial x} \end{array} \right. \quad (11.1)$$

$$\left\{ \begin{array}{l} \varepsilon v + \frac{y}{2} u = -\frac{\partial p}{\partial y} \end{array} \right. \quad (11.2)$$

$$\left\{ \begin{array}{l} \varepsilon p + \frac{\partial u}{\partial x} + \frac{\partial v}{\partial y} = -Q \end{array} \right. \quad (11.3)$$

$$\zeta \boxed{?} E \quad \frac{1}{2} v = \frac{y}{2} Q + \frac{y}{2} \varepsilon p - \varepsilon \zeta \quad (12)$$

q.:

## Modified Gill model:

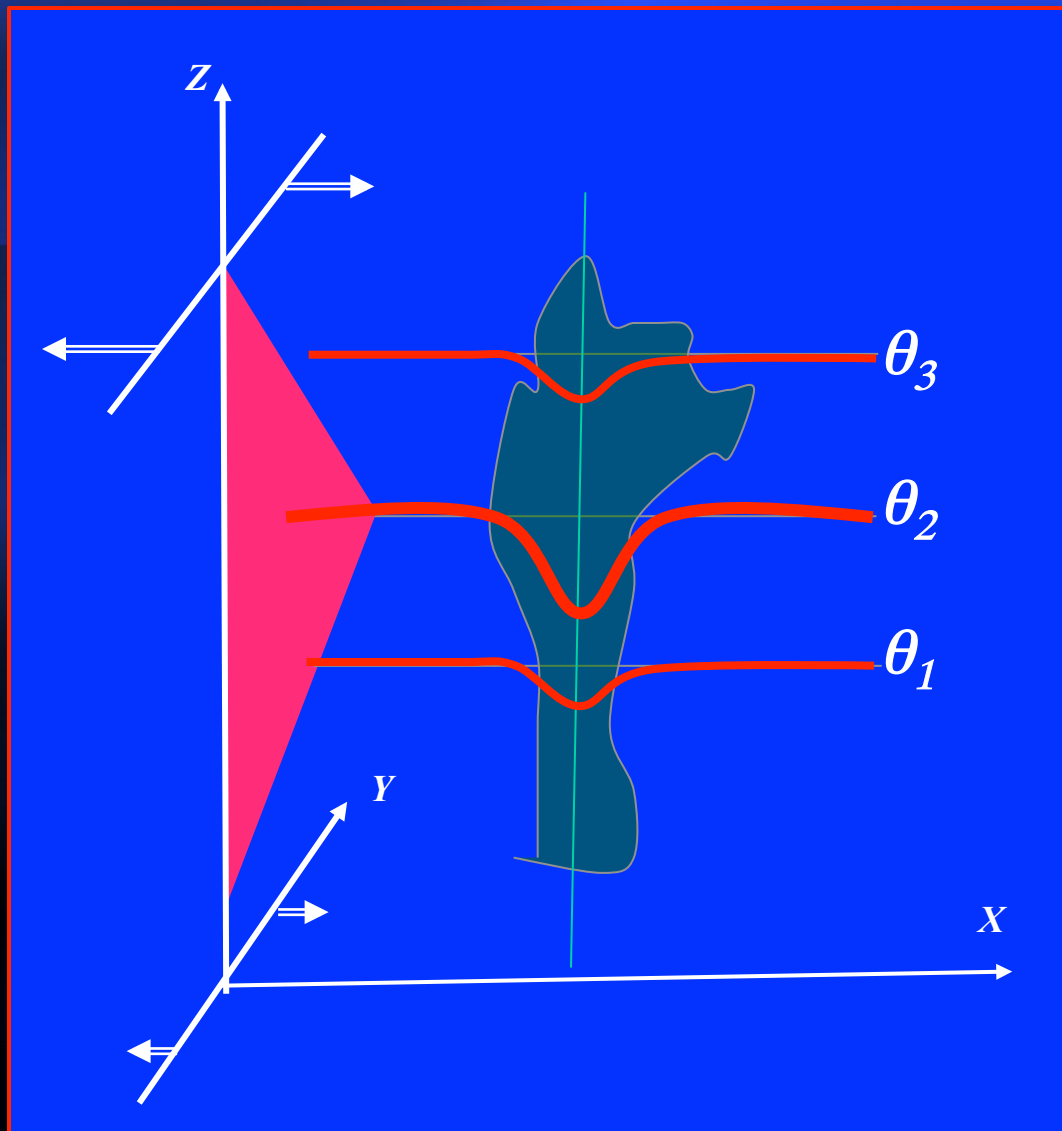
$$\left\{ \begin{array}{l} \varepsilon u - \frac{y}{2} v = -\frac{\partial p}{\partial x} \end{array} \right. \quad (11.1)$$

$$\left\{ \begin{array}{l} \varepsilon v + \frac{y}{2} u = -\frac{\partial p}{\partial y} \end{array} \right. \quad (11.2)$$

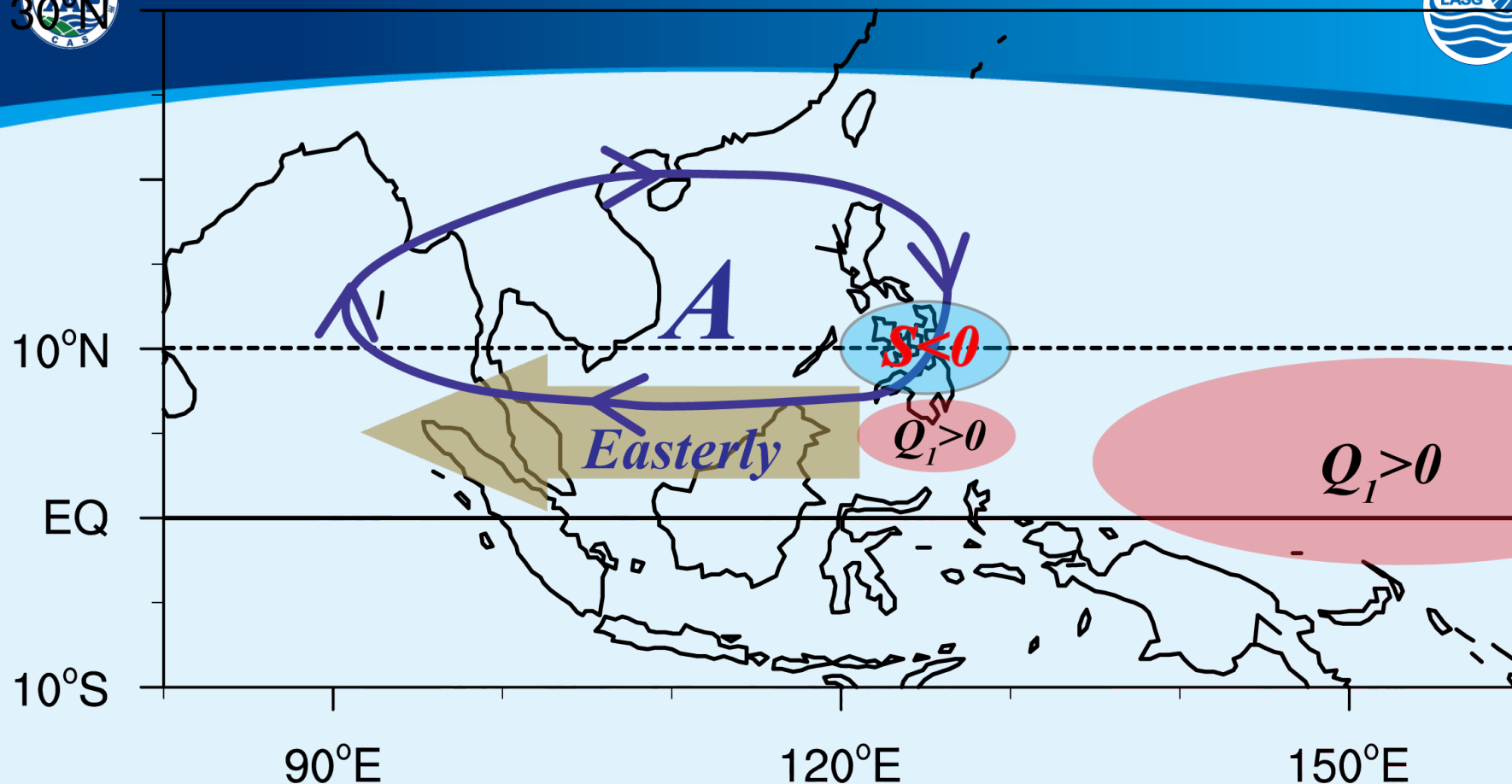
$$\left\{ \begin{array}{l} \varepsilon p + \frac{\partial u}{\partial x} + \frac{\partial v}{\partial y} = -\frac{\partial Q}{\partial z} \end{array} \right. \quad (11.3)$$

$$\zeta \boxed{?} E \quad \frac{1}{2} v = \frac{y}{2} \frac{\partial Q}{\partial z} + \frac{y}{2} \varepsilon p - \varepsilon \zeta \quad (12)$$

q.:



垂直非均匀对流加热（左边红色）引起的对流区（绿色）等位温面的变化：在最大加热区等熵面下凹最大，导致其下层等熵面厚度减小，涡度增大；其上等熵面厚度增大，涡度减小



Schematic diagram presenting the mechanism responsible for the SAH (marked by “A”) formation: persistent convective diabatic heating in spring over the south Philippines produces a sustained negative vorticity source over the Philippines, and the South Asian High is generated as a Gill-type atmospheric response to the negative forcing source. The marked area over the equatorial west Pacific denotes the diabatic heating which is isolated from the one over the south Philippines.

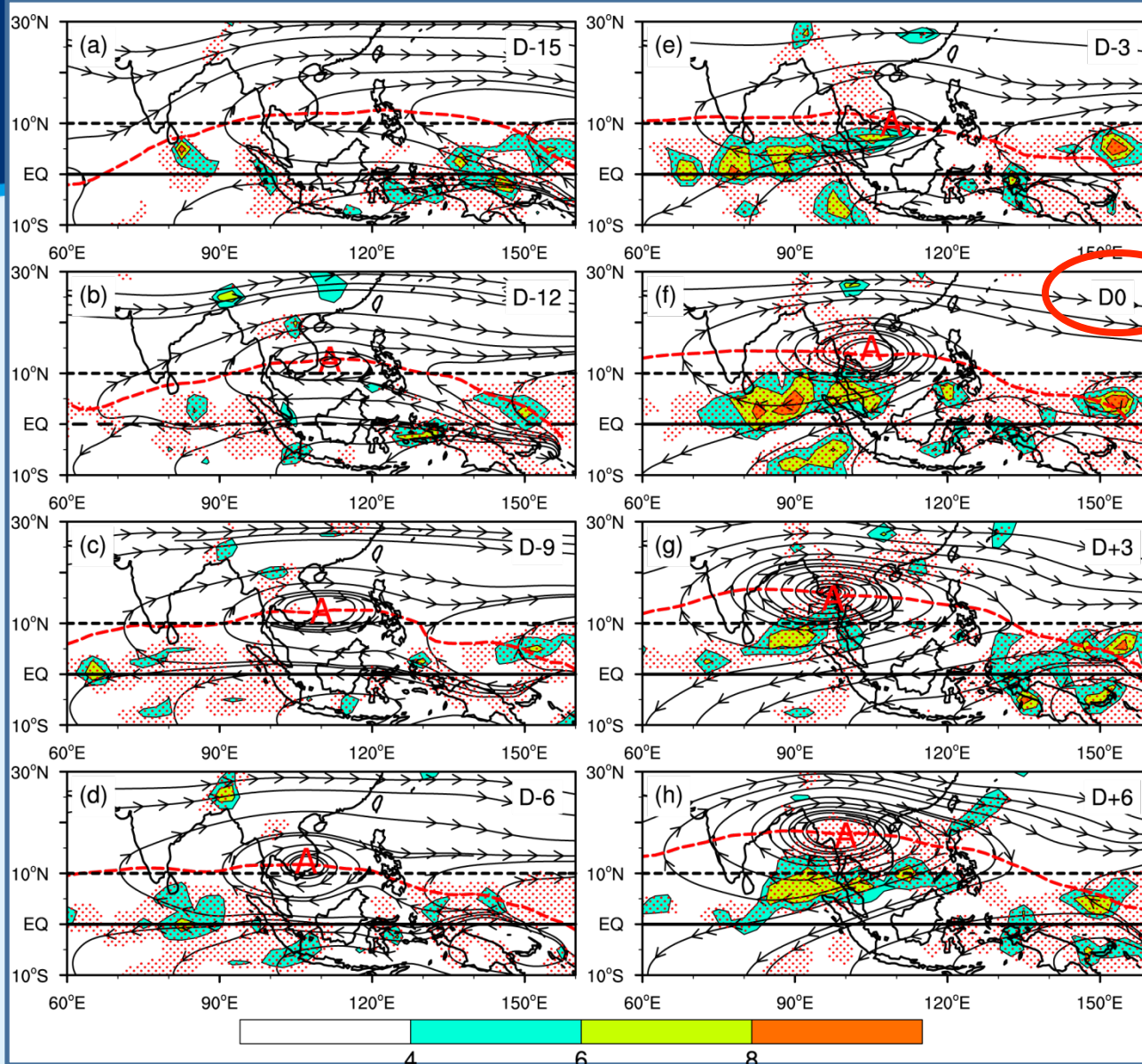


Fig. 1 Daily evolution of **150hPa streamline** and **divergent field** (shaded, units:  $10^{-6} \text{ s}^{-1}$ ), and **the diabatic heating** averaged from 500hPa to 200hPa (red stipple denotes greater than  $1.5 \text{ K day}^{-1}$ ) during the BOB summer monsoon onset period (a: D-15, b: D-12, c: D-9, d: D-6, e: D-3, f: D0, g: D+3, h: D+6). “A” denotes the anticyclone center, the ridgeline is plotted by the red dash line.



## Lower troposphere

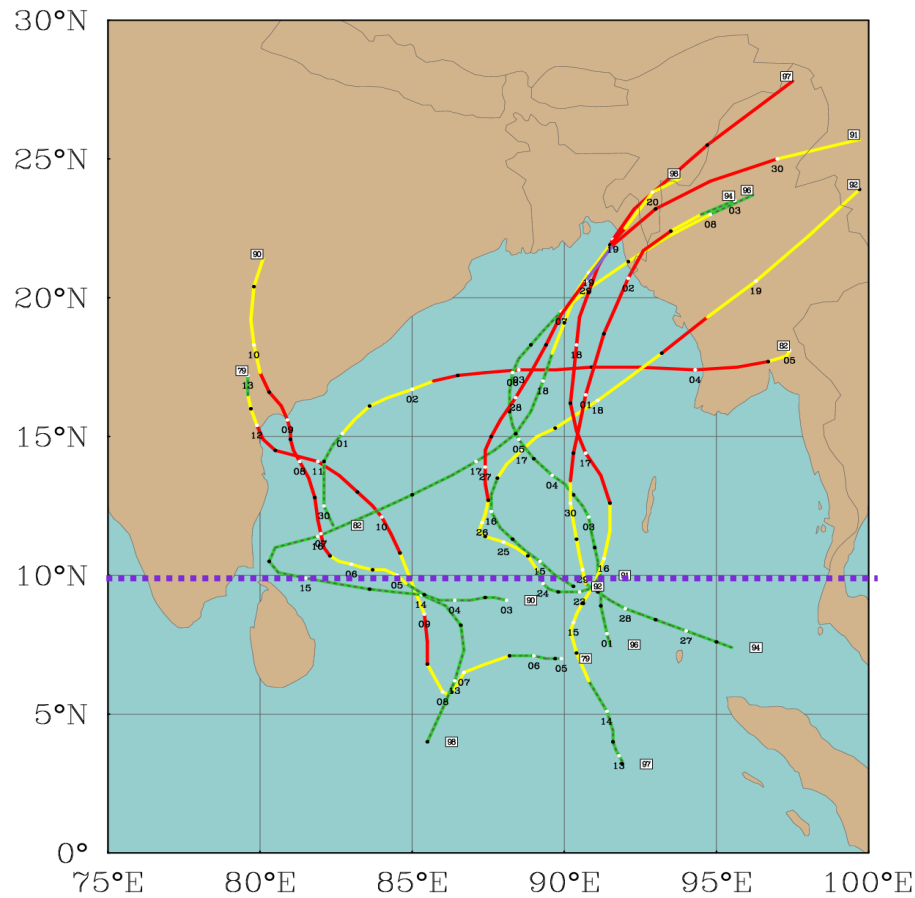
- BOB monsoon onset
- Indian monsoon onset



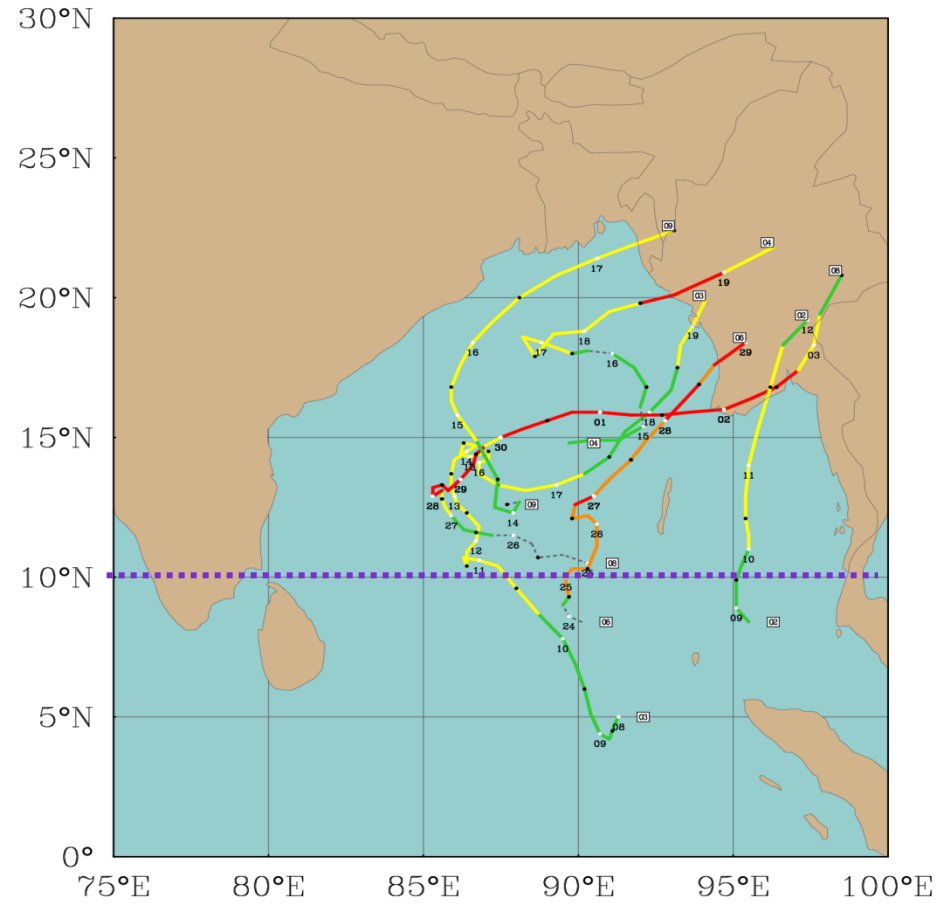
# Climatology: BOB vortex and seasonal transition



## Before 2000



## After 2000



— ST — TY — TS — TD — TC — — DB

● 0000 UTC Position ○ 1200 UTC Position/Date ◻ Tropical Cyclone year

# 4. Influence of the atmosphere and ocean mixing on SST evolution

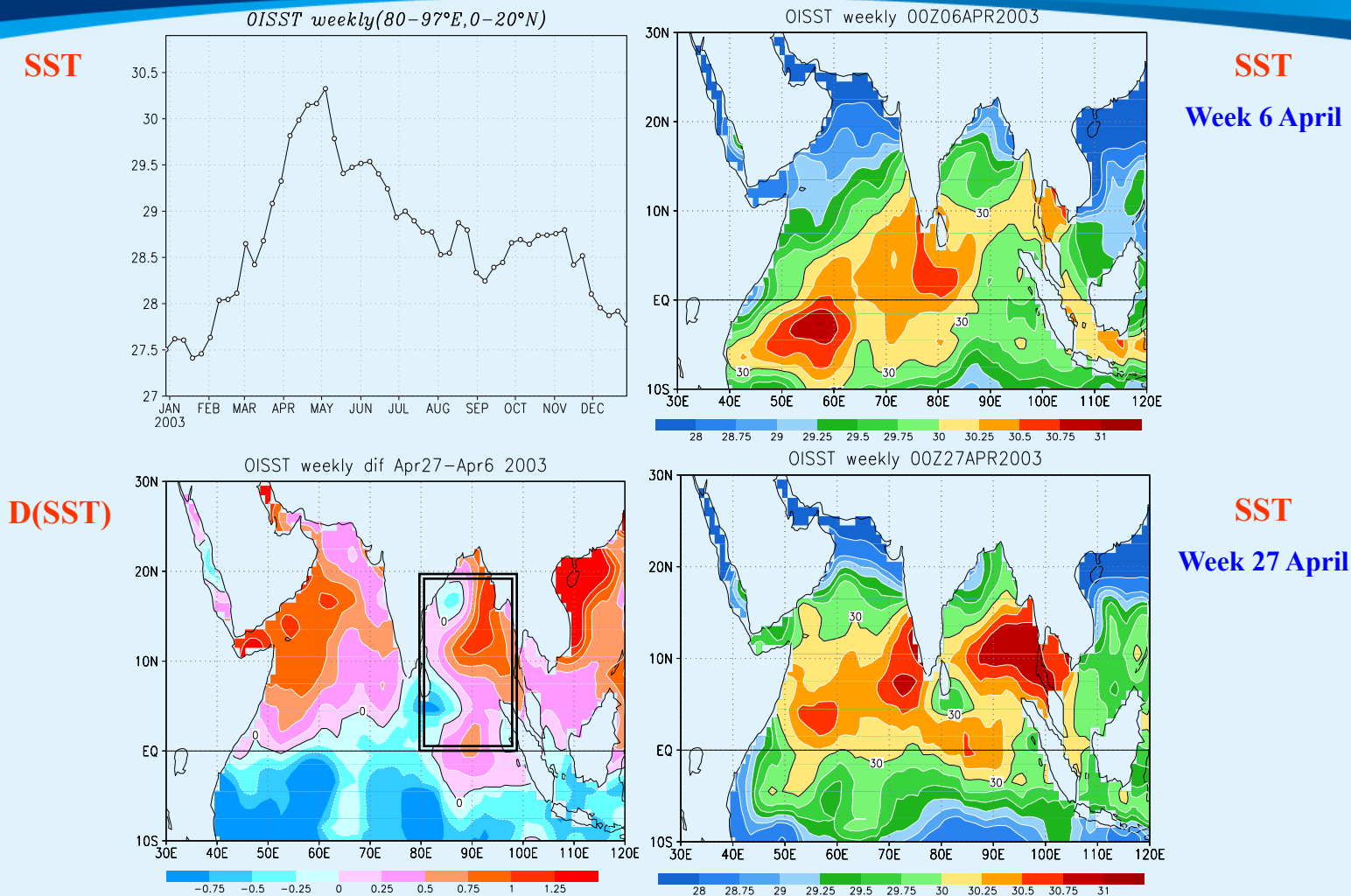


Fig. 9 (a) Time series of area-averaged weekly SST ( $^{\circ}\text{C}$ ) from OISST over the BOB area ( $80^{\circ}$ – $97^{\circ}\text{E}$ ,  $0^{\circ}$ – $20^{\circ}\text{N}$ ). (b) SST increase from the Week 6 April to the Week 27 April. (c) Weekly SST distribution for Week 6 April. (d) As in (c), except for Week 27 April.

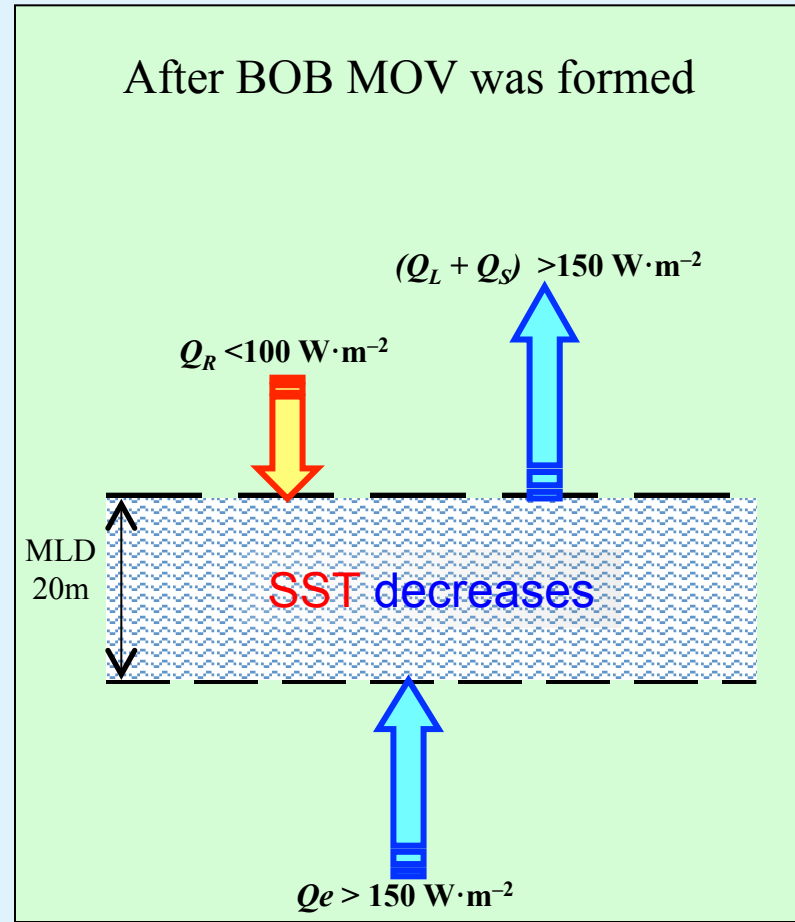
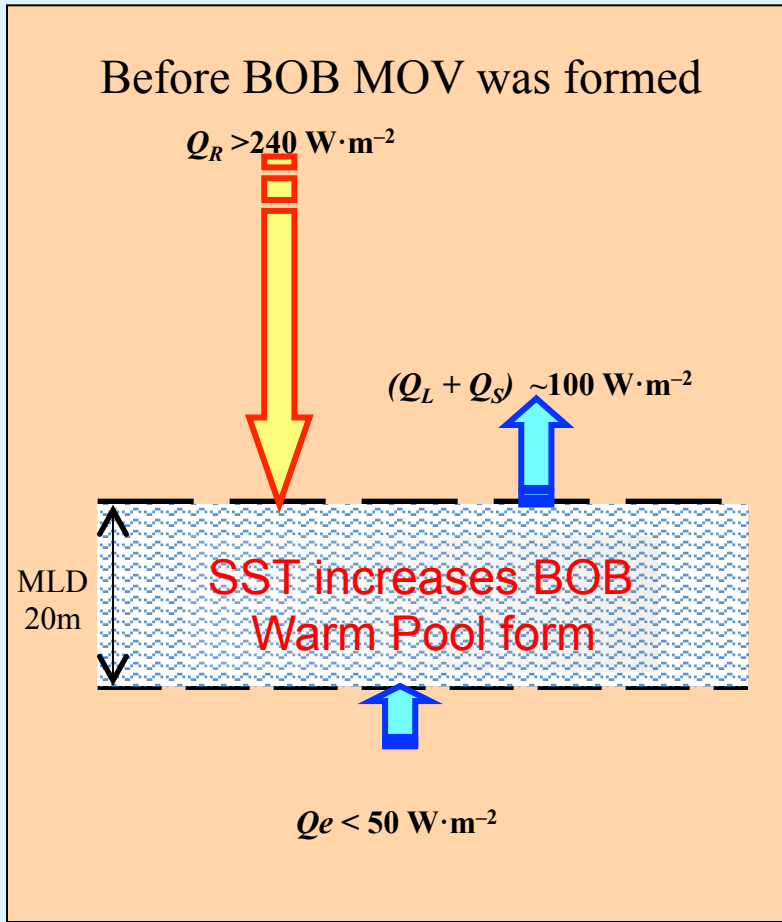


# Influence of the atmosphere and ocean mixing on SST evolution



## Mixed Layer energy budget in northern BOB

$$D(SST)/Dt \propto Q = Q_N - Q_v - Q_e \approx Q_R - (Q_L + Q_S) - Q_e$$



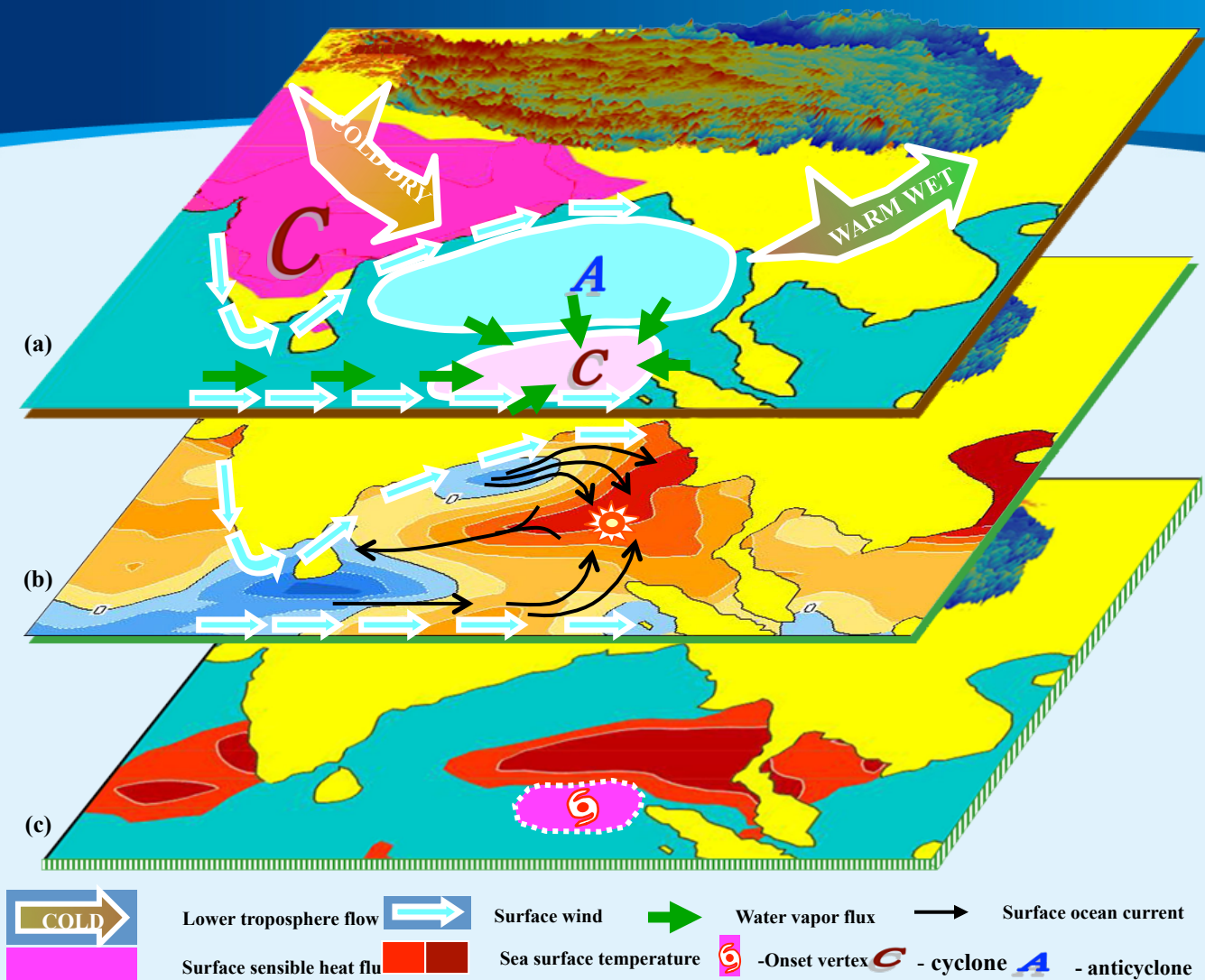


Fig. 7 Schematic diagram showing the formation of the BOB monsoon onset vortex as a consequence of *in situ* air–sea interaction modulated by the land–sea thermal contrast in South Asia and Tibetan Plateau forcing in spring. (adopted from Wu et al., 2012a)

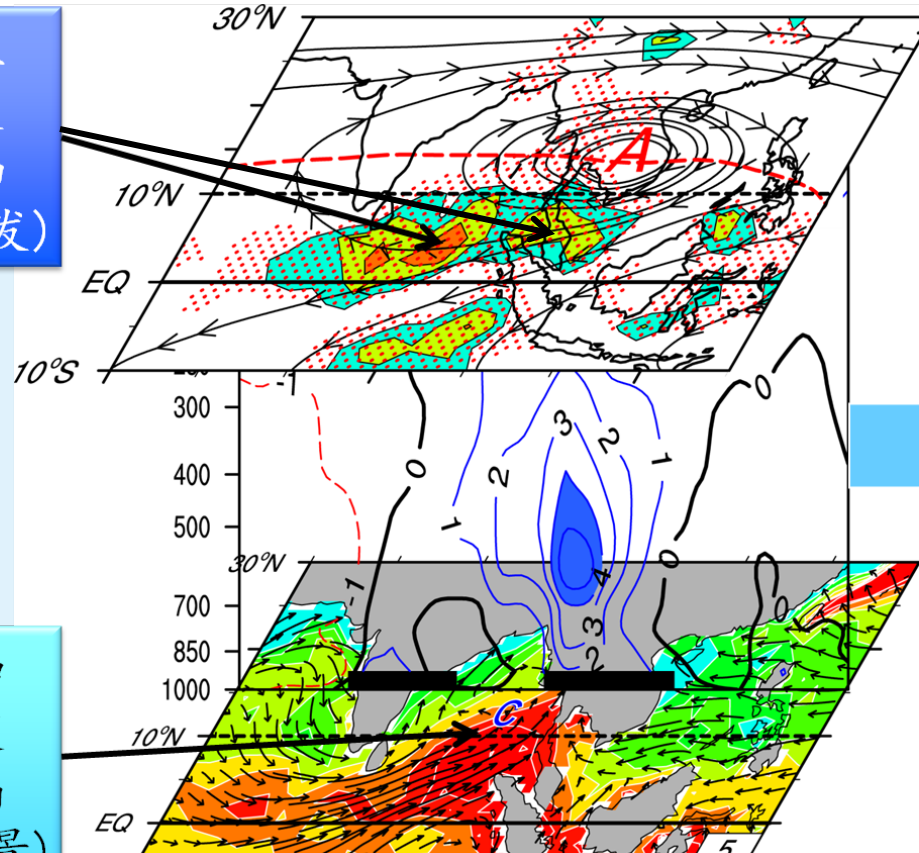
图7 春季在青藏高原强迫和南亚海陆热力对比共同作用下(a), 孟加拉湾暖池形成(b)和季风爆发涡旋激发(c)的示意图, 详见正文。引自 Wu等(2012a)



# Upper-lower troposphere coupling leads to earliest ASM onset over BOB

**TP forcing intensifies SAH so that the upper tropospheric divergence-pumping is located over the SE BOB**

高空：南亚高压西伸发展引起的抽吸作用(触发)



孟加拉湾MOV形成发展，亚洲夏季风开始爆发

低空：孟加拉湾春季暖池提供的涡旋动能(背景)

**TP forcing generates a warm pool and a MOV over the eastern BOB in the lower troposphere**



# Outline



- 1 **Introduction- general circulation**
- 2 **Dynamics of ASM onset**
- 3 **Evolution of the ASM onset**
- 4 **Maintenance of the ASM**
- 5 **Variability of the ASM**
- 6 **Conclusion**



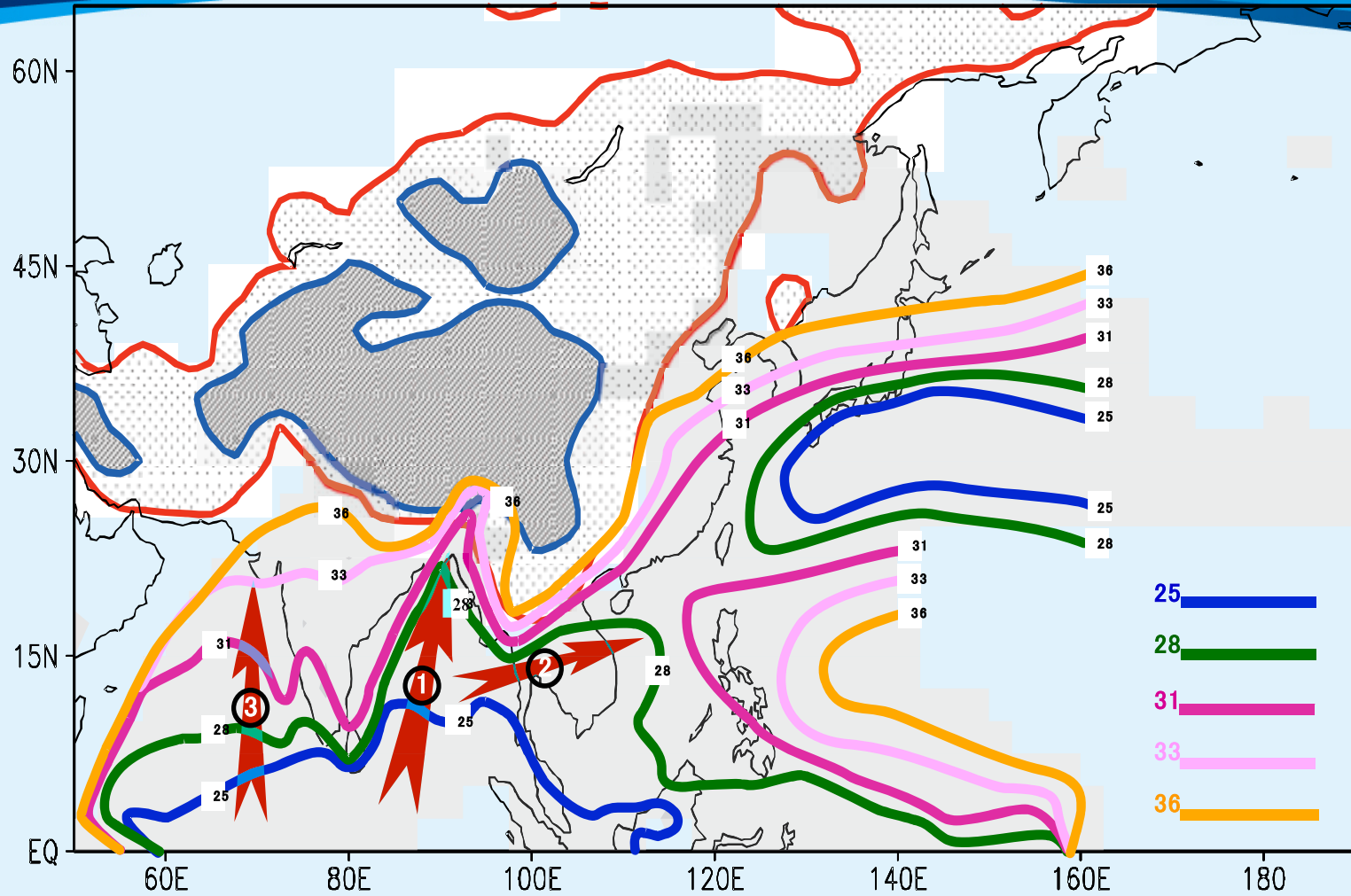
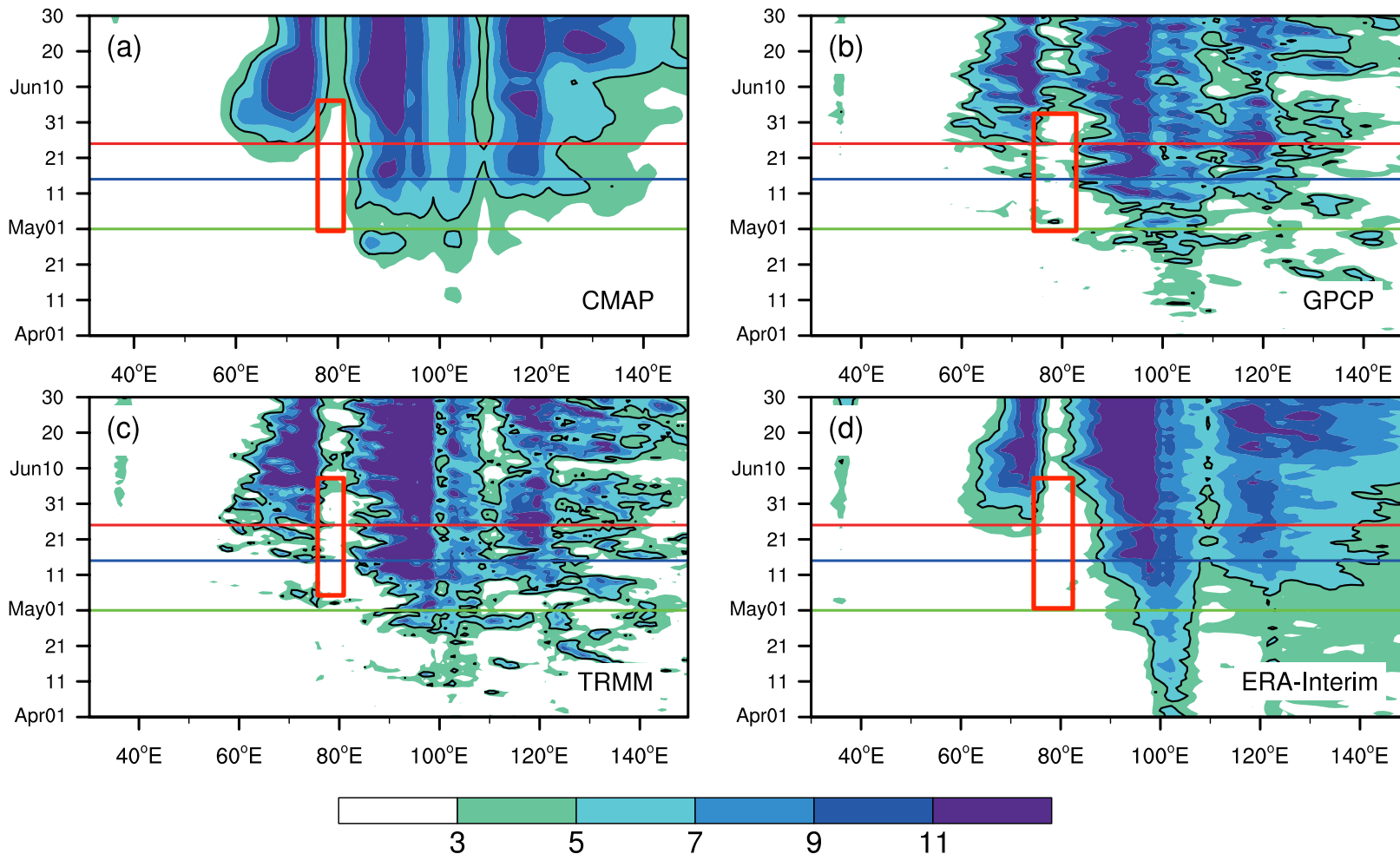


**Fig. 4 Climate-mean Pentad-isochrones indicating the evolution of the Asian summer monsoon onset, Unit: pentad**

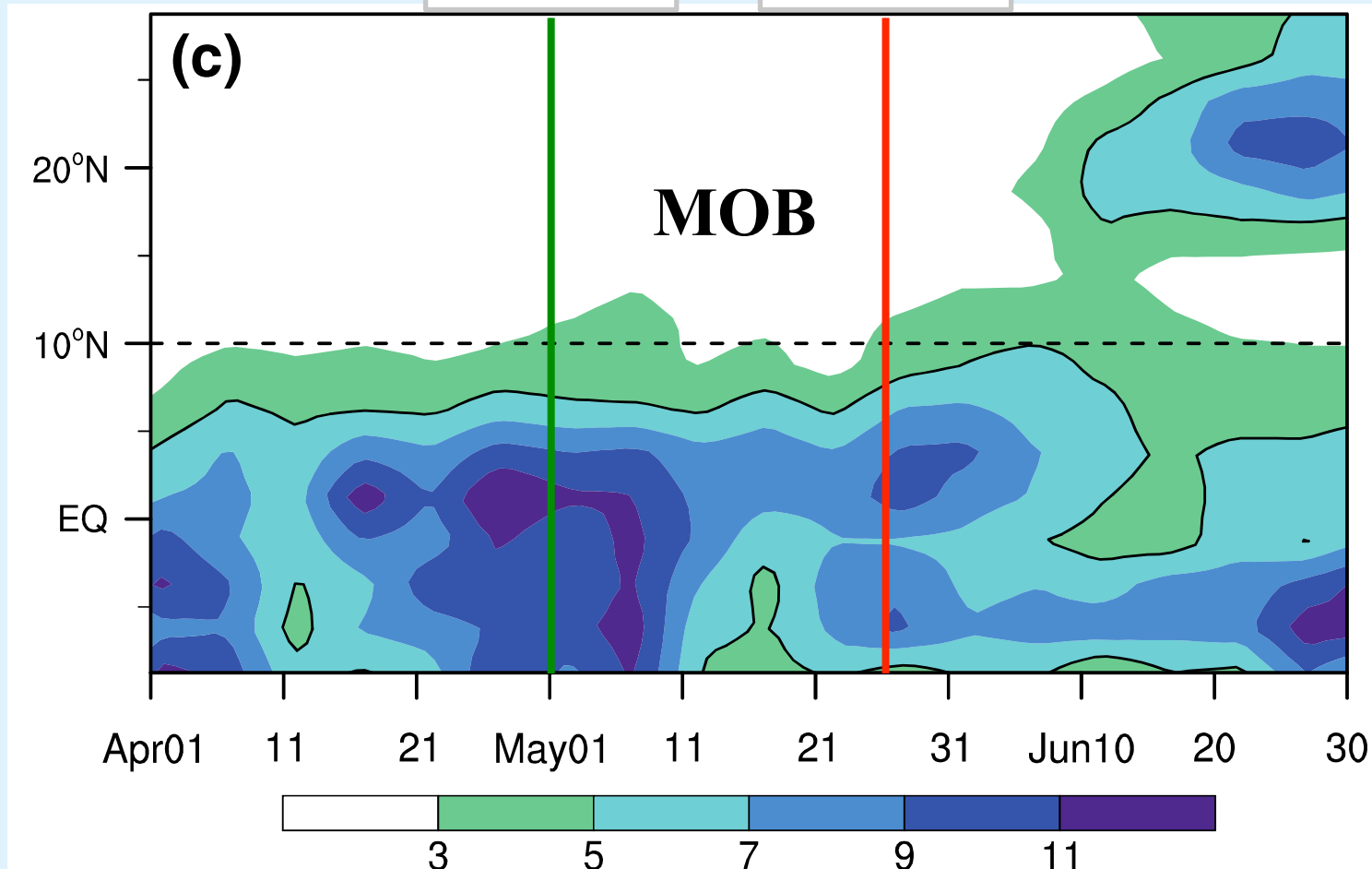


# 气候平均沿10-20N平均的降水时间-经度剖面 (mm day<sup>-1</sup>)



BOBSM

ISM

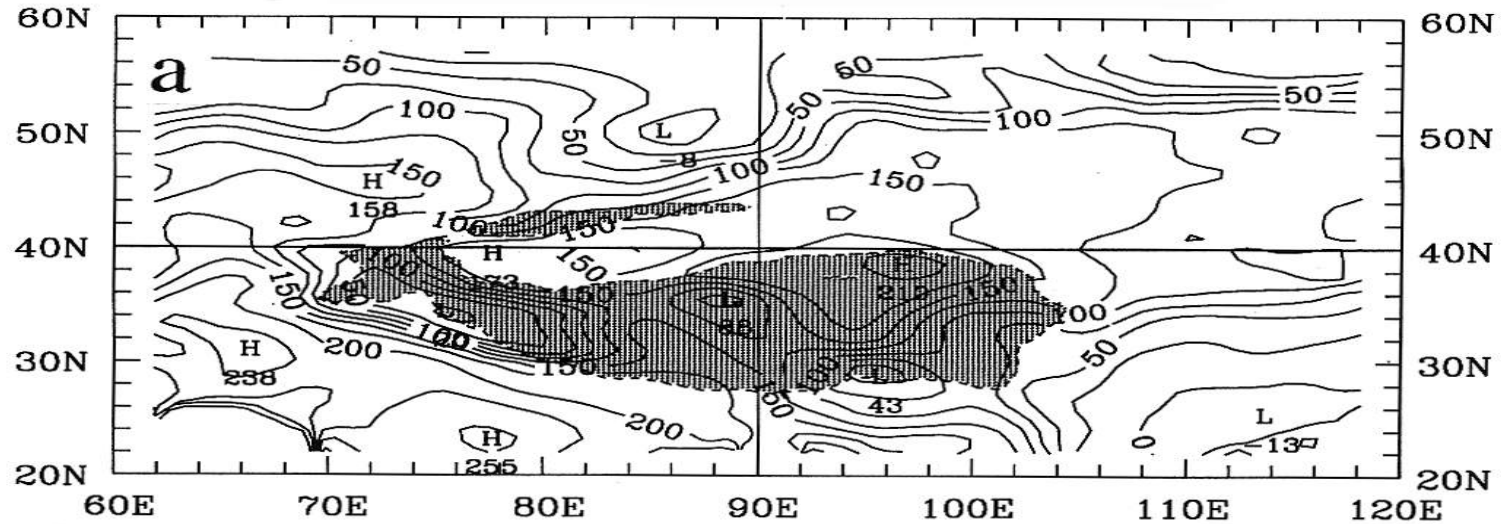


BOB夏季风爆发

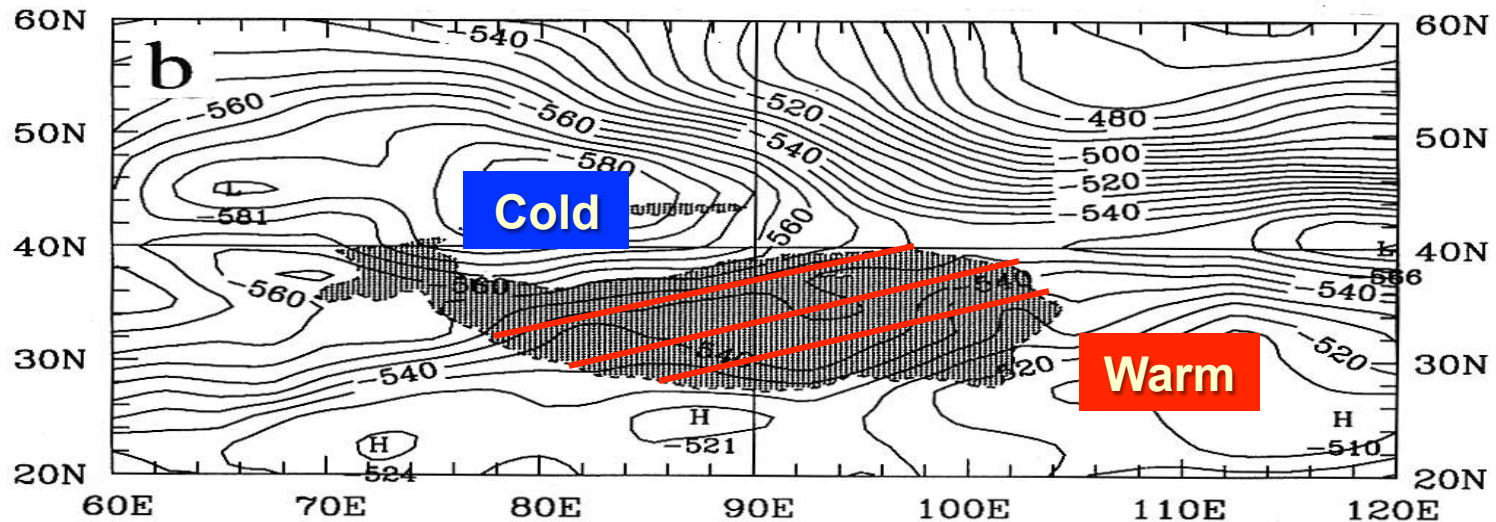


MOB形成

SH ( $\text{Wm}^{-2}$ ) Premonsoon, 1989

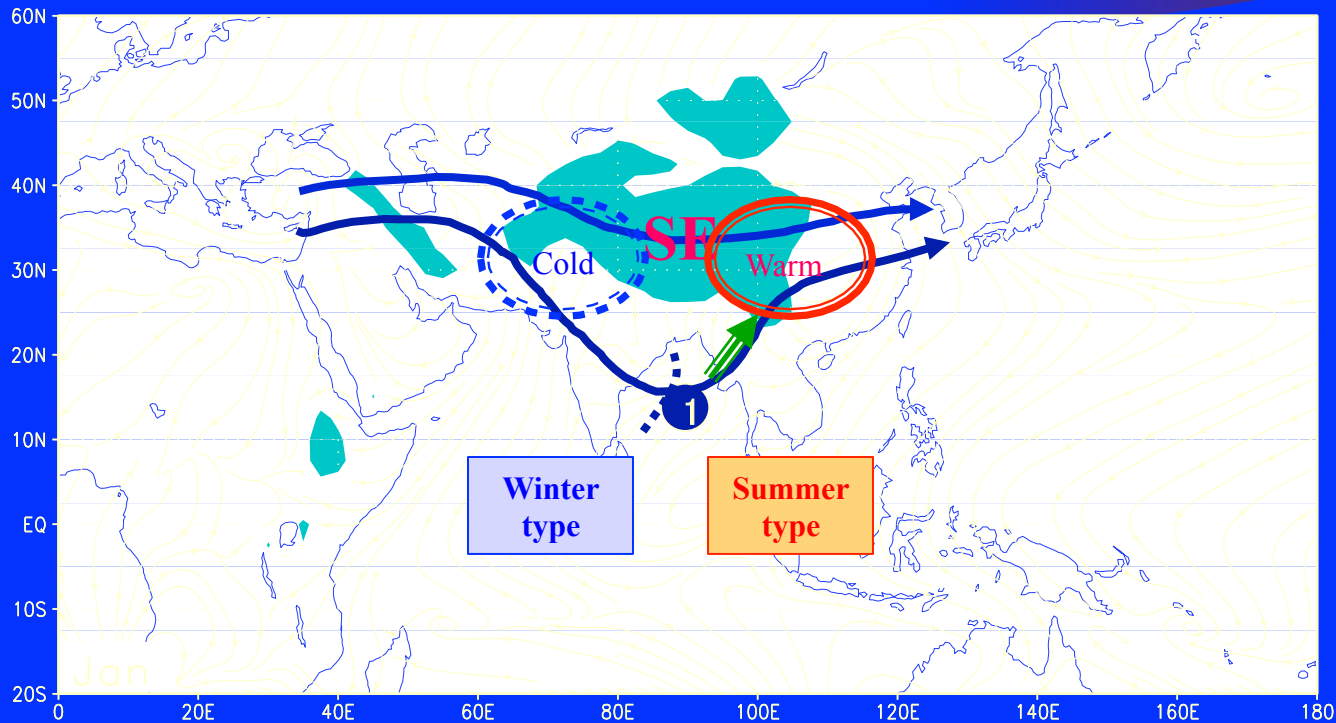


$T_{200}$  ( $0.1^\circ\text{C}$ ) Premonsoon, 1989



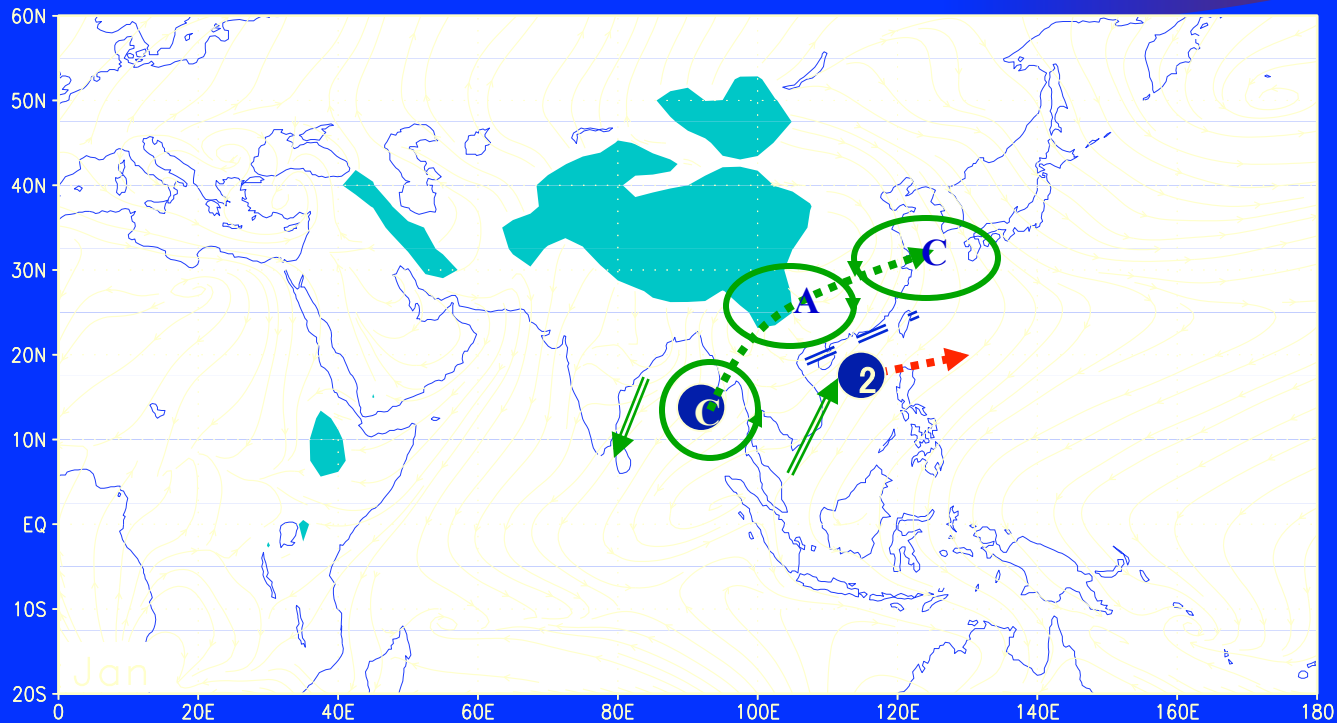
# MO Sequence: Three Stage Structure

## Stage 1: BOB Monsoon Onset



# MO Sequence: Three Stage Structure

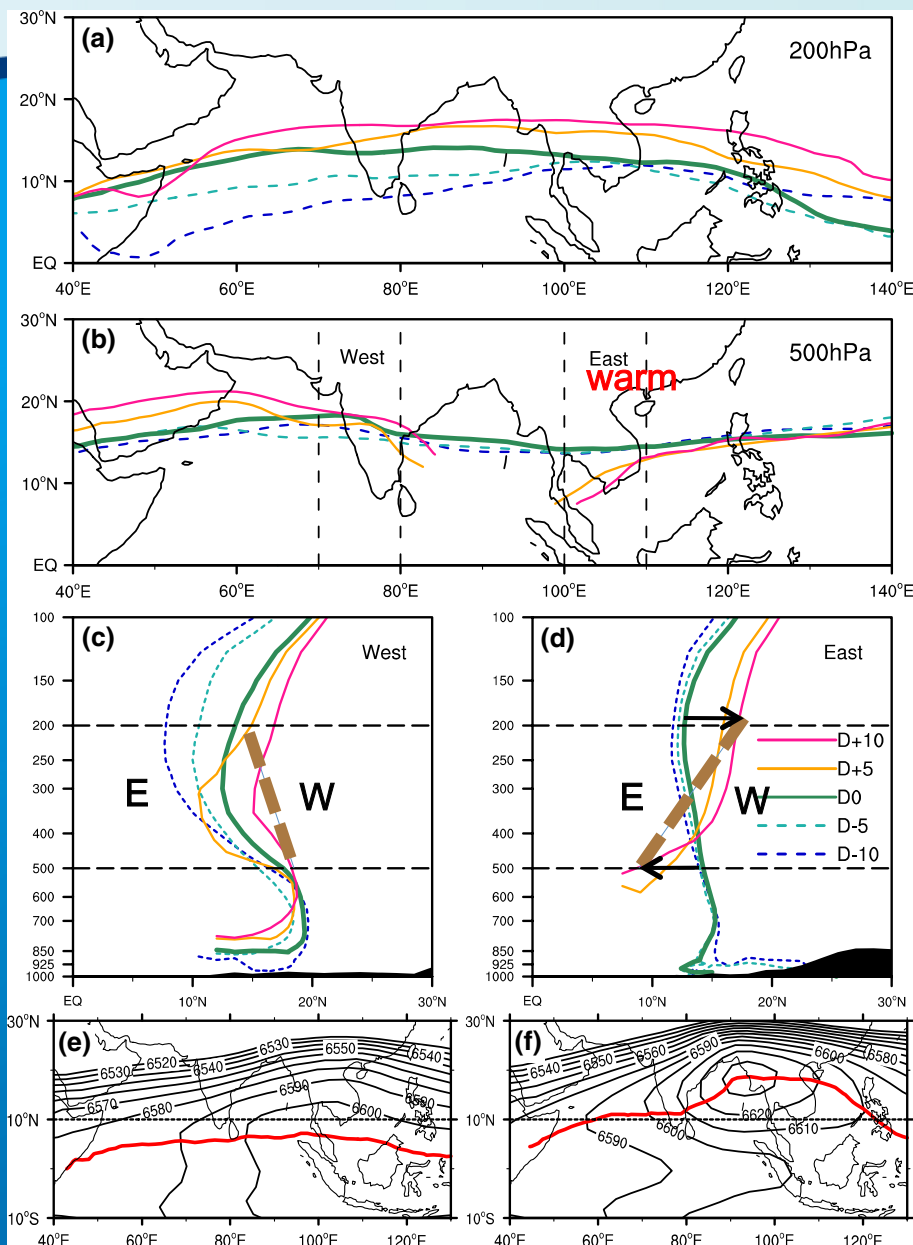
## Stage 2: SCS Monsoon Onset





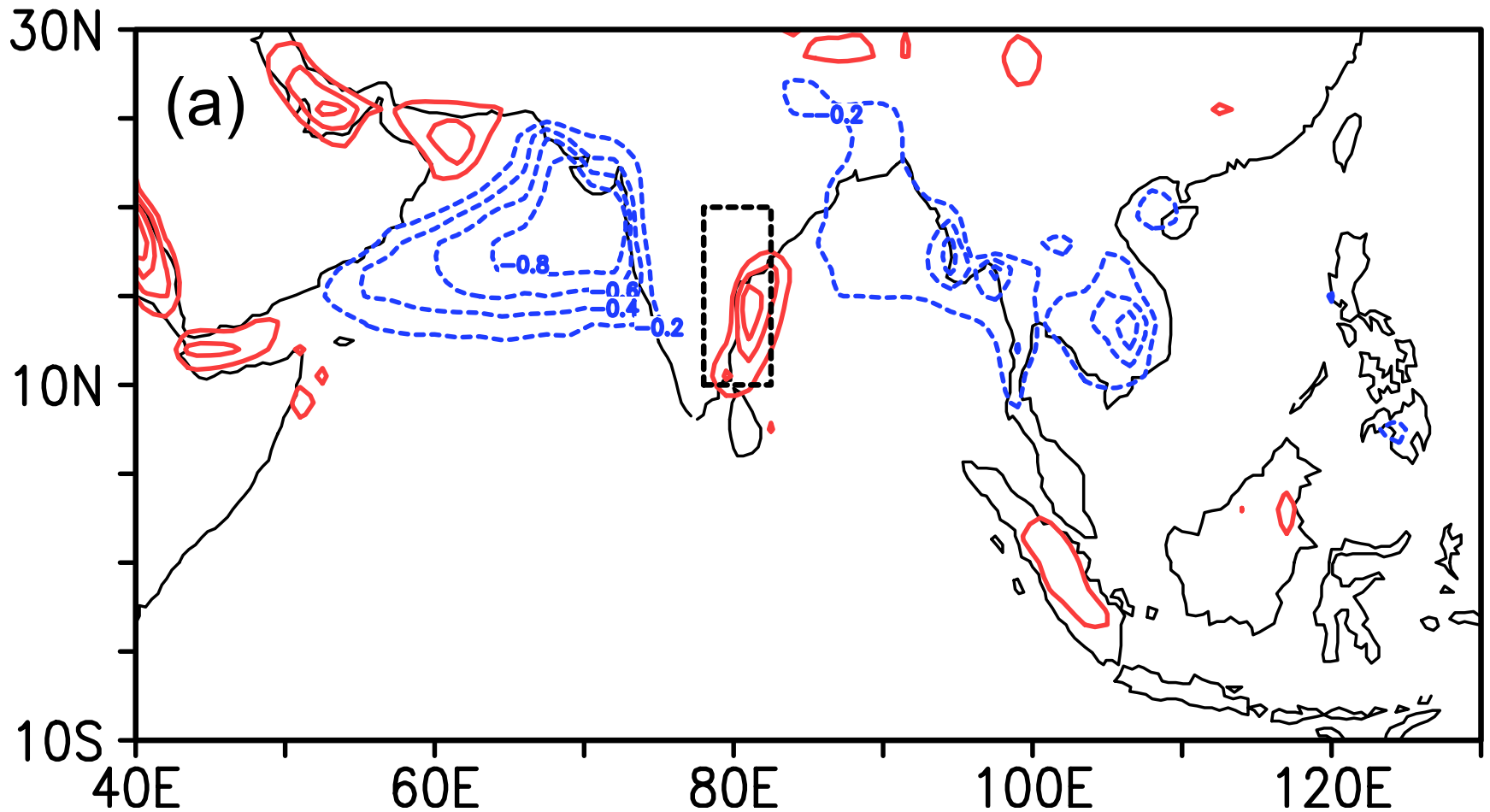
# ASM onset Barrier (MOB)

# Change in atmospheric circulation



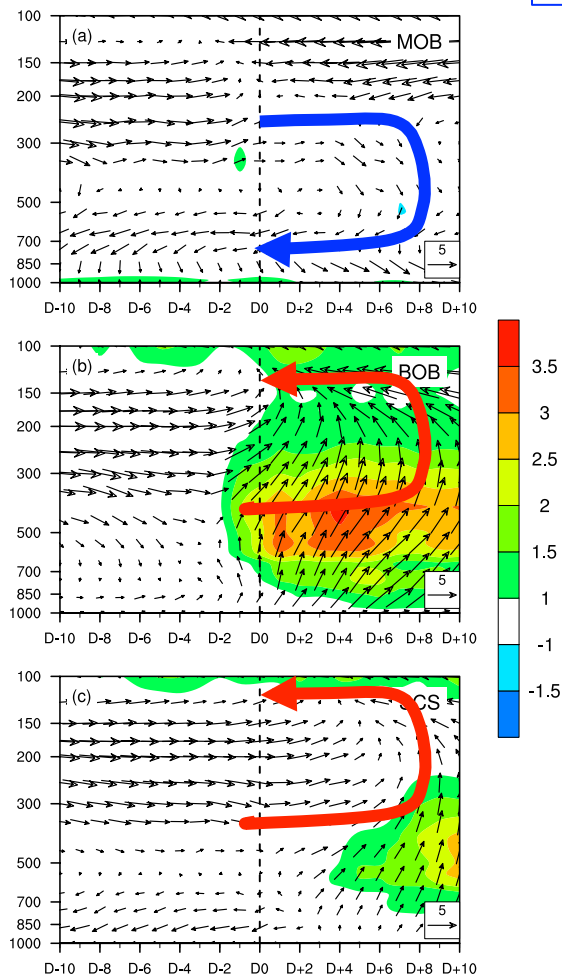
BOBSM爆发前后对流层中上部反气旋脊线的演变特征(a: 200hPa, b: 500hPa, c: 沿印度季风区剖面, d:沿中南半岛剖面, e, f: BOBSM爆发前后200-500hpa气层厚度, gpm)

- BOBSM爆发前：亚洲南部都是冬季型，高压脊面随高度向海洋倾斜。
- BOBSM爆发后：BOB对流以东变为夏季型（高压脊面随高度向大陆倾斜），以西仍为冬季型。

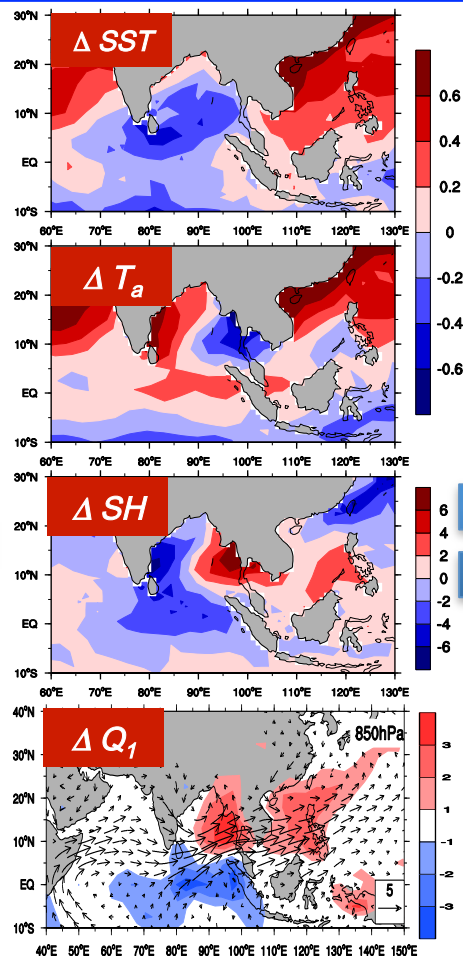


Onset changes of the difference between environmental and air parcel virtual temperature ( $T_{ve} - T_{va}$ , interval is 0.2 K) averaged from 1000 hPa to 900 hPa.

# Formation of MOB

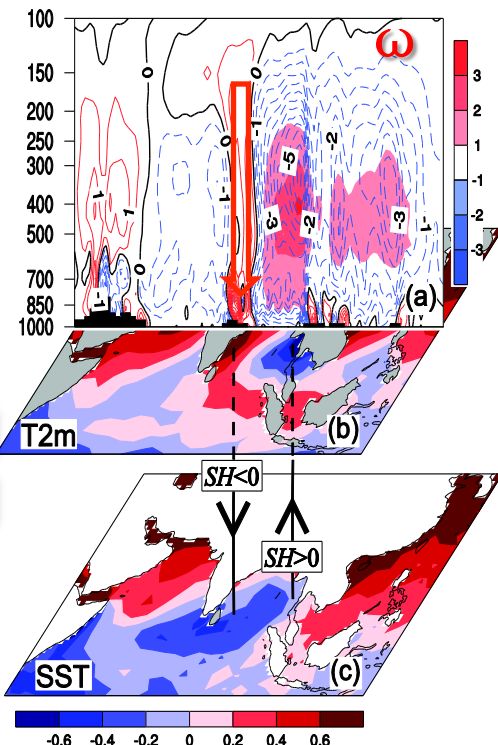


Change in atmos. circulation



Change in air-sea interaction

# Formation of MOB



孟加拉湾夏季风爆发后，季风对流释放的凝结潜热一方面在MOB地区激发出下沉运动，另一方面令MOB地区的海气热通量发生变化，在孟加拉湾西部-印度半岛东岸之间的海域上空形成向上负感热通量，两者的共同作用导致了MOB的出现。

Liu, BQ, YM Liu, GX Wu, JH Yan, JH He, SL Ren, 2014: Asian summer monsoon onset barrier and its formation mechanism. *Climate Dyn.*, 10.1007/s00382-014-2296-0.

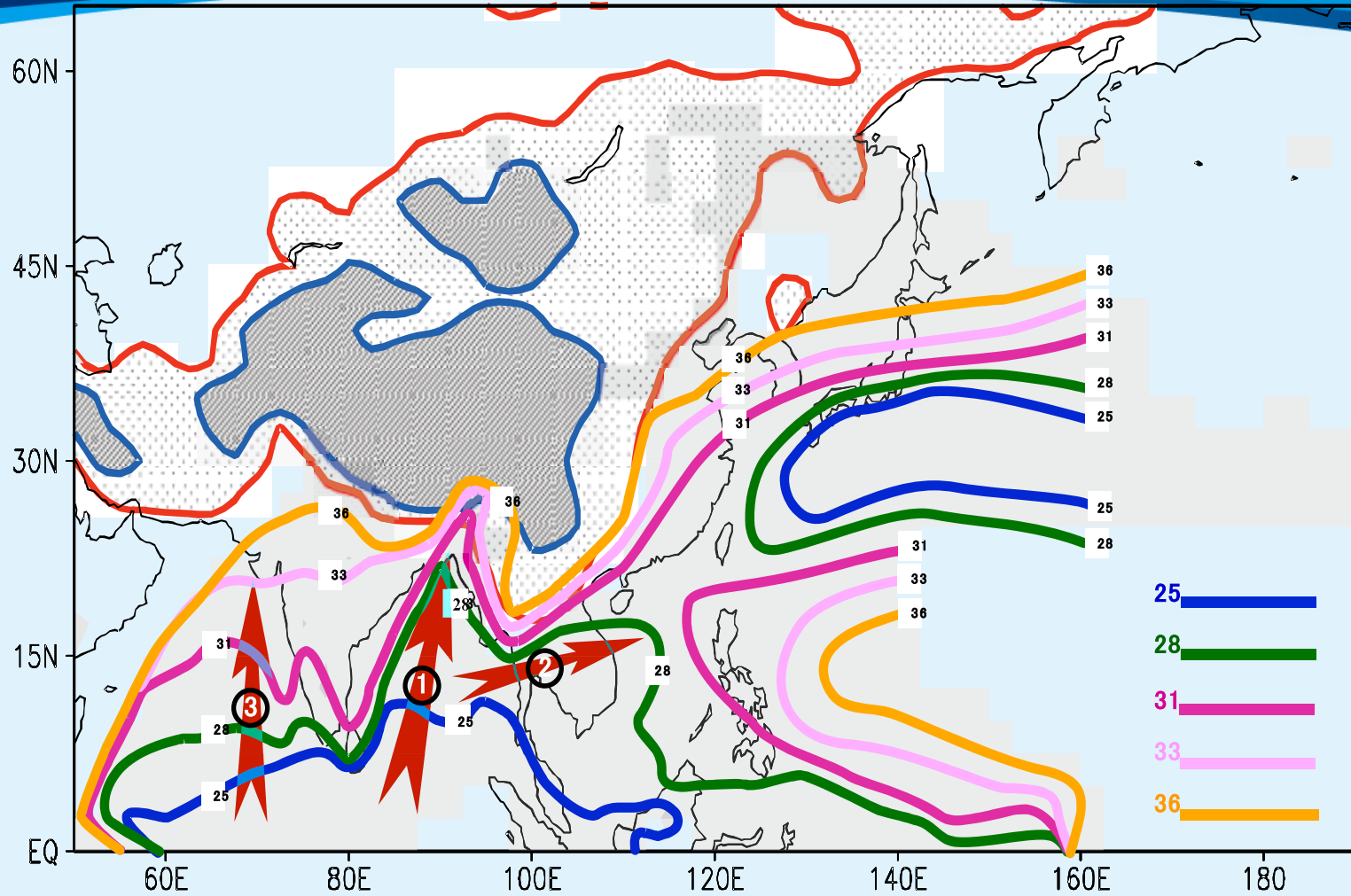
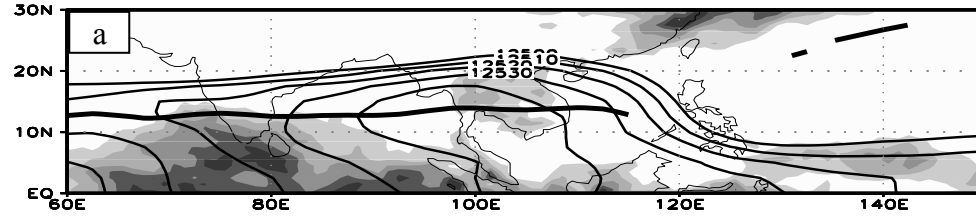


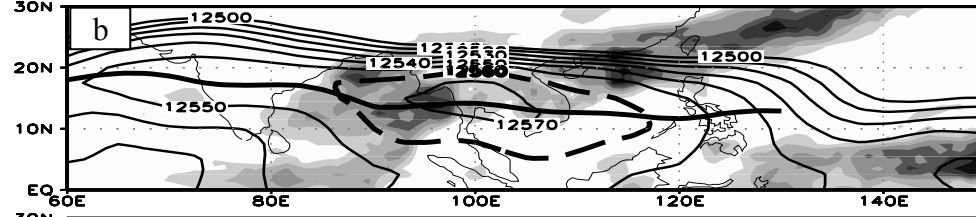
**Fig. 4 Climate-mean Pentad-isochrones indicating the evolution of the Asian summer monsoon onset, Unit: pentad**

# SCS monsoon onset and the unstable development of the SAH

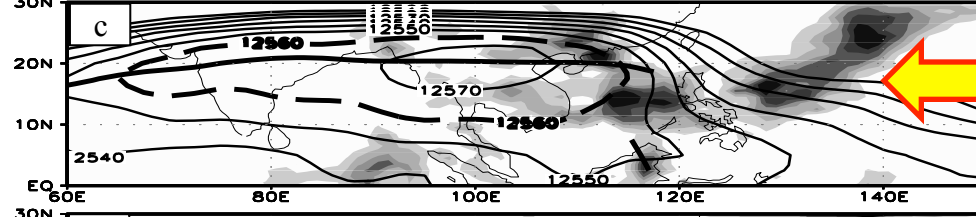
P. 27候: May11-15



P. 28候: May16-20

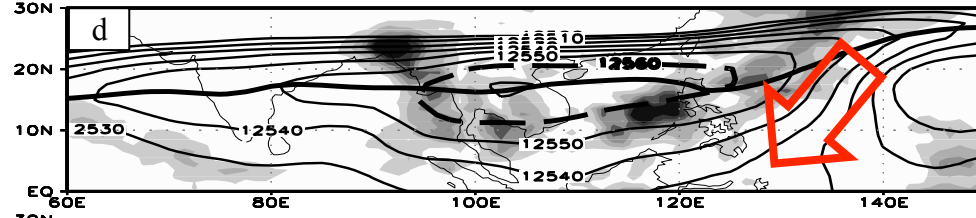


P. 29候: May21-25



SCS  
onset

P. 30候: May26-30



P. 31候: May31-Jun.4

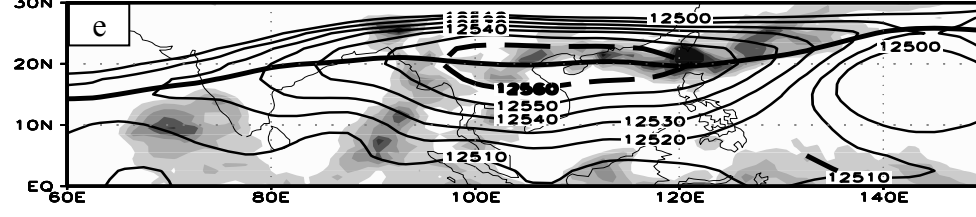


图5 1998年候平均降水 (阴影, 单位: mm/d) 和200hPa南亚高压 (单位: gpm) 的水平分布 (粗实线为副高脊线, 粗虚线为12560gpm线) (a) 27候: 5月11-15日 (b) 28候: 5月16-20日 (c) 29候: 5月21-25日 (d) 30候: 5月26-30日 (e) 31候: 5月31日-6月4日

May 27

Jun 4

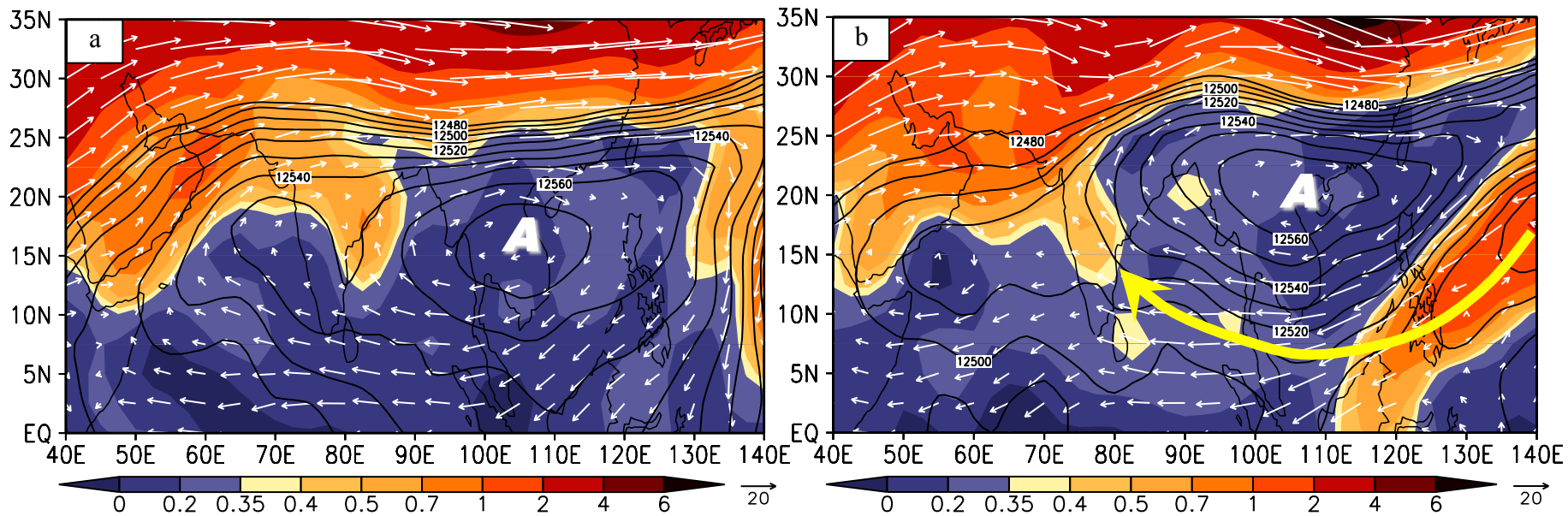


图7 355K等熵PV场（阴影，单位：PVU）、风场（单位：m/s）及200hPa高度场（单位：gpm）的水平分布：(a) 5月27日；(b) 6月4日

360K

355K

330K

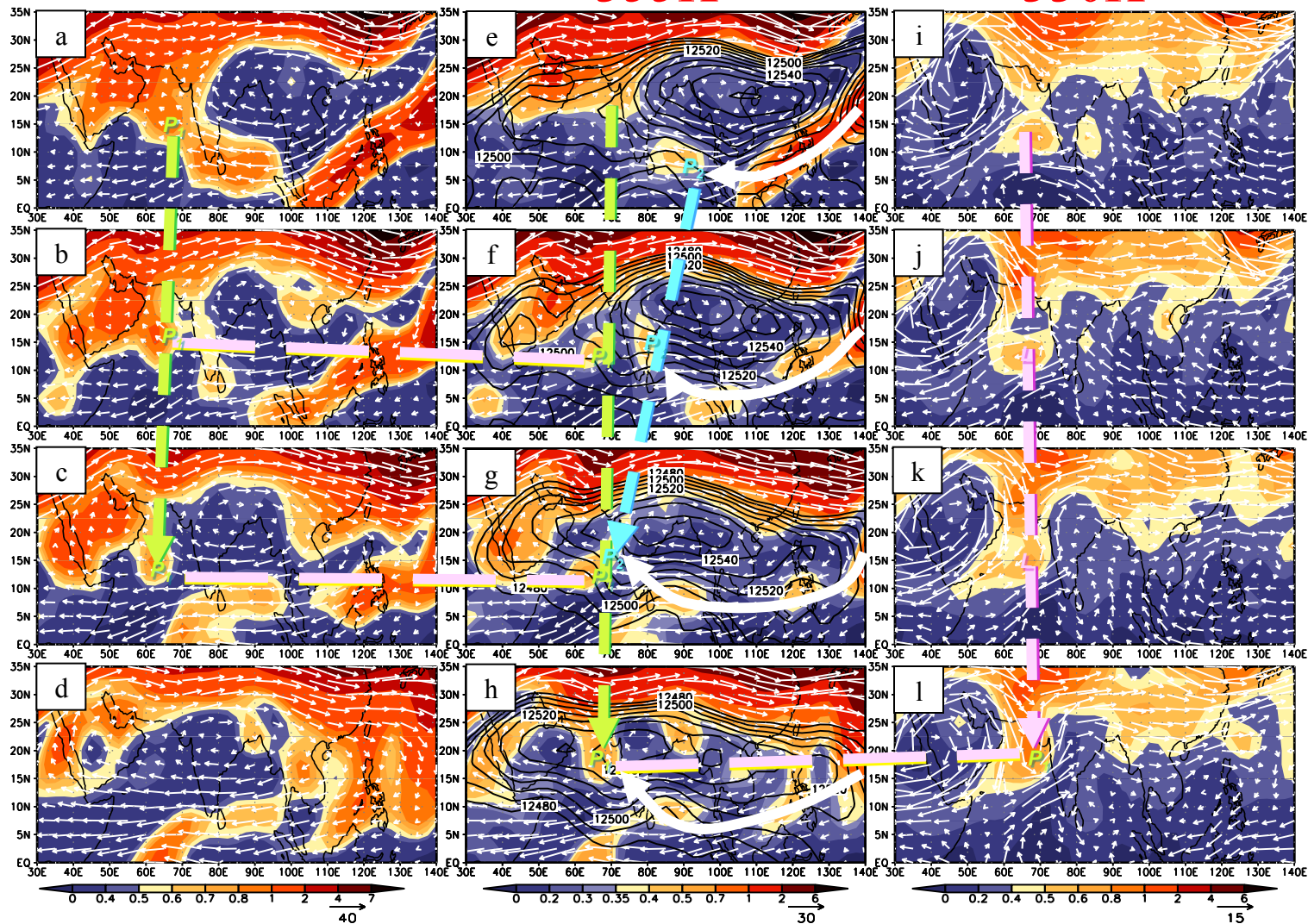
5  
□6  
□7  
□8  
□

图8 6月在360K(a-d)、355K(e-h)、和 330 K (i-l) 等熵面上PV场(阴影, 单位:PVU)、风场(单位:m/s)和200hPa高度场(实线, 单位:gpm)的水平分布。第1-4行依序分别为5-8日。垂直虚箭矢表示对流层高层涡旋系统 $P_1$ 、 $P_2$ 和对流层中层热带低压系统L的水平移动方向;水平粉红色长虚线指示低涡系统垂直向的锁相斜压发展。

Without friction:  $k=0$ , but N-S pressure gradient not uniform

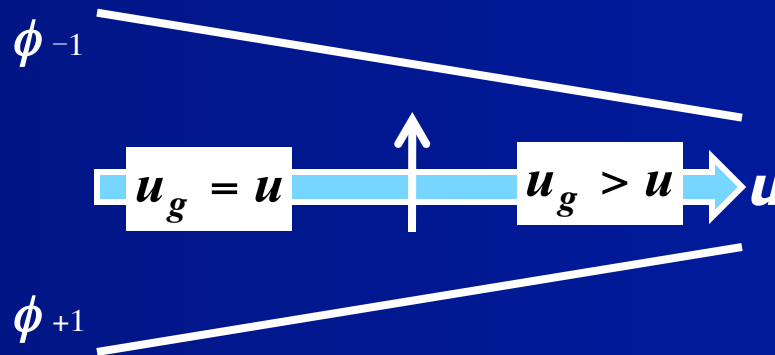
$$\frac{\partial}{\partial x} \left( \frac{\partial \phi}{\partial y} \right) \neq 0$$

$$\frac{D^2 \mathbf{v}}{Dt^2} + \lambda^2 \mathbf{v} = f \left( u \frac{\partial u_g}{\partial x} \right) \quad \lambda^2 = f \left( f - \frac{\partial u_g}{\partial y} \right)$$

$$v_1 = \frac{1}{f - \frac{\partial u_g}{\partial y}} \left( \frac{\partial u_g}{\partial t} + u \frac{\partial u_g}{\partial x} \right) \approx \frac{1}{f - \frac{\partial u_g}{\partial y}} \cdot u \frac{\partial u_g}{\partial x} = -\lambda^{-2} u \frac{\partial}{\partial x} \left( \frac{\partial \phi}{\partial y} \right)$$

Mechanism

$$\frac{Dv}{Dt} = -fu + fu_g - Kv = f(u_g - u)$$



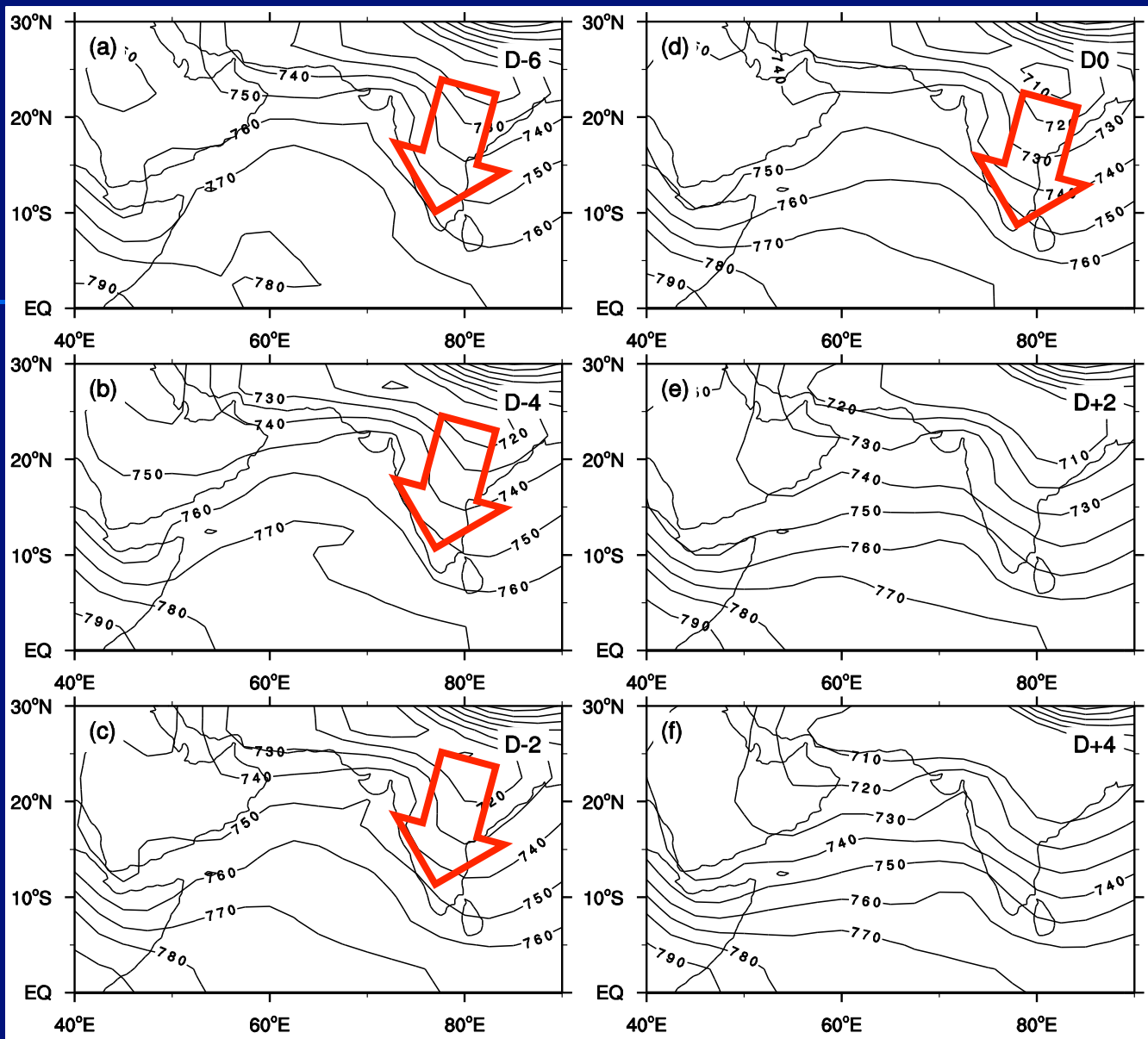
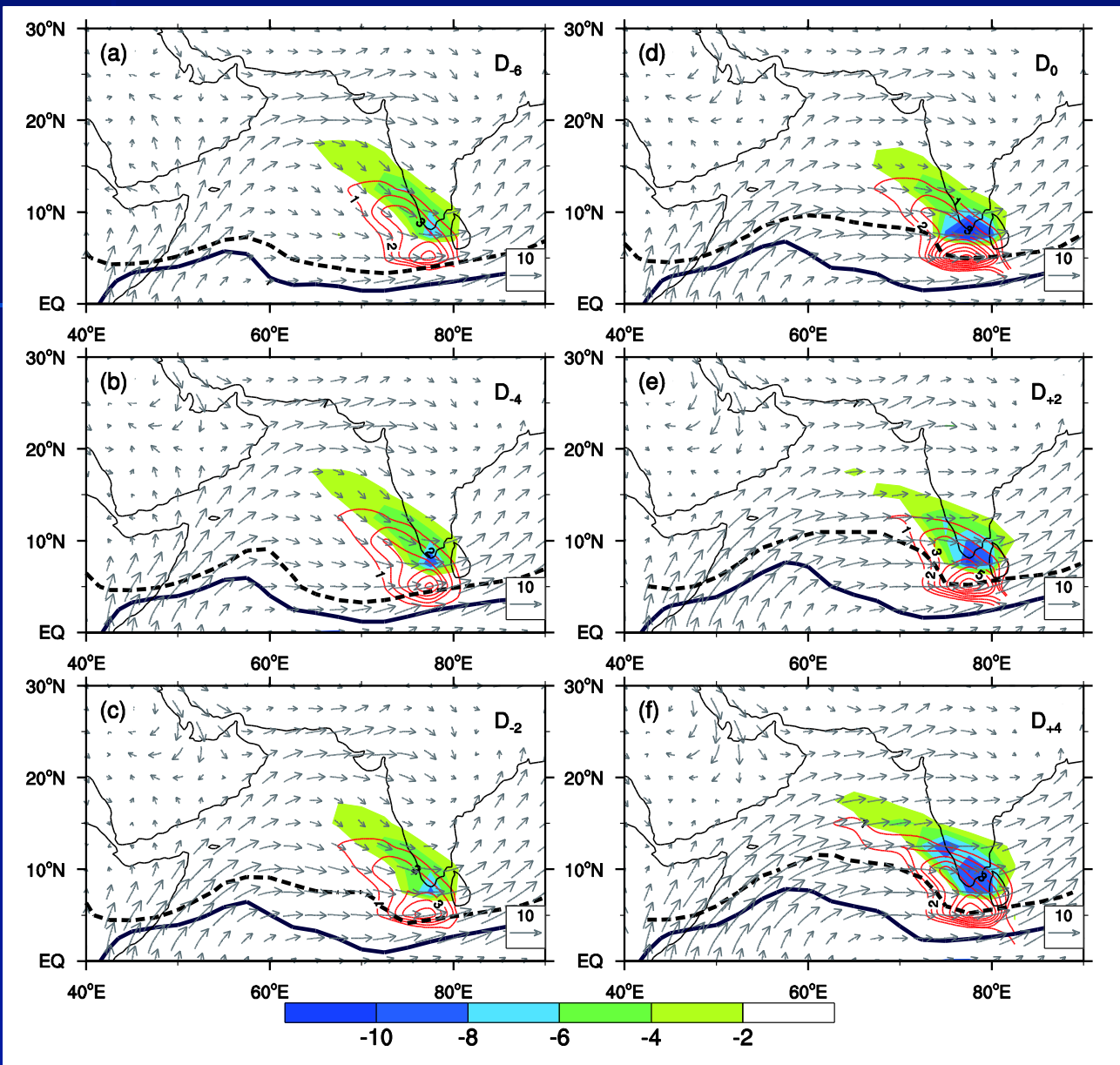
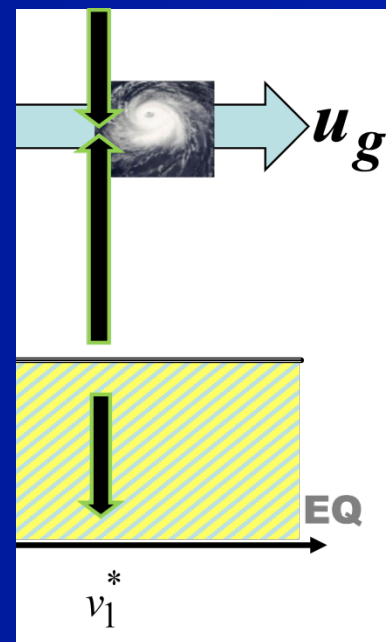


图 5 印度夏季风爆发过程中925hPa 等压面上位势高度(单位: dgpm)的演变特征。  
 Evolution of geopotential height at 925hPa during the ISM onset (interval is 10 gpm)



$$v_1^* \approx -\lambda^2 \cdot u \frac{\partial}{\partial x} \left( \frac{\partial \varphi}{\partial y} \right)$$



强迫作用

图6 矢量: 925hPa风场 (m/s); ; 等值线: 925hPa  $v_1^*$  (m/s); 阴影:  $d(v_1^*)/dy$  ( $10^{-6} s^{-1}$ ); 粗实线: 绝对涡度零线; 粗虚线: 地转西风急流轴



# Outline



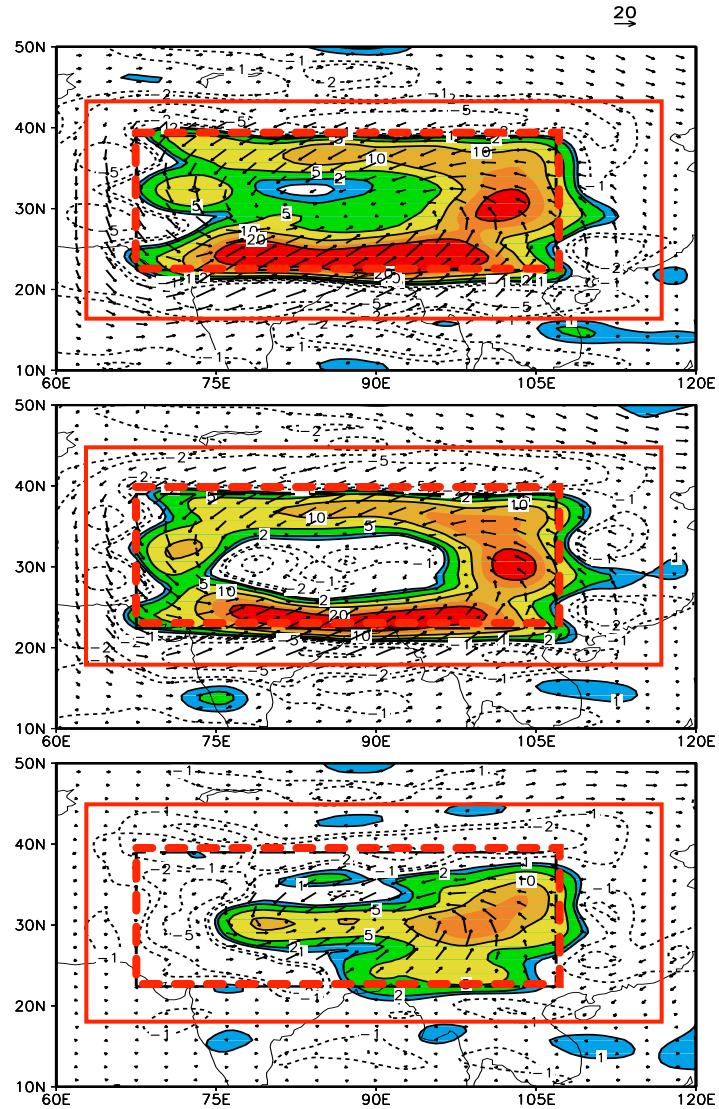
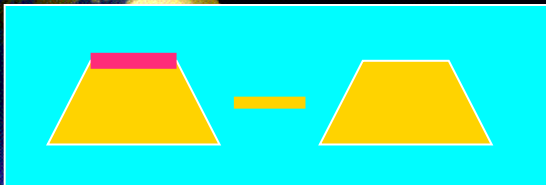
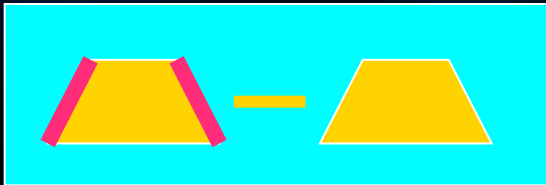
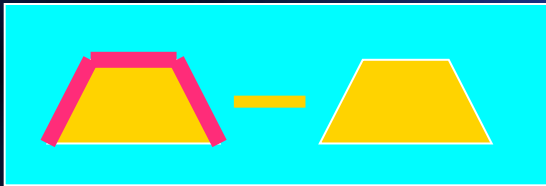
- 1 **Introduction- general circulation**
- 2 **Dynamics of ASM onset**
- 3 **Evolution of the ASM onset**
- 4 **Maintenance of the ASM**
- 5 **Variability of the ASM**
- 6 **Conclusion**



# **Tibetan Plateau- Sensible Heat driven Air-Pump (TP-SHAP)**

**Heating on the mountain slope surface is crucial for uplifting water vapor from the surface to free atmosphere to form monsoon cloud and precipitation!**

# Aqua-Planet Experiment (APE): Diff of $V$ and $w$ at $s=0.991$

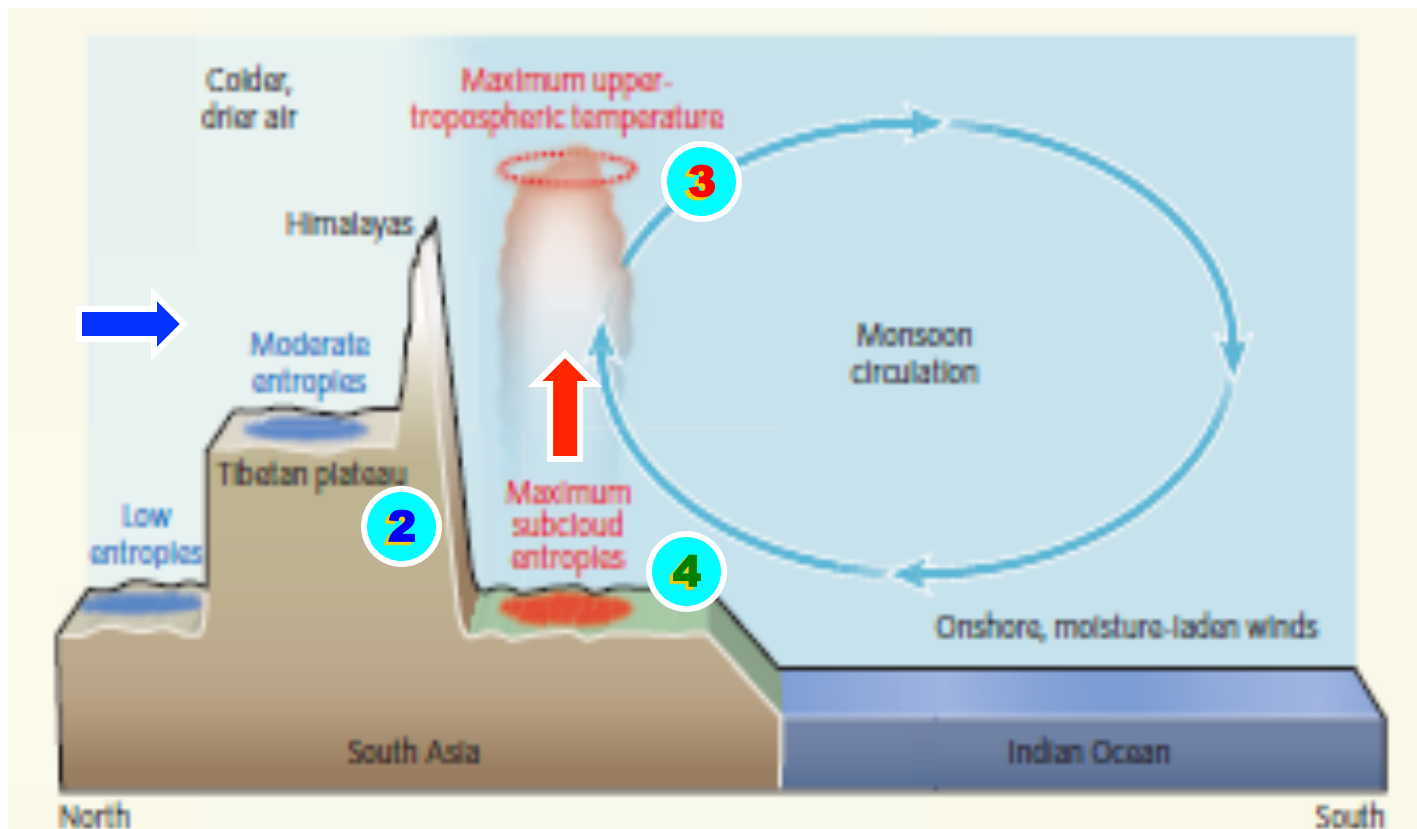




# Mechanical forcing hypothesis: blocking impact of the TP :

1. Shield the India from cold and dry advection

2. High surface energy and UTTM are coupled by monsoon convection



# Does there exist the TP Shielding of India from cold and dry advection?

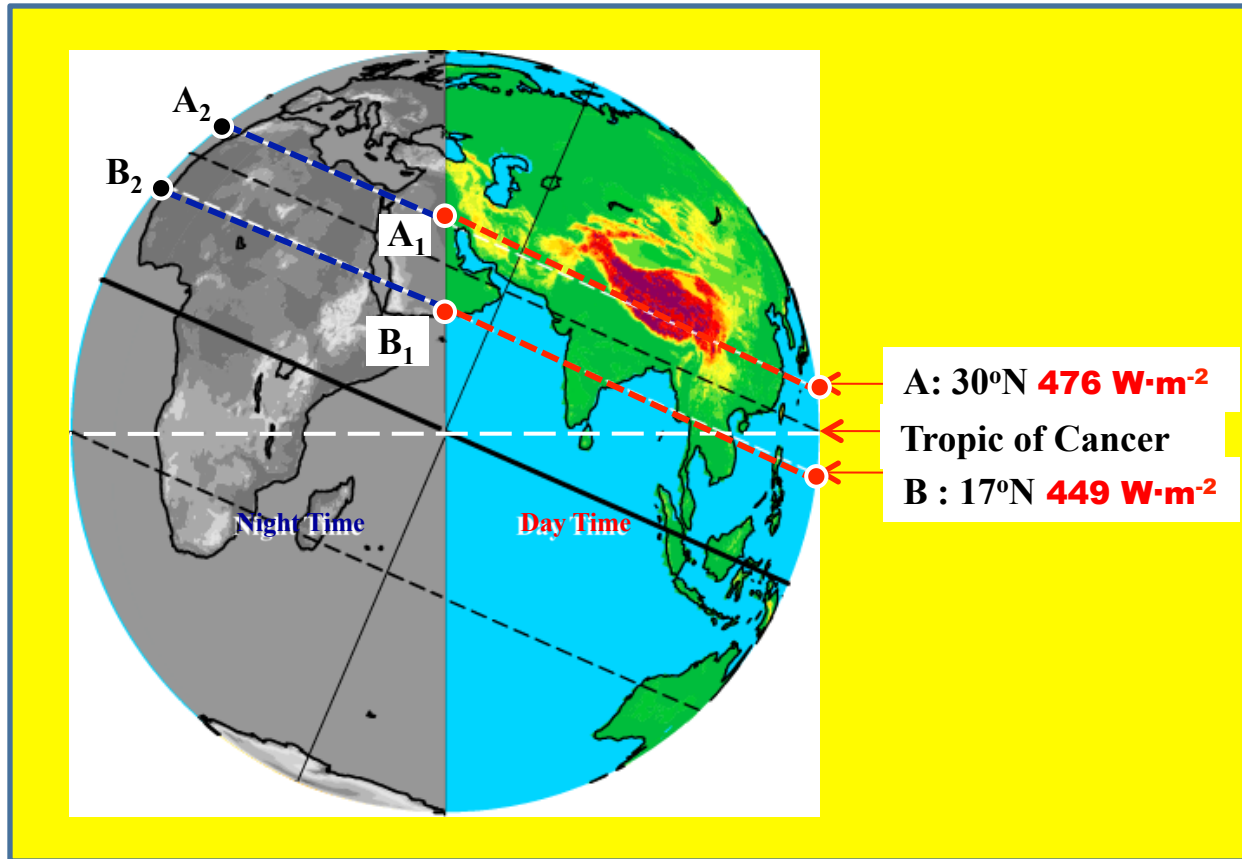


**Fig. 1 (a)** At the summer solstice, the solar zenith angle at noon is zero at the Tropic of Cancer ( $\phi = 23.5^\circ\text{N}$ ). At the top of the atmosphere (TOA), the intensity of solar radiation (SR) at latitude A ( $30^\circ\text{N}$ ) in the subtropics is the same as that at latitude B ( $17^\circ\text{N}$ ) in the tropics. **However, the length of day (LOD) at A ( $AA_1/AA_2$ ) is about one hour longer than the LOD at B ( $BB_1/BB_2$ ).** Thus the daily solar radiation (DSR) at  $30^\circ\text{N}$  is more than that at  $17^\circ\text{N}$

# Summer months Daily solar radiation (DSR) in $Wm^{-2}$

CERES climate JJA mean insolation

	17°N	30°N
Jun	444	474
Jul	443	466
AUG	438	436
JJA	442	458

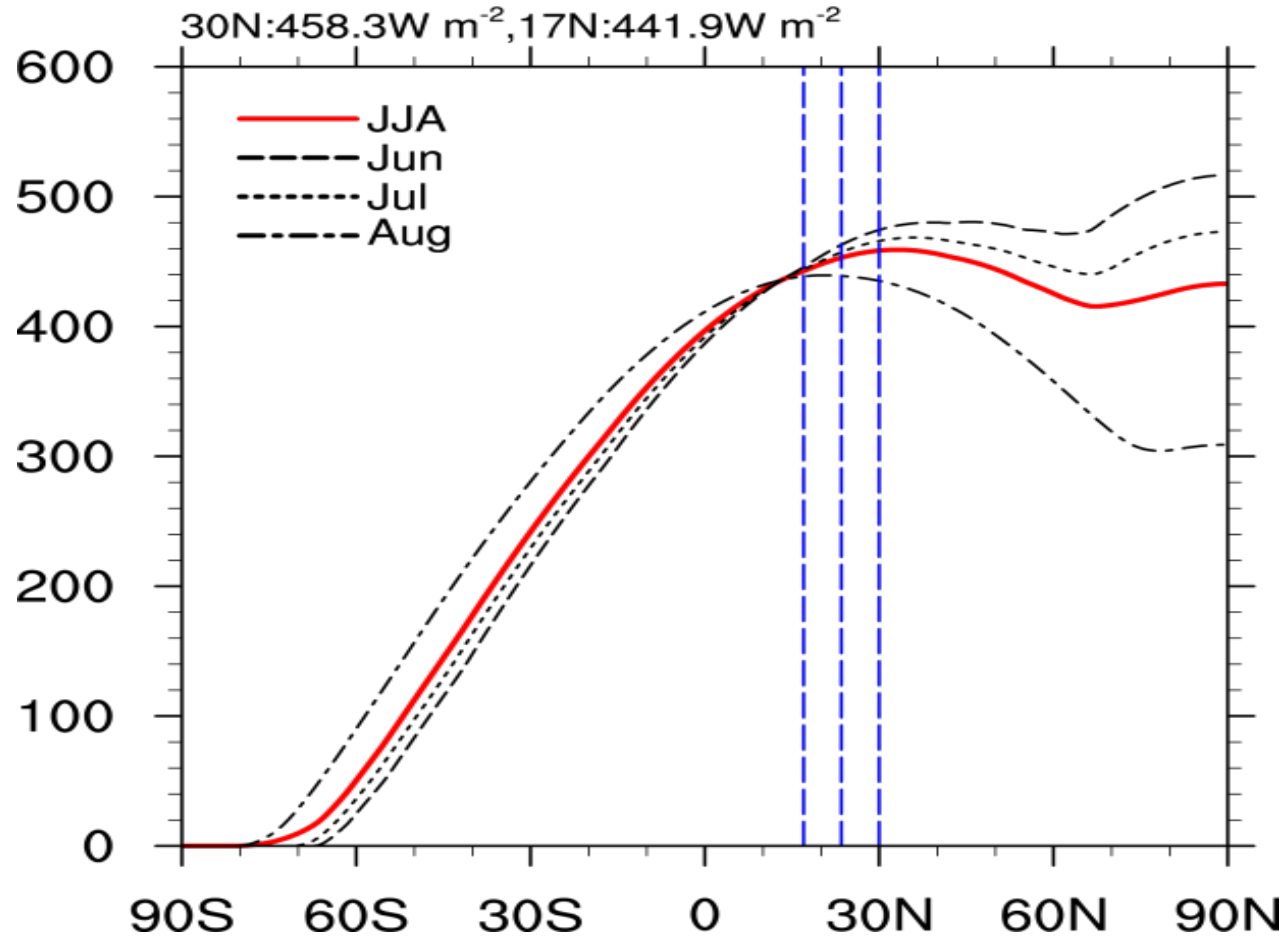


**Fig. 1 (b)** The climate mean latitude distributions of DSR in summer months are calculated from the CERES reanalysis

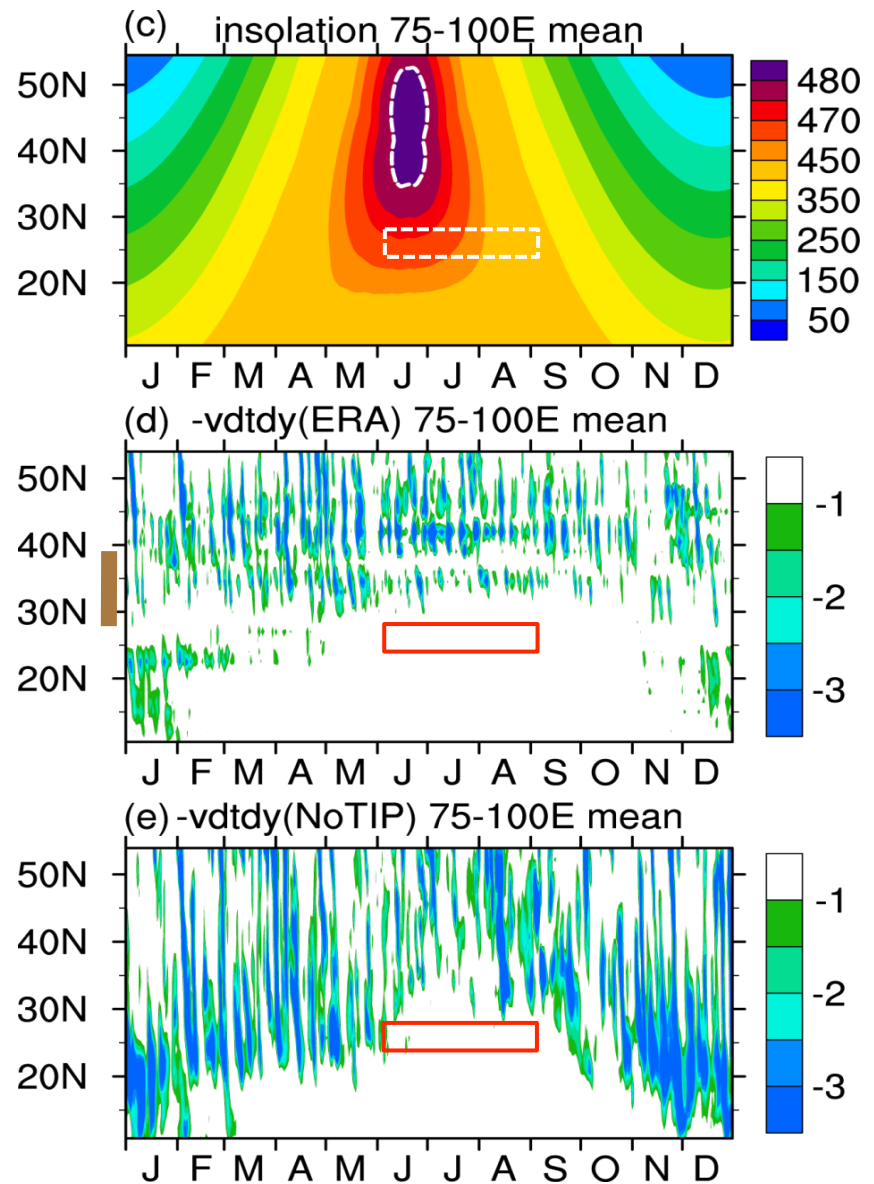
**Unpublished**

the daily evolutions in 2001 across the longitude domain 75–100°E of

(c) DSR ( $\text{W m}^{-2}$ ), with the white dashed curve denoting the  $480 \text{ W m}^{-2}$  contour,

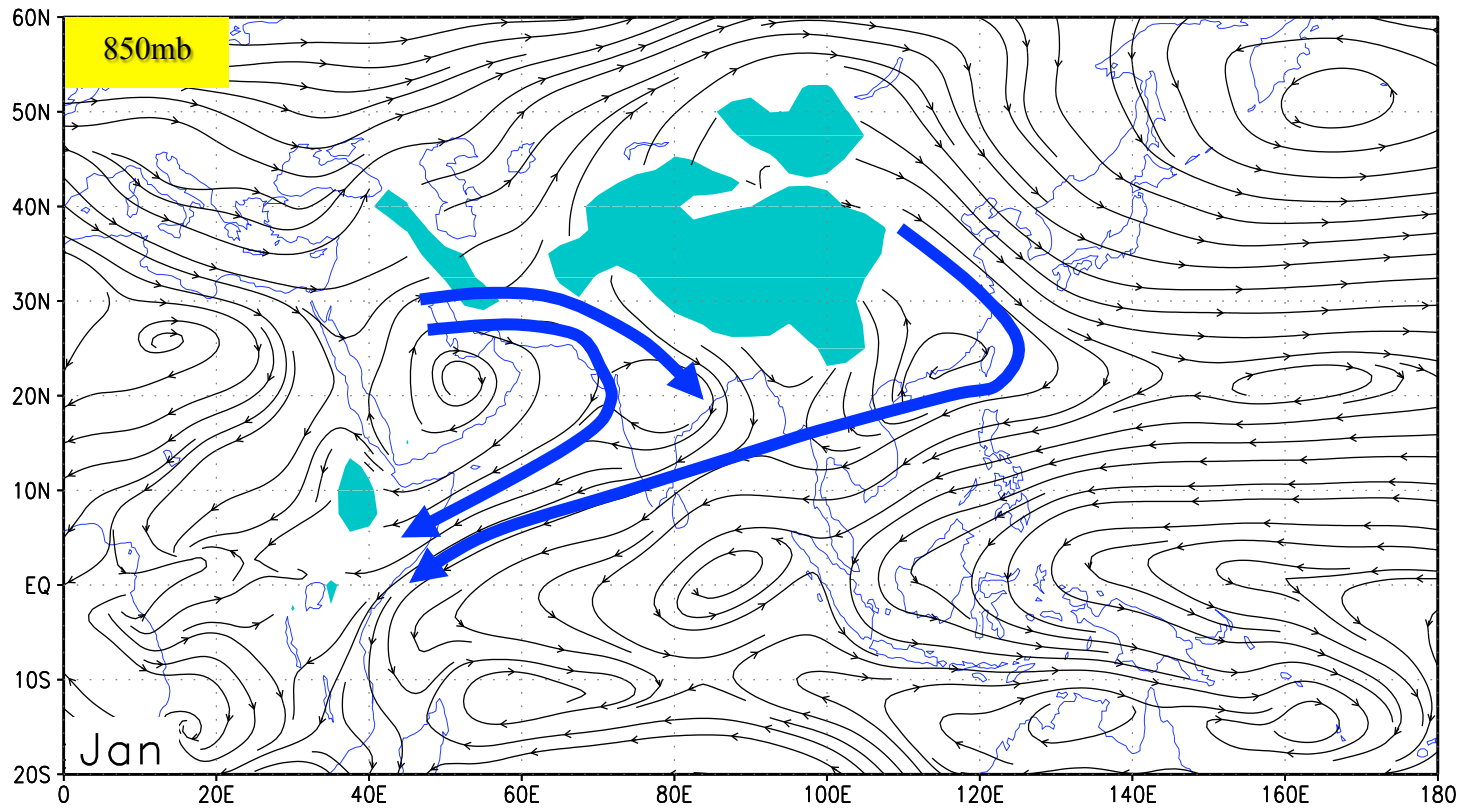
(d) the cold temperature advection ( $v < 0$ ) at the surface ( $\sigma = 0.99$ ) from ERA-interim and

(e) from the NoTIP experiment, which is driven with the SST in 2001 and with the removal of the mountain range TIP. The square in (c-e) indicates the South Asian summer monsoon region between  $24^\circ\text{N}$  and  $28^\circ\text{N}$  and during June to August.



**Summer: Shielding not need!**

**Winter: TP cannot block cold advection!**



**Jan mean streamline at 850 hPa**

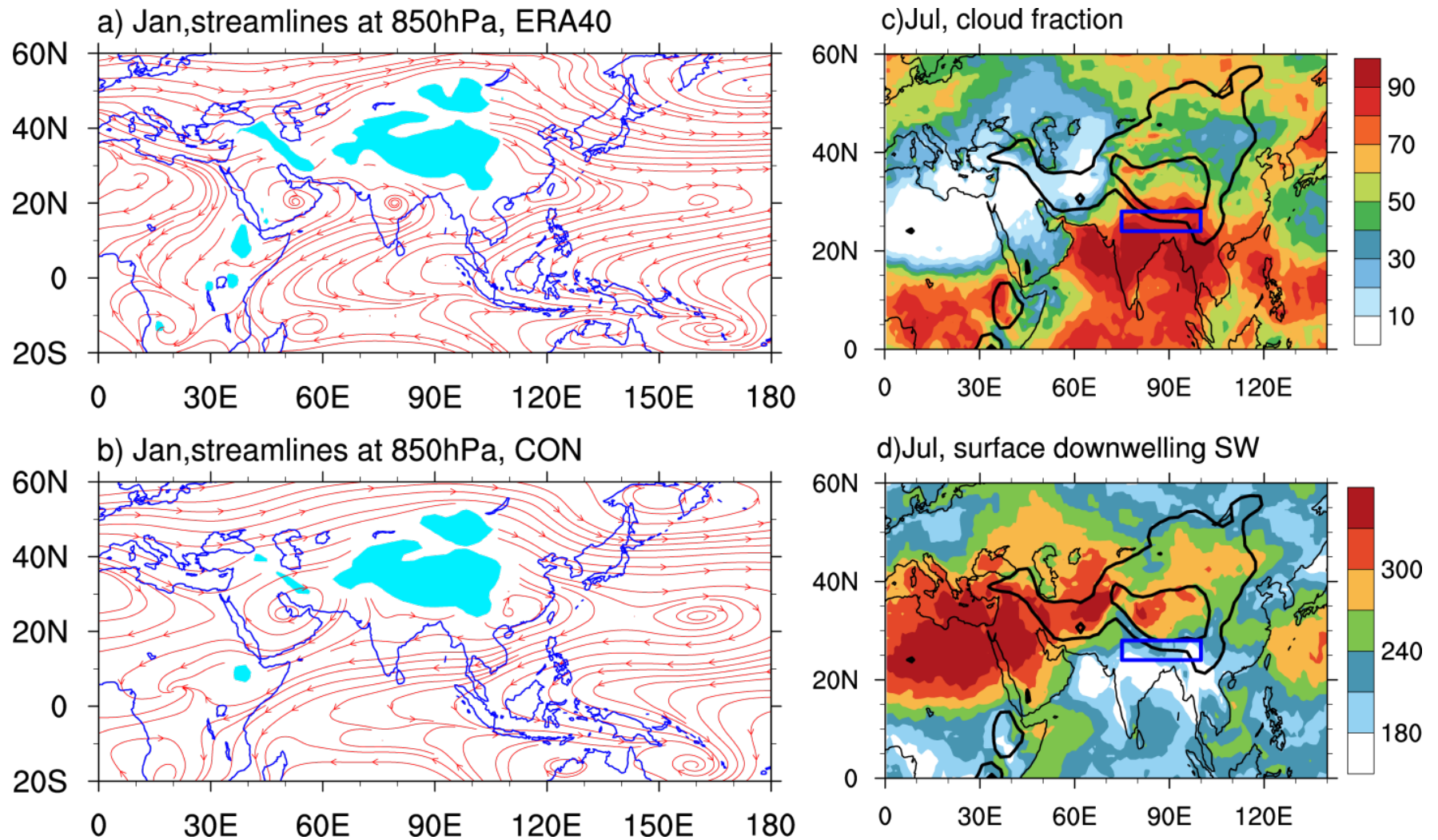


Fig. 2 Climatological mean January streamfield at 850 hPa produced from (a) ERA40 and (b) CON Experiment; and the monthly mean of July, 2001 of (c) cloud fraction in percentage and (d) downward shortwave radiation at the surface ( $\text{Wm}^{-2}$ ) produced from CERES.

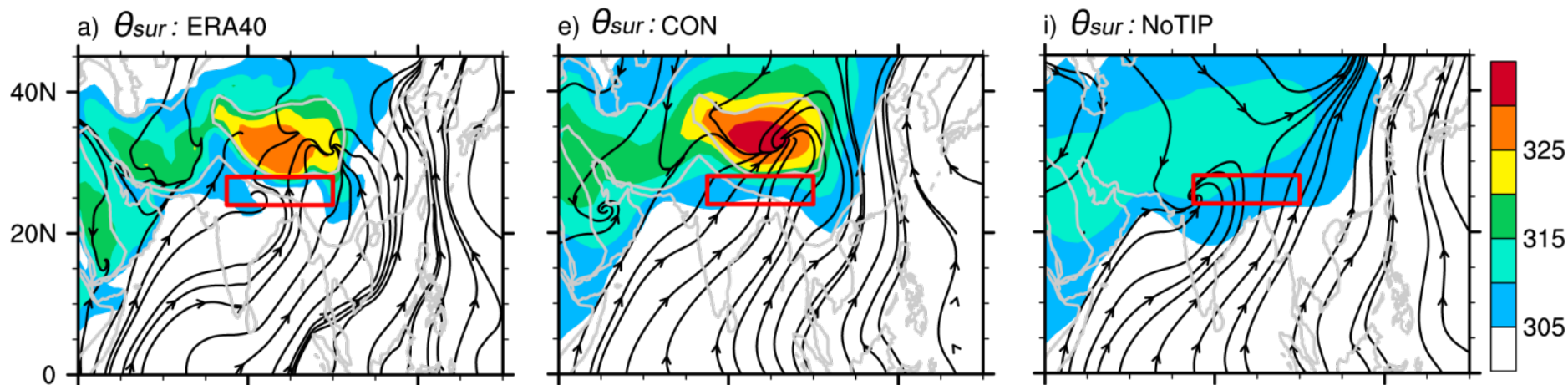


Fig. 3 JJA-means of  $\theta_{sur}$  (K) and streamfield (top row),  $q_{sur}$  ( $\text{g kg}^{-1}$ ) and 850-hPa water-vapor-fluxes (vector,  $\text{kg m}^{-1}\text{s}^{-1}$ ) (second row), and  $\theta_{env}$  (K) and precipitation ( $\text{mm d}^{-1}$ , contours) (third row); and of profiles of environmental temperature (K, red) and rising air-parcel temperature (K, blue) averaged over the four pale-blue-grid-points over North India shown in the third row (bottom row), calculated from ERA-40 (a-d), CON (e-h) and NoTIP (i-l).

## **Conclusion**

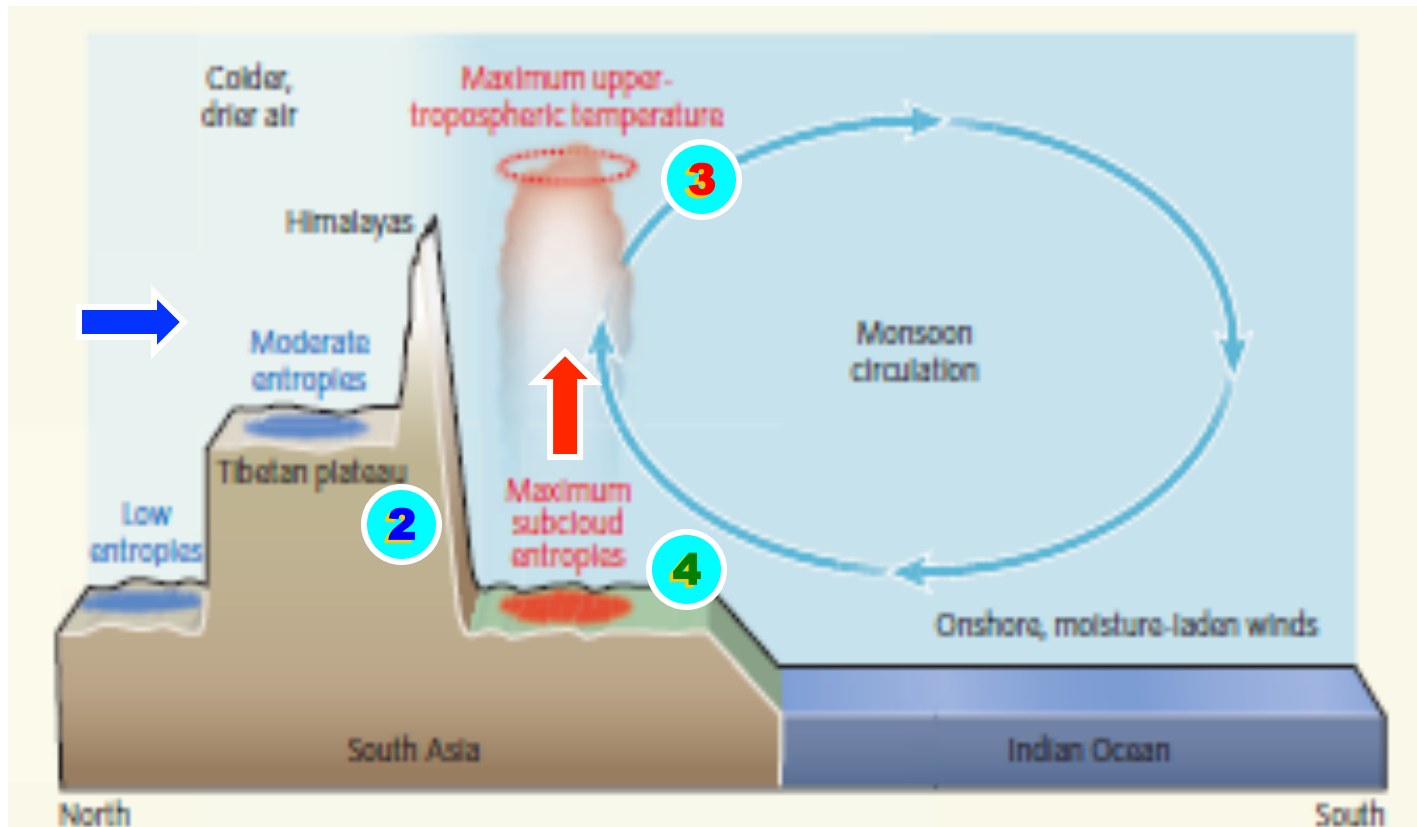
**In Summer: Shielding/blocking of the TIP is not need since there is no cold advection from higher latitudes!**

**In Winter: TIP cannot block cold advection because the cold northwesterly or northeasterly can move around the TIP and intrude India!**

# Mechanical forcing hypothesis: blocking impact of the TP :

1. Shield the India from cold and dry advection

2. High surface energy and UTTM are coupled by monsoon convection



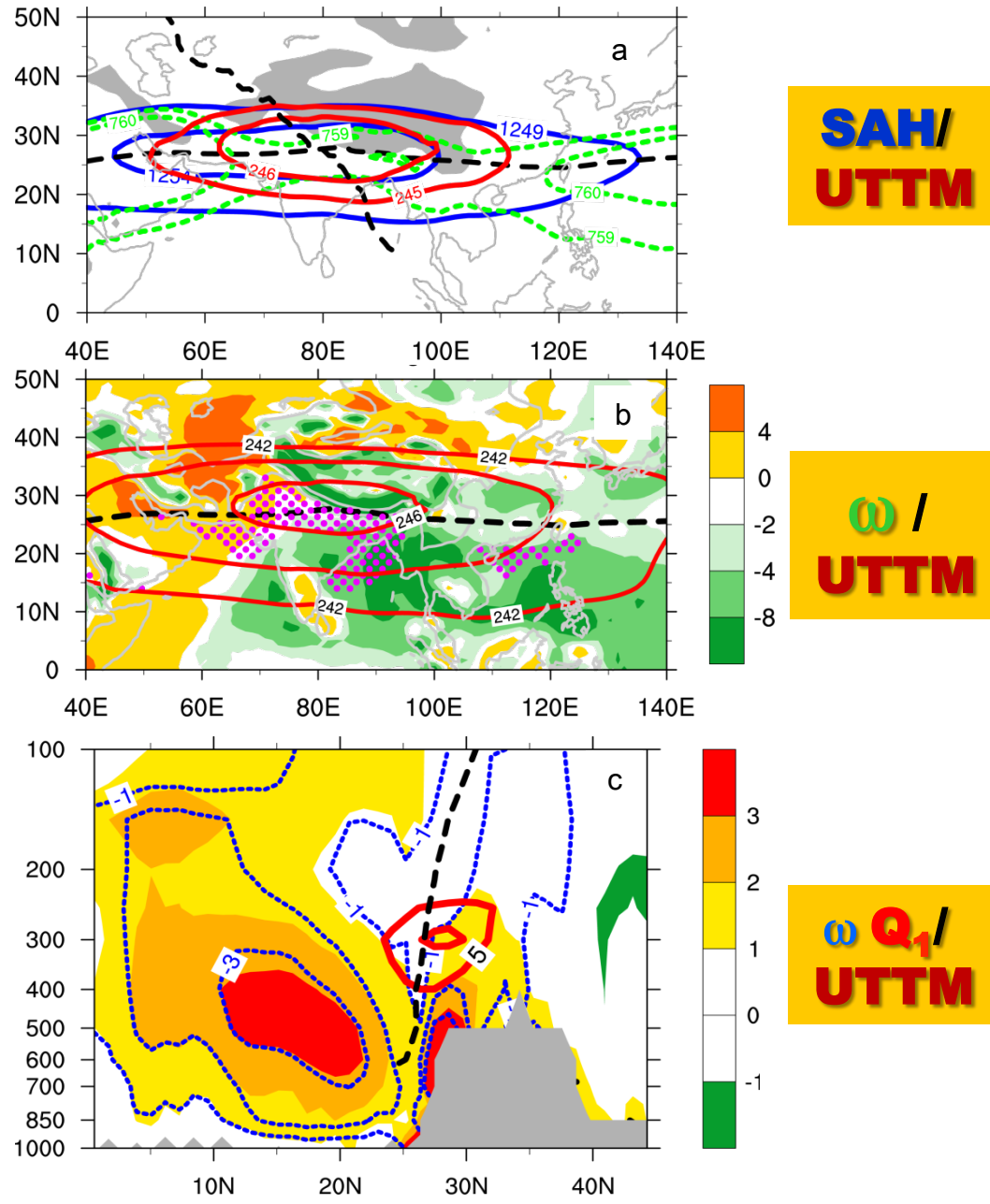
# Dynamic forcing and W

## Vertical coupling

$$W \propto \frac{\partial}{\partial z} [-\vec{V} \cdot \nabla (f + \zeta)]$$



**Fig. 1 The JJA mean distributions** of (a) geopotential height (unit: dgpm) at 200 hPa (blue solid) and 400 hPa (green dashed), 200–400 hPa mass-weighted mean temperature (red solid, unit: K), and zero zonal and meridional wind contours at 200 hPa (black dashed); (b) 500-hPa vertical velocity (shading, unit: hPa s<sup>-1</sup>), 200–400 hPa mass-weighted mean temperature (red contour, unit: K), surface entropy > 356 K (purple stippled; unit: K), and contour of u=0 at 300 hPa (black dashed); and (c) 60°–100°E mean diabatic heating  $Q_1/C_p$  (shading, unit: K d<sup>-1</sup>) and adiabatic heating (blue dotted contour, unit: K d<sup>-1</sup>), ridgeline (black dashed line), and temperature deviation from the (40°–160°E, 0°–50°N) area mean (red contour, interval: 5°C).



**In response to an axisymmetric diabatic heating, the meridional circulation adopts two distinct regimes:**

- **the thermal equilibrium (TE) regime in extra-tropics**
- **the angular momentum conservation (AMC) regime in the tropics.**



$$W \propto \frac{\partial}{\partial z} [-\vec{V} \cdot \nabla (f + \zeta)]$$

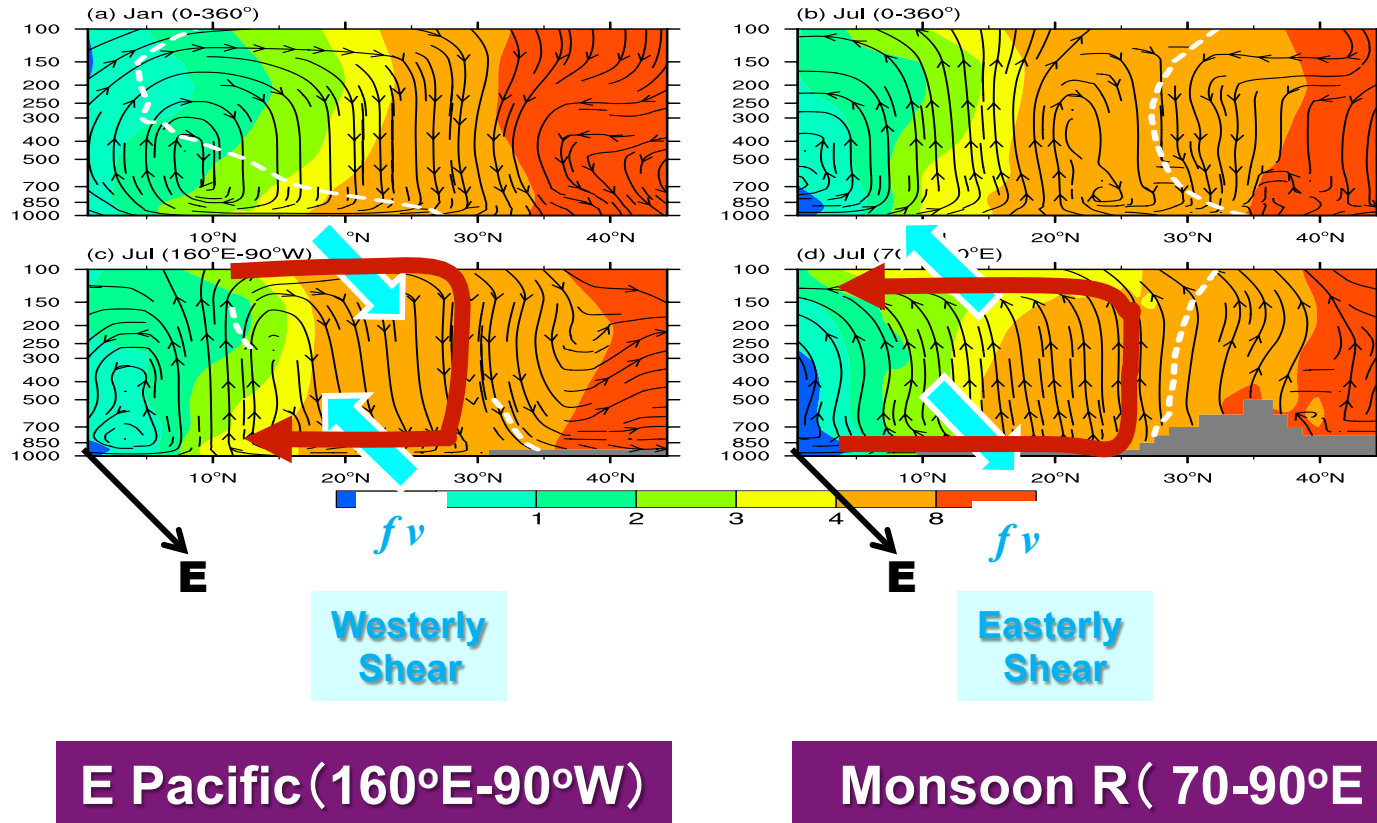


图4. 平均经圈环流(流线)、绝对涡度( $10^{-5} \text{ s}^{-1}$ , 彩色)和纬向风零线(白断线)的气压-纬度分布的剖面图:(a)1月纬向平均;(b)7月纬向平均;(c)7月东太平洋(160°E-90°W)平均, (d)7月亚洲季风区(70-90°E)平均<sup>63</sup>

AMC

TE

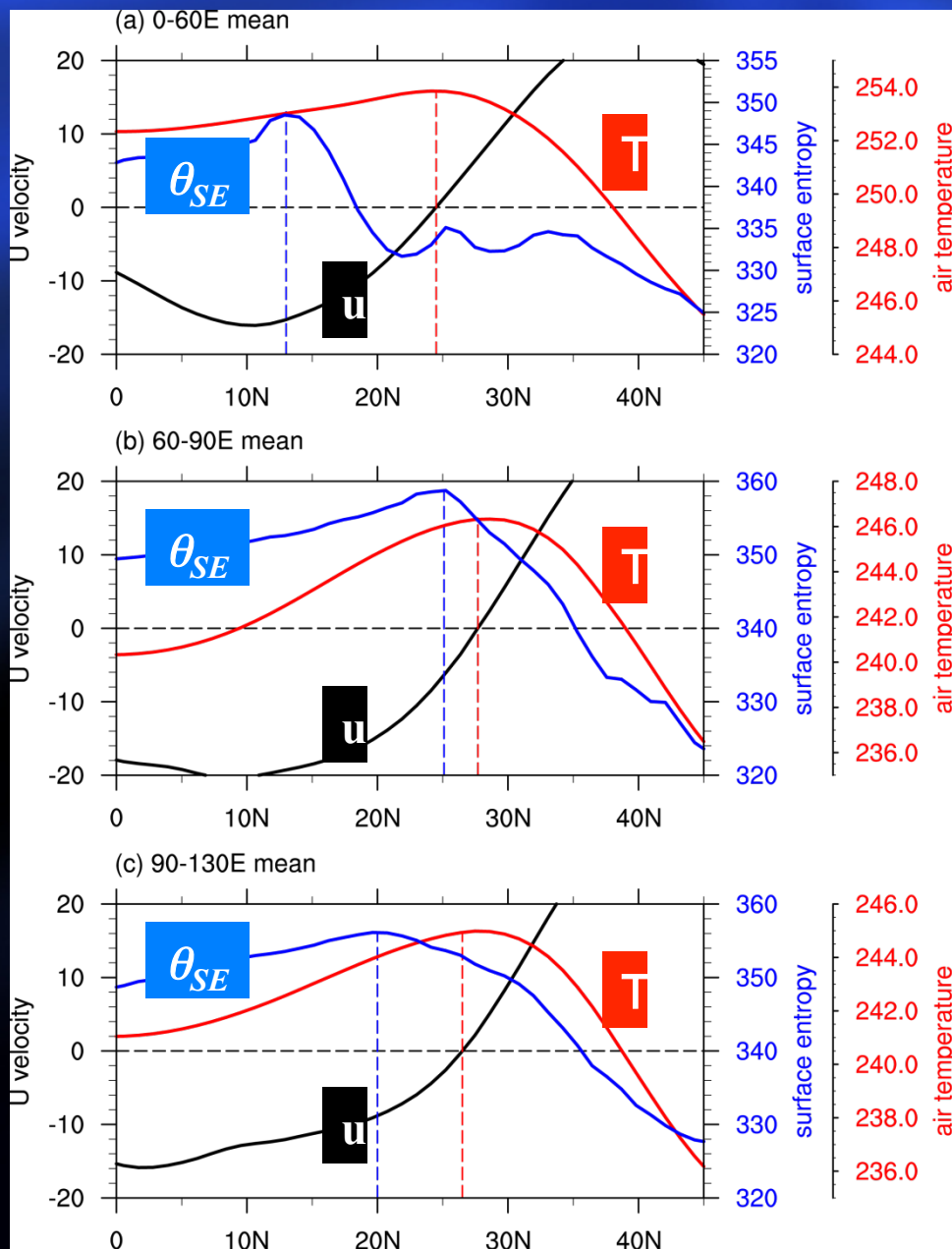
$$\frac{\partial u}{\partial \ln p} = \frac{R}{f} \left( \frac{\partial T}{\partial y} \right)$$

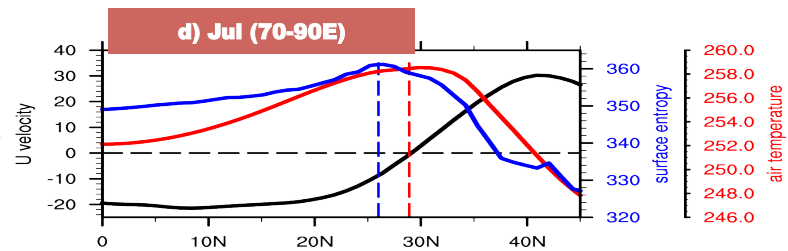
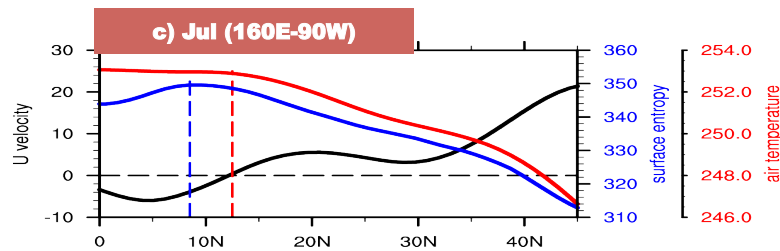
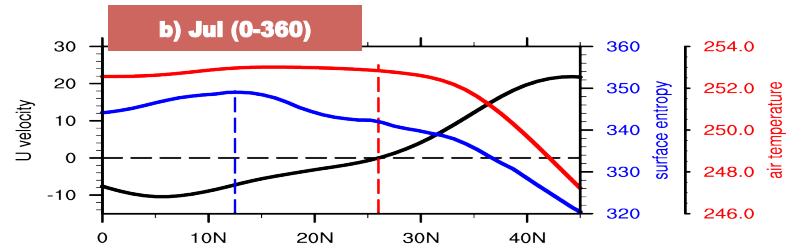
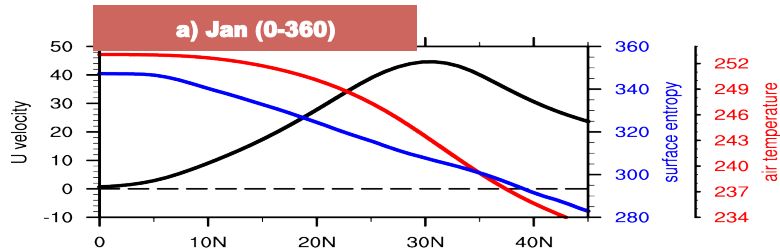
**Monsoon AMC regime:  
Vertical Easterly shear  
T increases with latitude!** →

Fig. 2 ERA40 July- mean profiles of surface  $\theta_{SE}$  (K, blue), 200-400hPa mass

**Latitude location of the SAH and UTMM**

°E mean, and (c) 90-130 °E mean. The black dashed line indicates  $u=0$ .





Westerly Shear

$$\frac{\partial u}{\partial \ln p} = \frac{R}{f} \left( \frac{\partial T}{\partial y} \right) < 0$$

E Pacific (160°E-90°W)

Easterly Shear

$$\frac{\partial u}{\partial \ln p} = \frac{R}{f} \left( \frac{\partial T}{\partial y} \right) > 0$$

Monsoon R (70-90°E)

(a) **Latitude location of the SAH and UTTM**

分布：  
平均

$$\beta v \approx (f + \zeta) \theta_z^{-1} (\partial Q / \partial z) \quad \theta_z \neq 0 \quad \vec{V} \cdot \nabla z \rightarrow 0 \quad z = -$$

$$\left\{ \begin{array}{l} \frac{\partial^2 T}{\partial x^2} \approx \gamma \frac{\partial}{\partial x} \left( \frac{\partial^2 Q}{\partial z^2} \right) \\ \gamma = f(f + \zeta) H / (R \beta \theta_z), \quad \theta_z \neq 0 \end{array} \right. \quad H \cdot \ln p,$$

## Longitude location of the SAH and UTTM

$$\left\{ \begin{array}{l} Q = Q(x) \cos\left(\frac{\pi z}{H_Q}\right) \\ T = T(x) \cos\left(\frac{\pi z}{H_Q}\right) \\ T(x) = T_0 \cos\left(\frac{\pi x}{L}\right) \end{array} \right.$$

$$\left\{ \begin{array}{l} T(x) \approx \gamma L^2 H_Q^{-2} \partial Q(x) / \partial x = \lambda \partial Q(x) / \partial x. \quad \vec{V} \cdot \nabla \zeta \rightarrow 0; \end{array} \right.$$

$$\left\{ \begin{array}{l} \lambda = \gamma L^2 H_Q^{-2} \end{array} \right.$$

$$\frac{\partial v}{\partial \ln p} = -\frac{R}{f} \left( \frac{\partial T}{\partial x} \right)$$

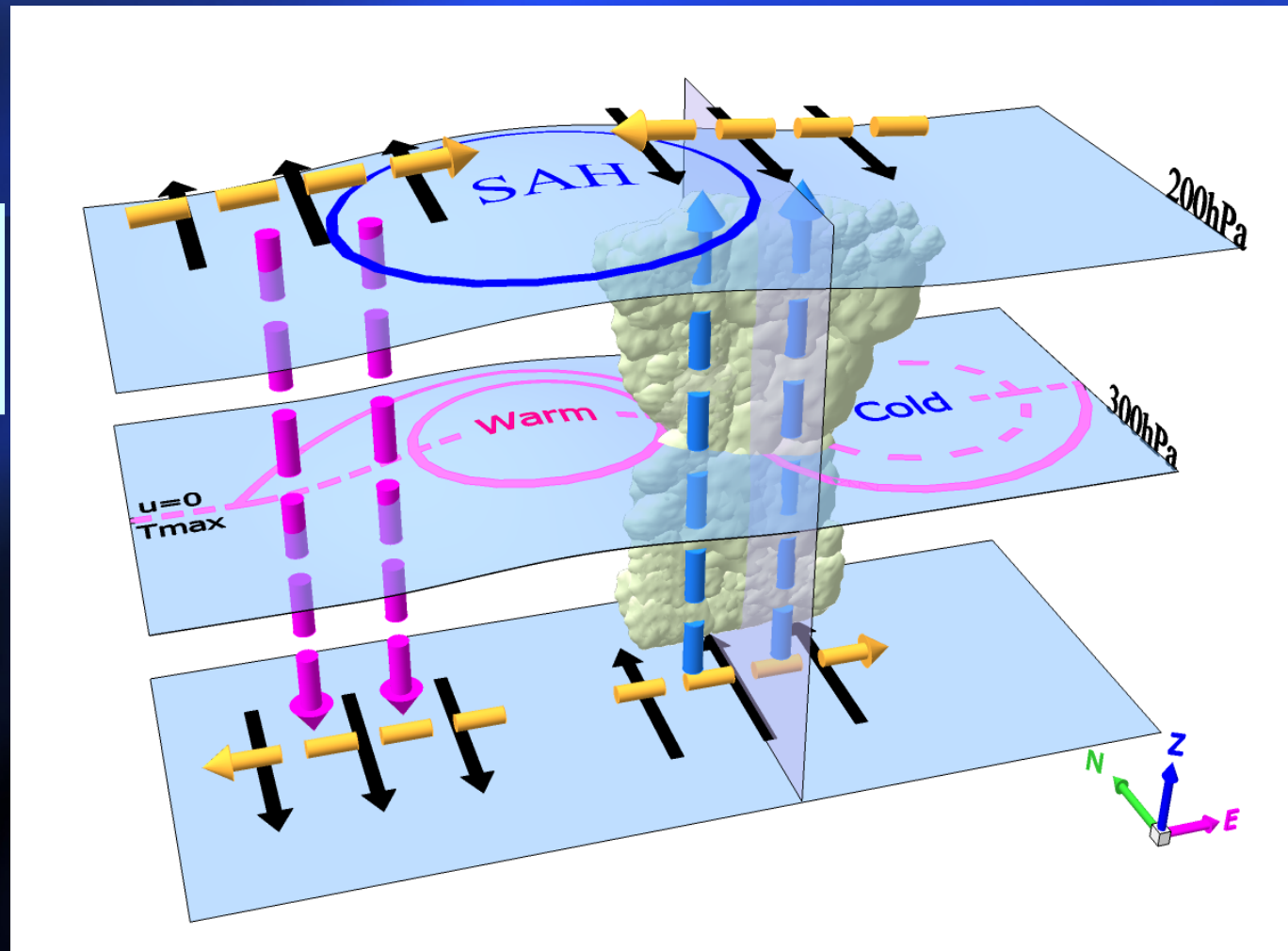


**Fig. 5** Schematic diagram of the  $T-Q_z$  mechanism contributing to the longitude location of the upper-troposphere temperature maximum (UTTM): Strong monsoon convective latent heating along the subtropics (blue upward arrow) results in the local development of a vertical northerly shear (black arrow) and induces an eastward decreasing temperature gradient. The induced Coriolis force ( $fv$ , orange arrow) is in geostrophic balance with the pressure gradient force. The heating and longwave radiation cooling (red downward arrow) in the upper troposphere, contributes to the occurrence of the UTTM and SAH on the eastern end of the cooling. Refer to text for details.

## Longitude location of the SAH and UTTM

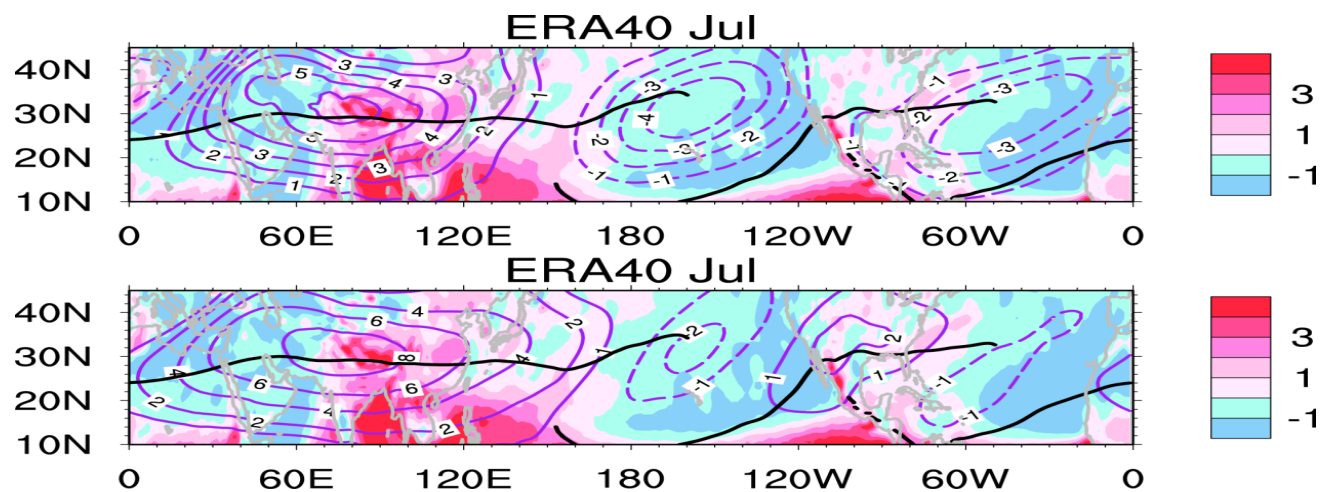
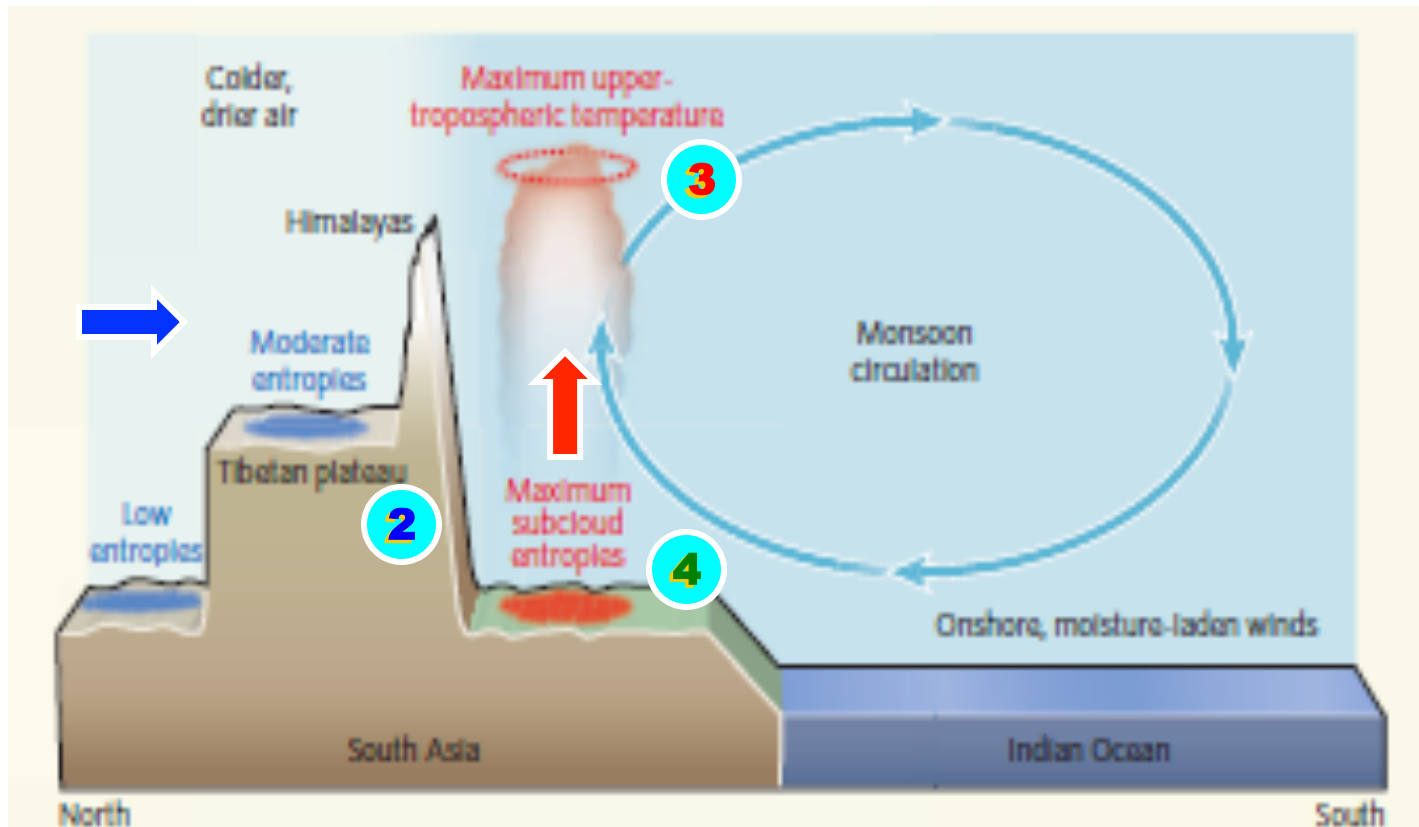


图2. 1979-1989年7月平均200-400hPa高度上的非绝热加热分布(阴影,  $Kd^{-1}$ ), 以及温度对纬向平均的偏差(a)及对(180-360°)平均的偏差(b)的分布(兰线, K)。粗实线为副高轴线(Wu et al., 2015)

# Mechanical forcing hypothesis: blocking impact of the TP :

1. Shield the India from cold and dry advection

2. High surface energy and UTTM are coupled by monsoon convection



Boos and Kuang, 2010, Nature  
Cane, 2010, Nature

**Table.** The AGCM SAMIL is used here for all the experiments. Its climate mean is termed CON. The topography is modified in NoTIP by removing the Tibetan and Iranian Plateau (TIP) if the local altitude is above 500m. The no-sensible-heating runs are performed by preventing the atmosphere from surface heating over the TIP if the local altitude is above 500m. In the dry experiments, CON\_dry and TIP\_NS\_dry, moist atmospheric processes are excluded by setting the atmospheric water vapor to zero globally.

<b>Experiments</b>	<b>TIP Topography</b>	<b>TIP Sensible heating</b>	<b>Moist process</b>
<b>CON</b>	<b>Yes</b>	<b>Yes</b>	<b>Yes</b>
<b>NoTIP</b>	<b>No</b>	<b>Yes</b>	<b>Yes</b>
<b>TIP_NS</b>	<b>Yes</b>	<b>No</b>	<b>Yes</b>
<b>CON_dry</b>	<b>Yes</b>	<b>Yes</b>	<b>No</b>
<b>TIP_NS_dry</b>	<b>Yes</b>	<b>No</b>	<b>No</b>

## Definition:

$$\theta_e = \theta \exp\left(\frac{L q}{C_p T}\right)$$

## Relative change:

$$\frac{\Delta\theta_e}{\theta_e} = \frac{L}{C_p} \frac{\Delta q_{sur}}{T_{sur}} + \frac{\Delta\theta_{sur}}{\theta_{sur}}$$

$$\left|\frac{\Delta\theta_e}{\theta_e}\right| = 2.5 \times 10^3 \left|\frac{\Delta q_{sur}}{T_{sur}}\right| + \left|\frac{\Delta\theta_{sur}}{\theta_{sur}}\right|$$

**(e)**

**(f):** moisture

**(g):** temperature

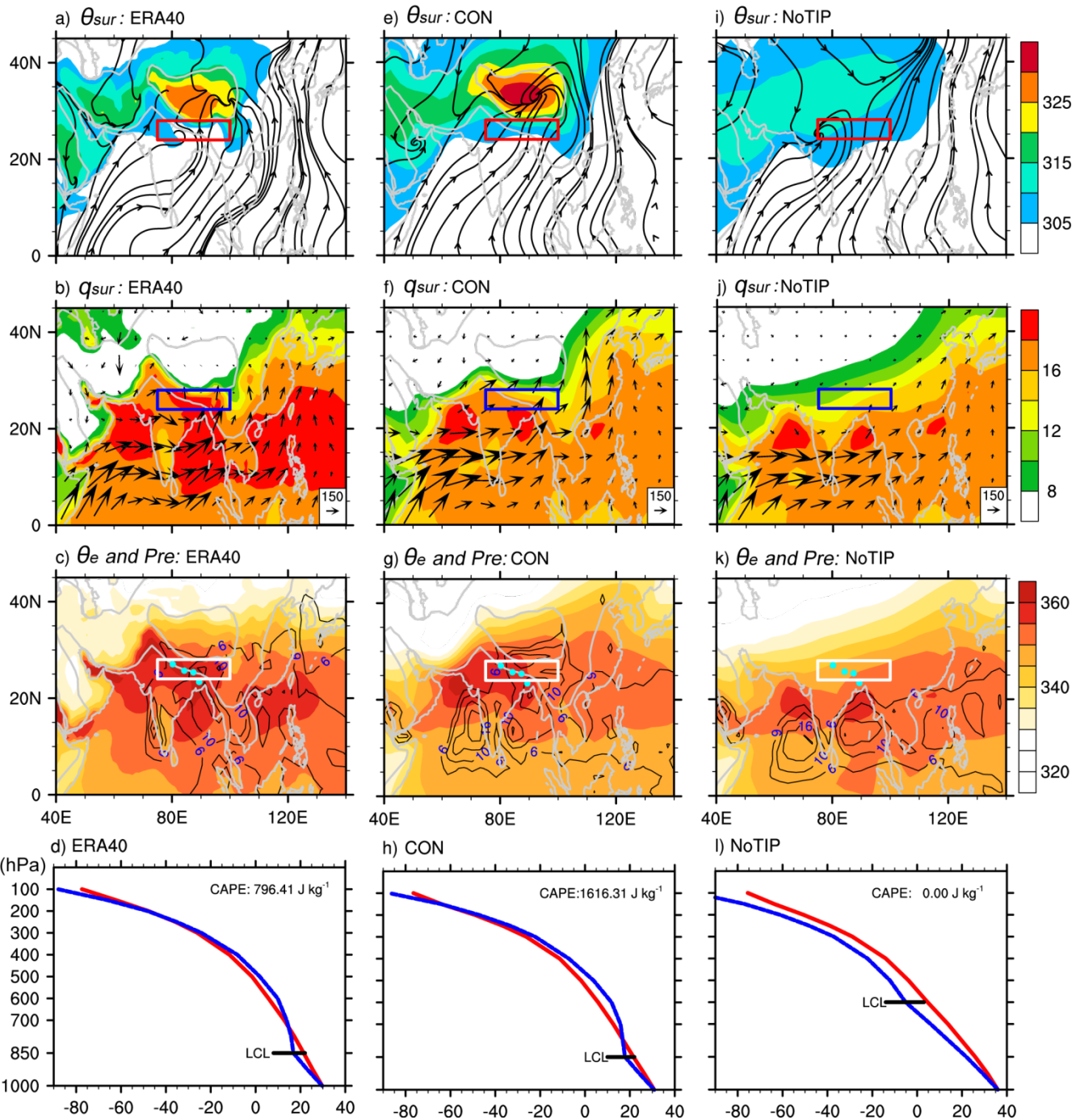
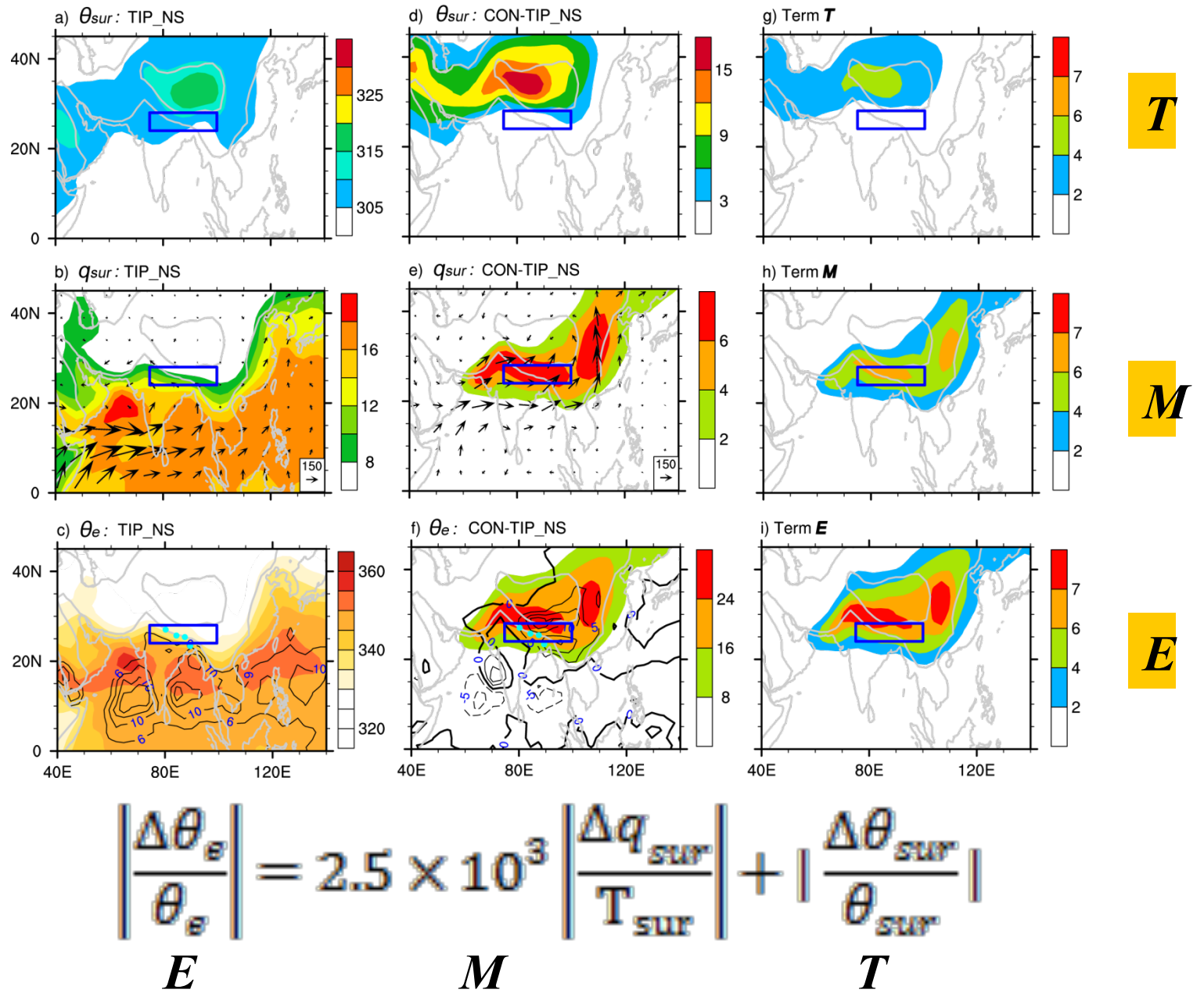
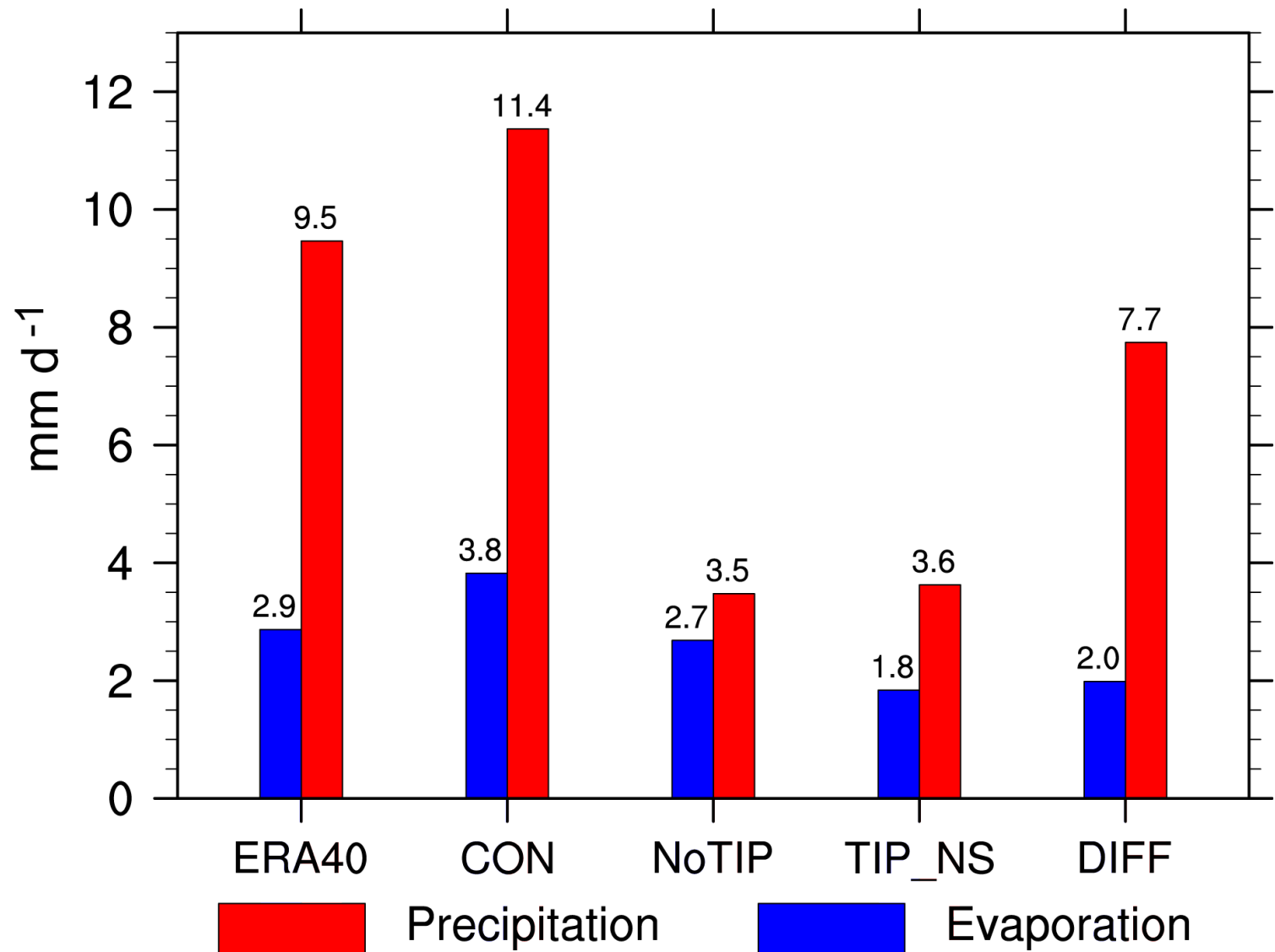


Fig. 3 JJA-means of  $\theta_{sur}$  (K) and streamfield (top row),  $q_{sur}$  ( $\text{g kg}^{-1}$ ) and 850-hPa water-vapor-fluxes (vector,  $\text{kg m}^{-1}\text{s}^{-1}$ ) (second row), and (K) and precipitation ( $\text{mm d}^{-1}$ , contours) (third row); and of profiles of environmental temperature (K, red) and rising air-parcel temperature (K, blue) averaged over the four pale-blue-grid-points over North India shown in the third row (bottom row), calculated from ERA-40 (a-d), CON (e-h) and NoTIP (i-l).



**Fig. 4** (a-c) and (d-f) are the same as Fig. 3 (a-c) but, respectively, for TIP\_NS and (CON-TIP\_NS); and (g-i) the JJA-mean distributions of the  $T$ ,  $M$  and  $E$  terms in Formular (3).



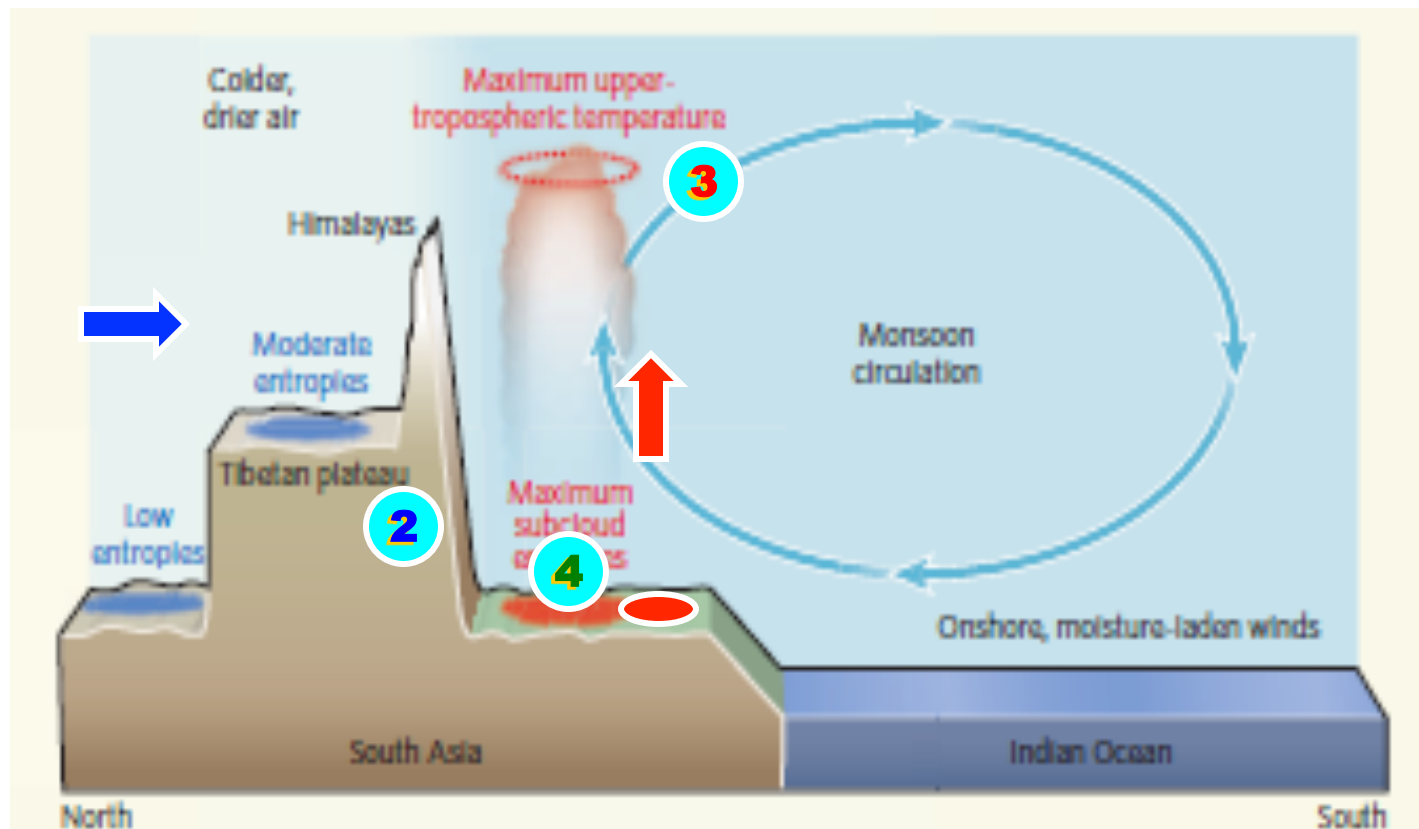
**Fig. 5 Hydrological budgets (mm d<sup>-1</sup>) in the SASM region of (24–28°N, 75–100°E) for ERA-40 and experiments CON, NoTIP, and TIP\_NS. DIFF denotes the difference (CON-TIP\_NS).**

## Conclusion

**Water vapor content is more important than temperature for maintaining high surface energy!**

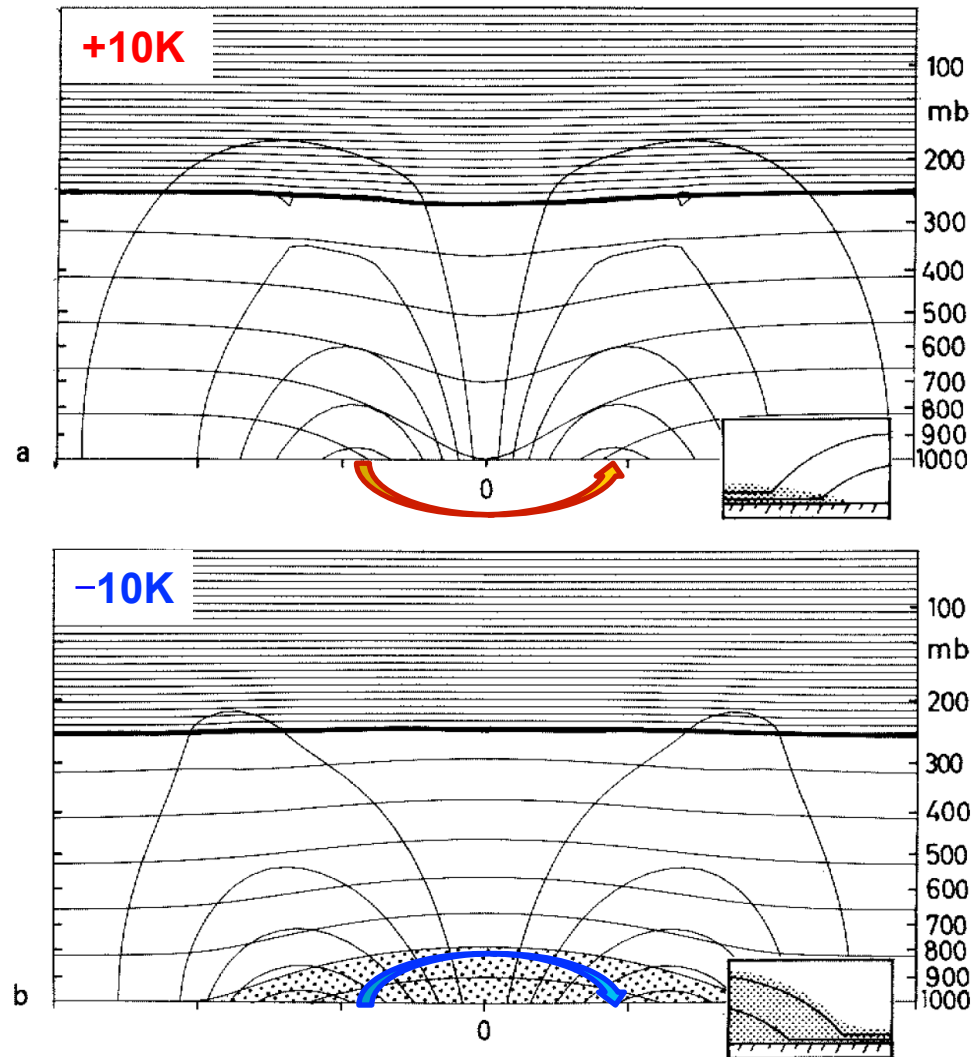
## Mechanical forcing hypothesis: blocking impact of the TP :

1. Shield the India from cold and dry advection
2. High surface energy and UTTM are coupled by monsoon convection

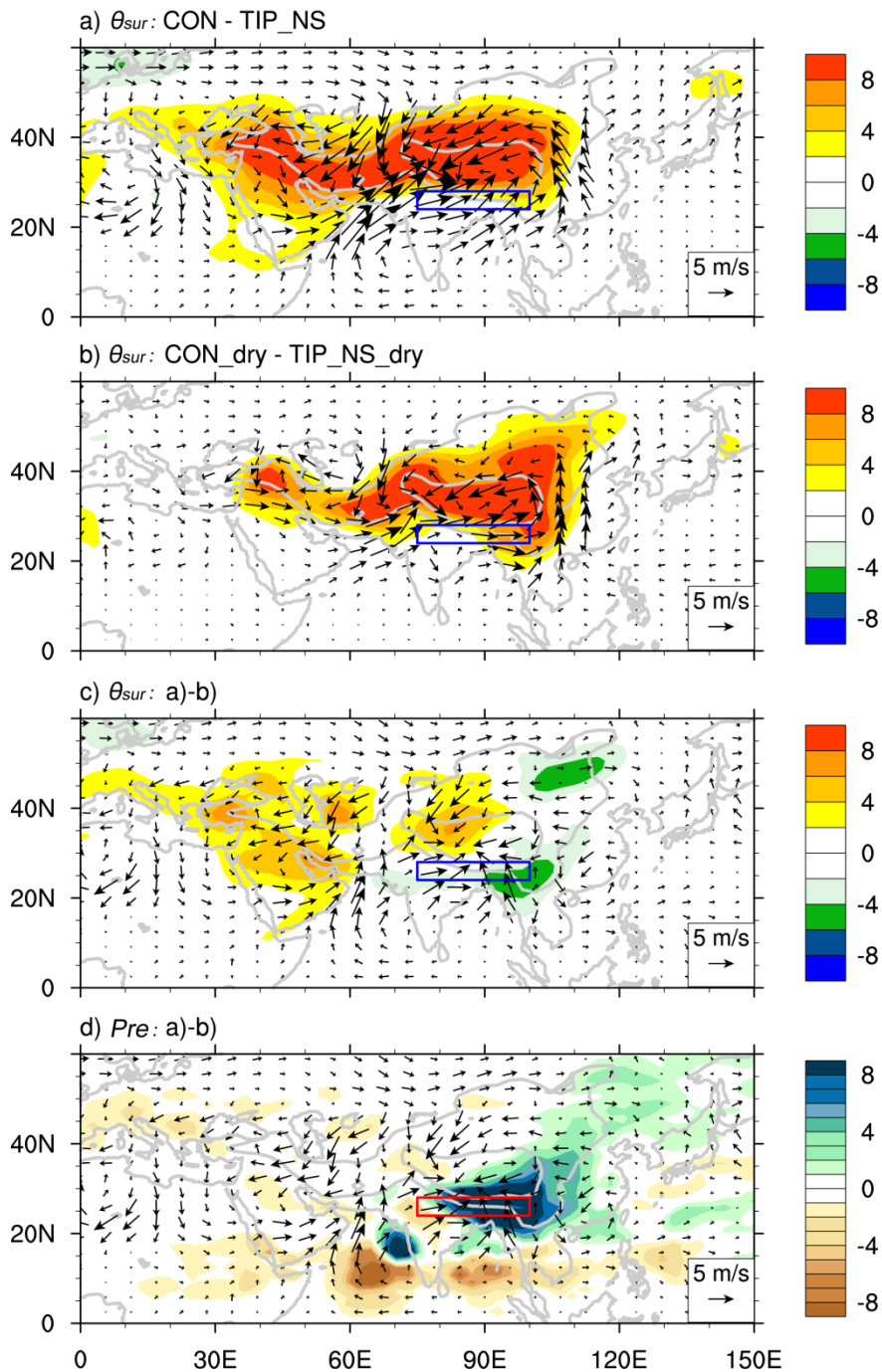


**How can the high Water vapor content over land be maintained for the continental monsoon?**

# Circulation symmetric flows induced by boundary temperature anomalies



Thorpe AJ (1985) Diagnosis of balanced vortex structure using potential vorticity. *J Atmos Sci* 42(4): 397-406.



**MOIST**

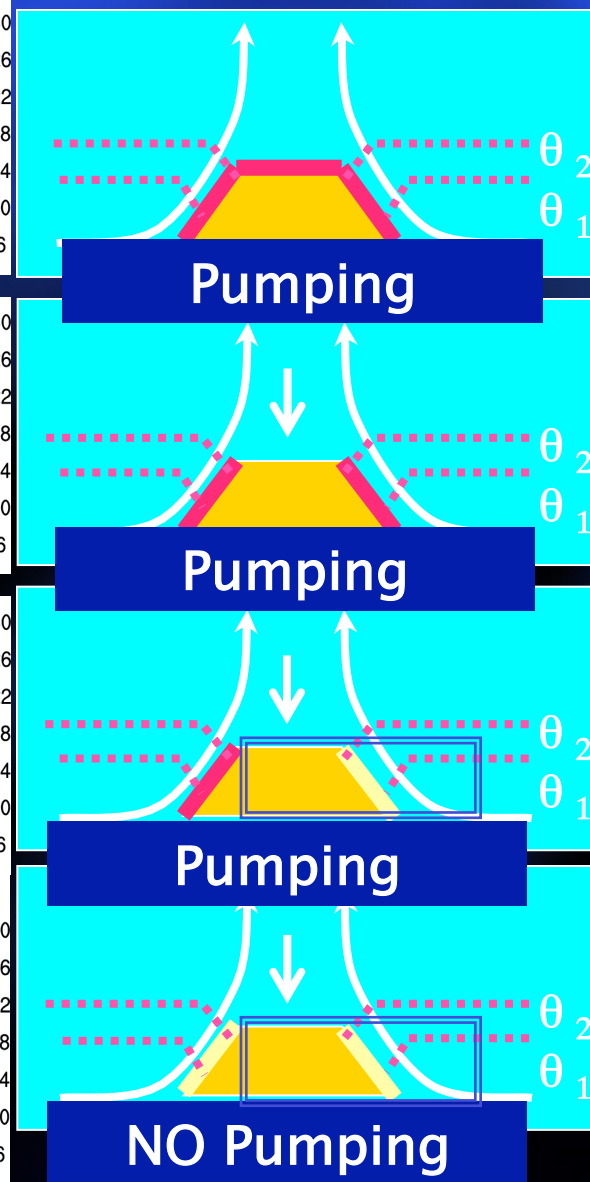
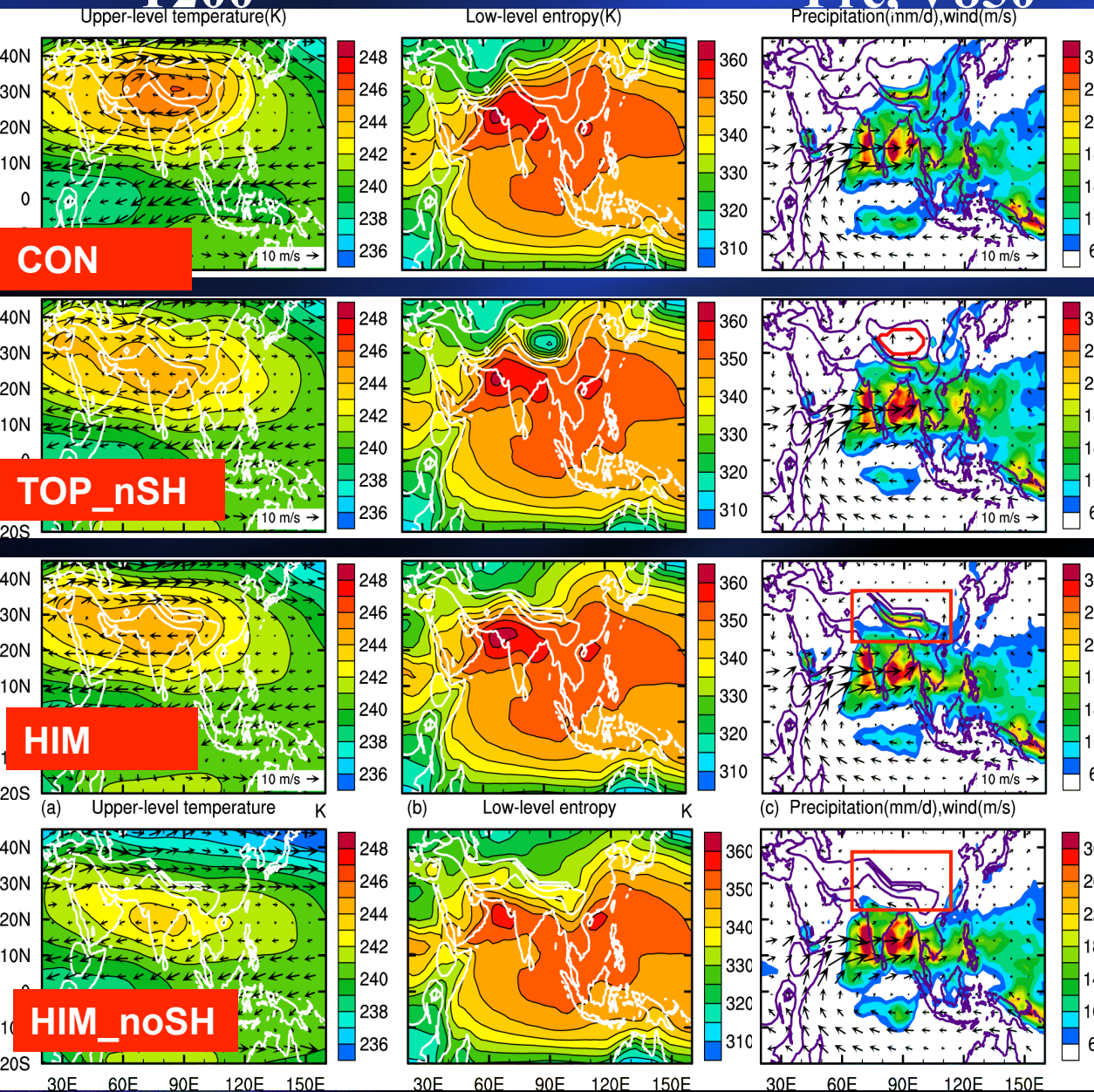
**DRY**

**Fig. 6 JJA-mean differences of  $\theta_{sur}$  (shading, K) and circulation (vectors, m s<sup>-1</sup>) between (a) CON and TIP\_NS, (b) CON\_dry and TIP\_NS\_dry, (c) difference between (a) and (b); (d) is the same as (c) but for precipitation (mm d<sup>-1</sup>). The square indicates the SASM region of (24–28°N, 75–100°E).**

# Experiments by SAMIL/LASG

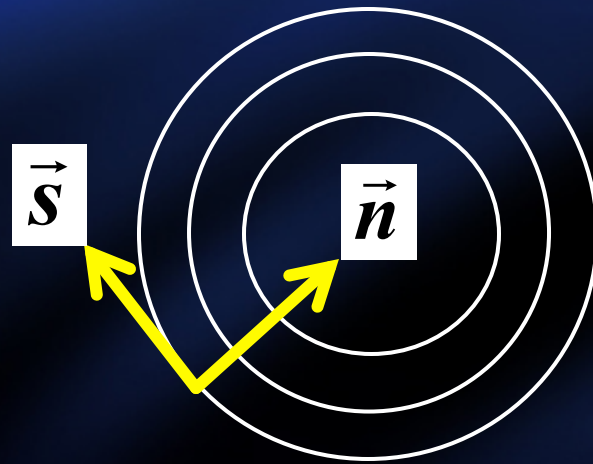
## T200

## Pre. V850



$$\vec{V} \cdot \nabla H = \vec{V}_n \cdot \nabla H_n + \vec{V}_s \cdot \nabla H_s$$

*climbing encircling*



# TP heating produce pumping

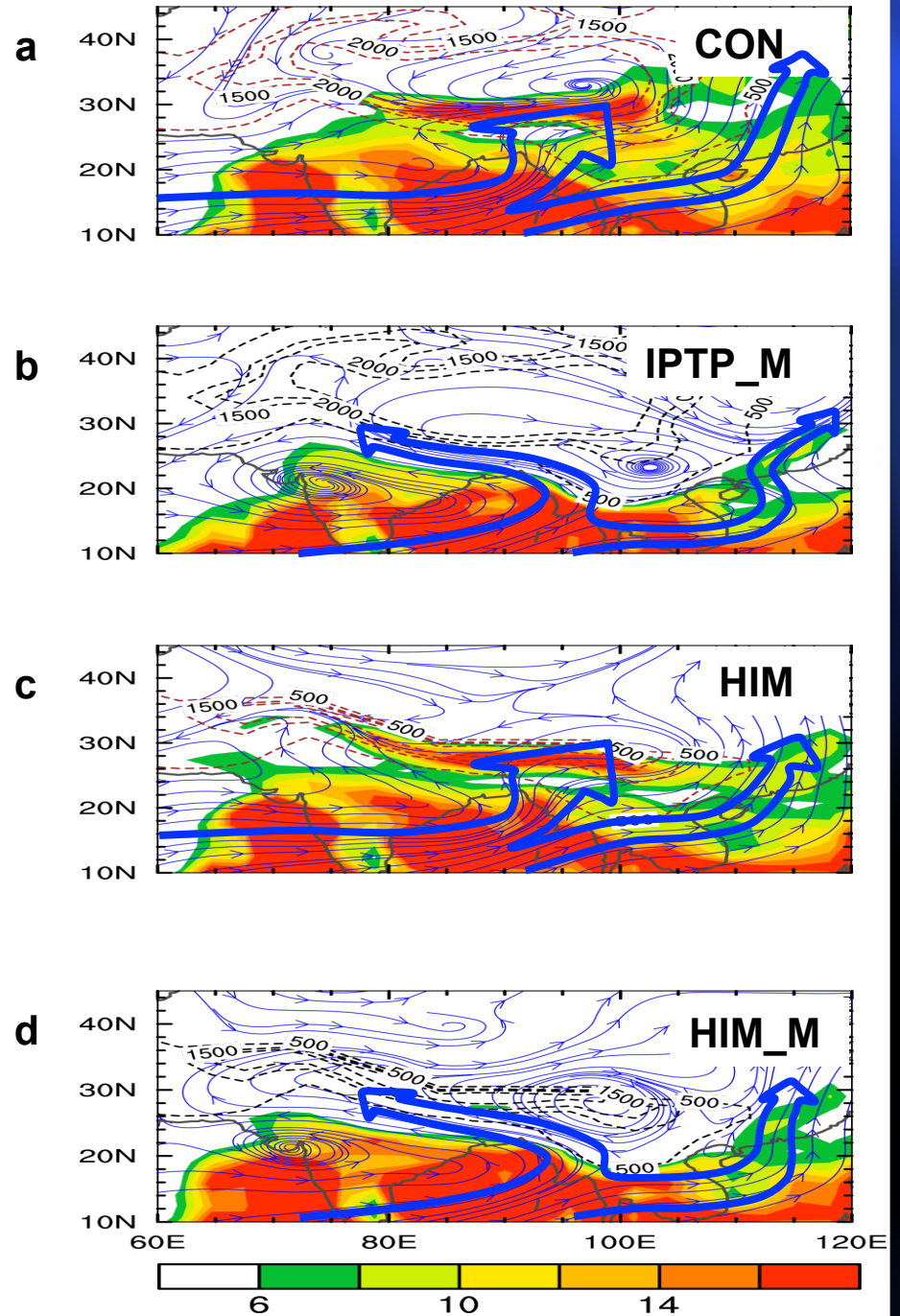
$$\vec{V}_s \cdot \nabla H_s \approx 0 \quad \vec{V} \cdot \nabla H \approx \vec{V}_n \cdot \nabla H_n$$

# No TP heating, no pumping

$$\vec{V}_n \cdot \nabla H_n = 0 \quad \vec{V} \cdot \nabla H = \vec{V}_s \cdot \nabla H_s$$

☆ Boos and Kuang (2010)-  
Insulation of the Himalaya?

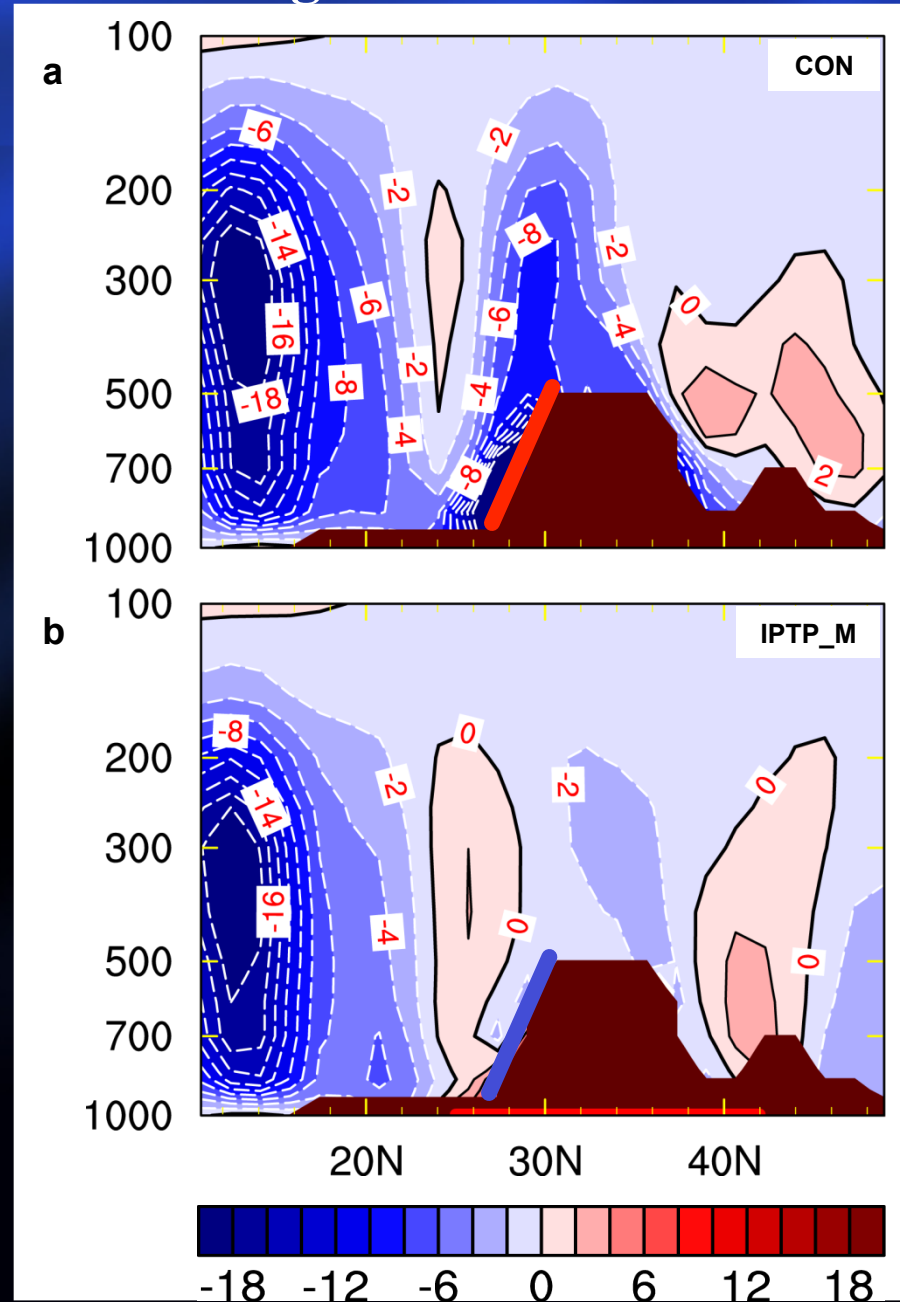
☆ Boos and Kuang (2010)-  
Himalaya without heating



**With TP surface  
sensible heating**

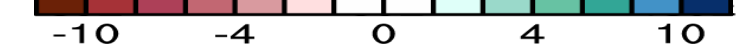
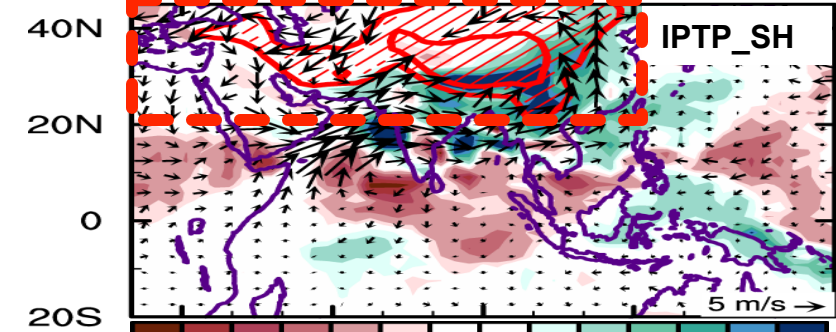
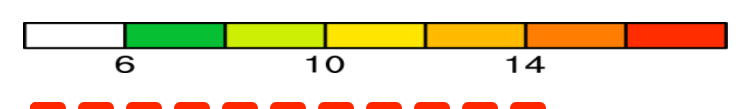
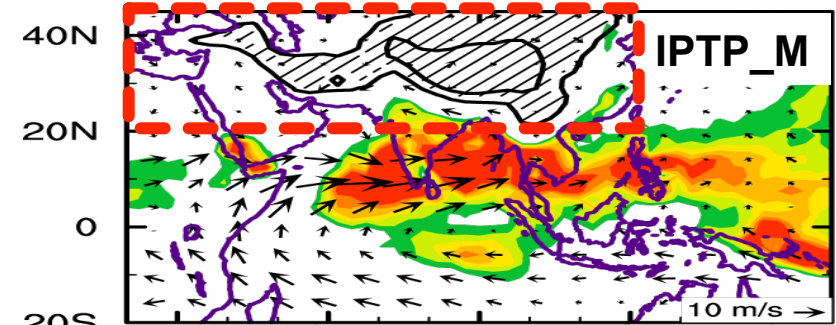
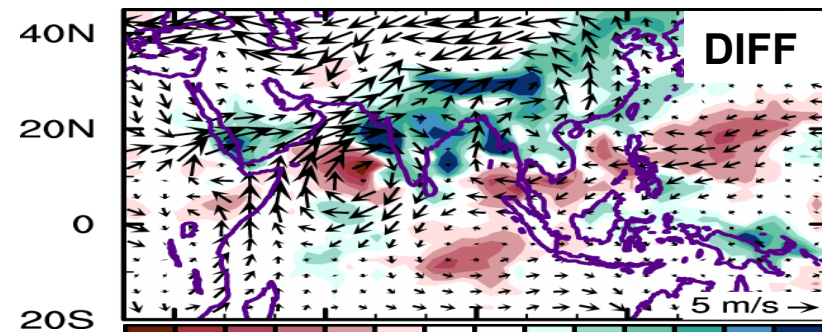
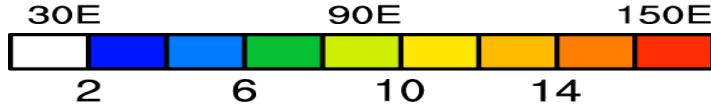
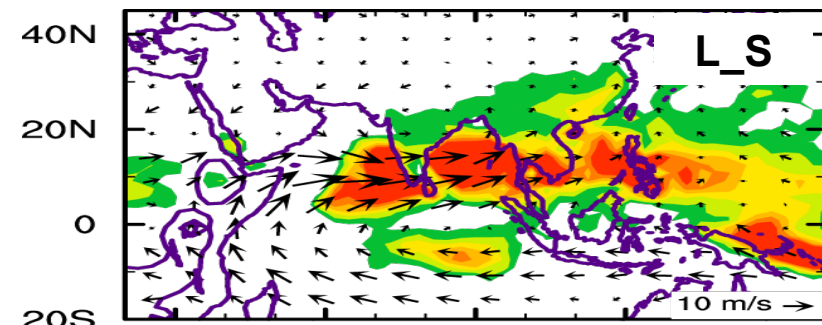
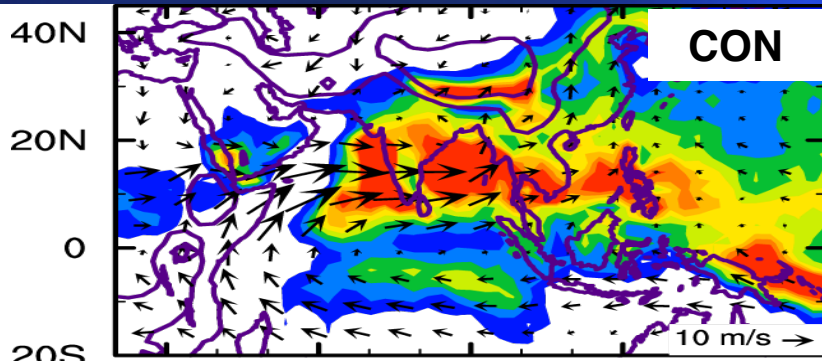
**Without TP  
surface sensible  
heating**

## Omega of 80°E–90°E



**Structure of the South Asian  
summer monsoon, showing  
80°E–90°E**

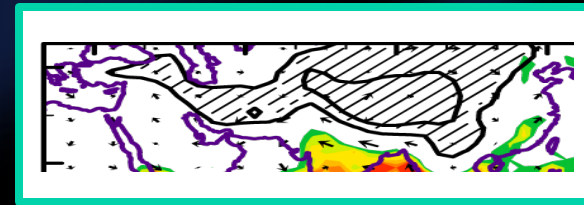
# Impacts of mountain mechanical ~ thermal forcing



Required Circul. and Precip. to make up the Asian summer monsoon

# PV-Q perspective of the TIP impact on the Asian summer monsoon

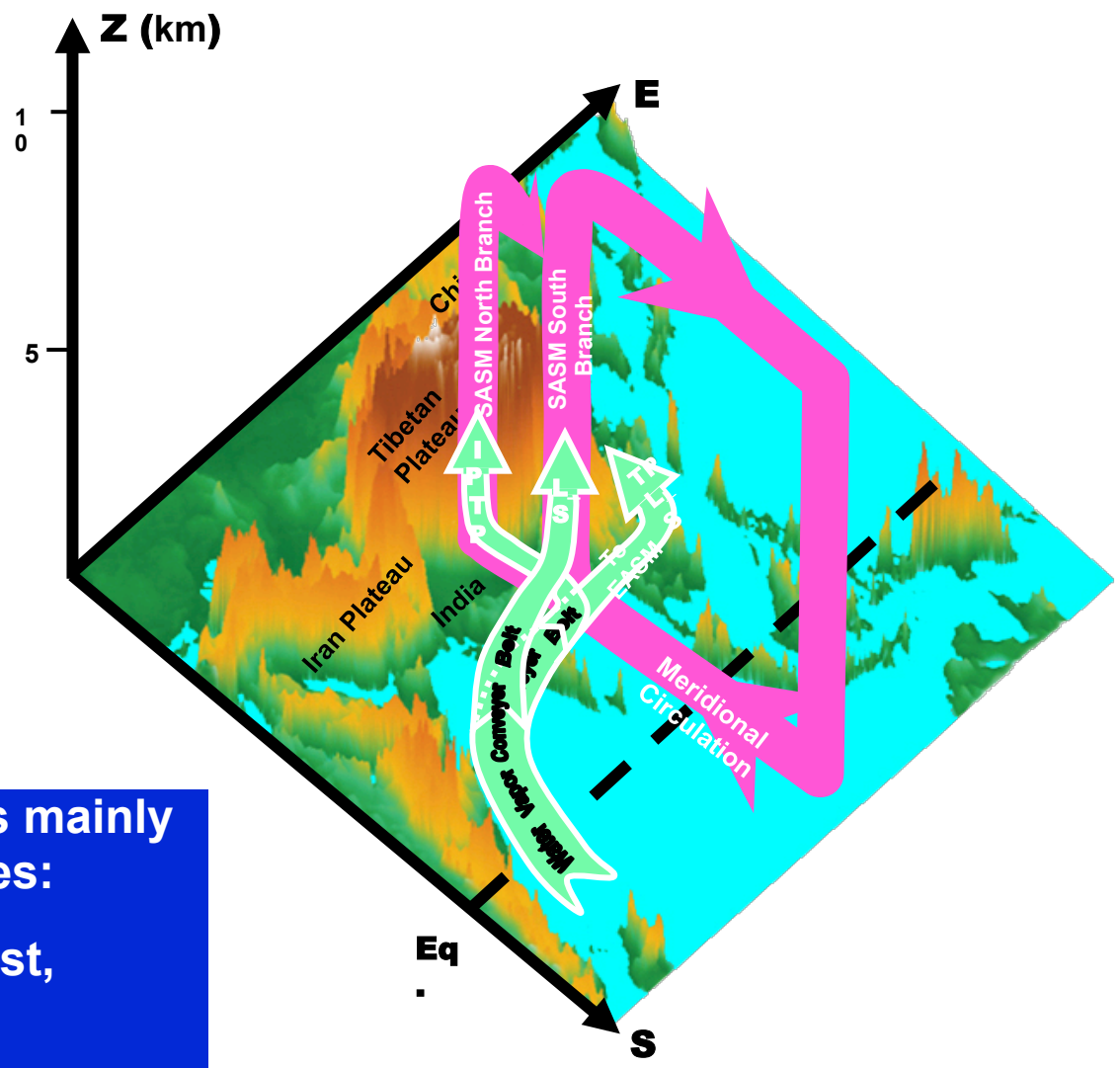
IPTP\_M



IPTP\_SH



# Highlight 7: Tibetan Plateau thermal forcing and Asian summer monsoon



The Asian summer monsoon is mainly controlled by thermal processes:

- Land\_Sea thermal contrast,
- TP thermal forcing and
- Iran Plateau thermal forcing



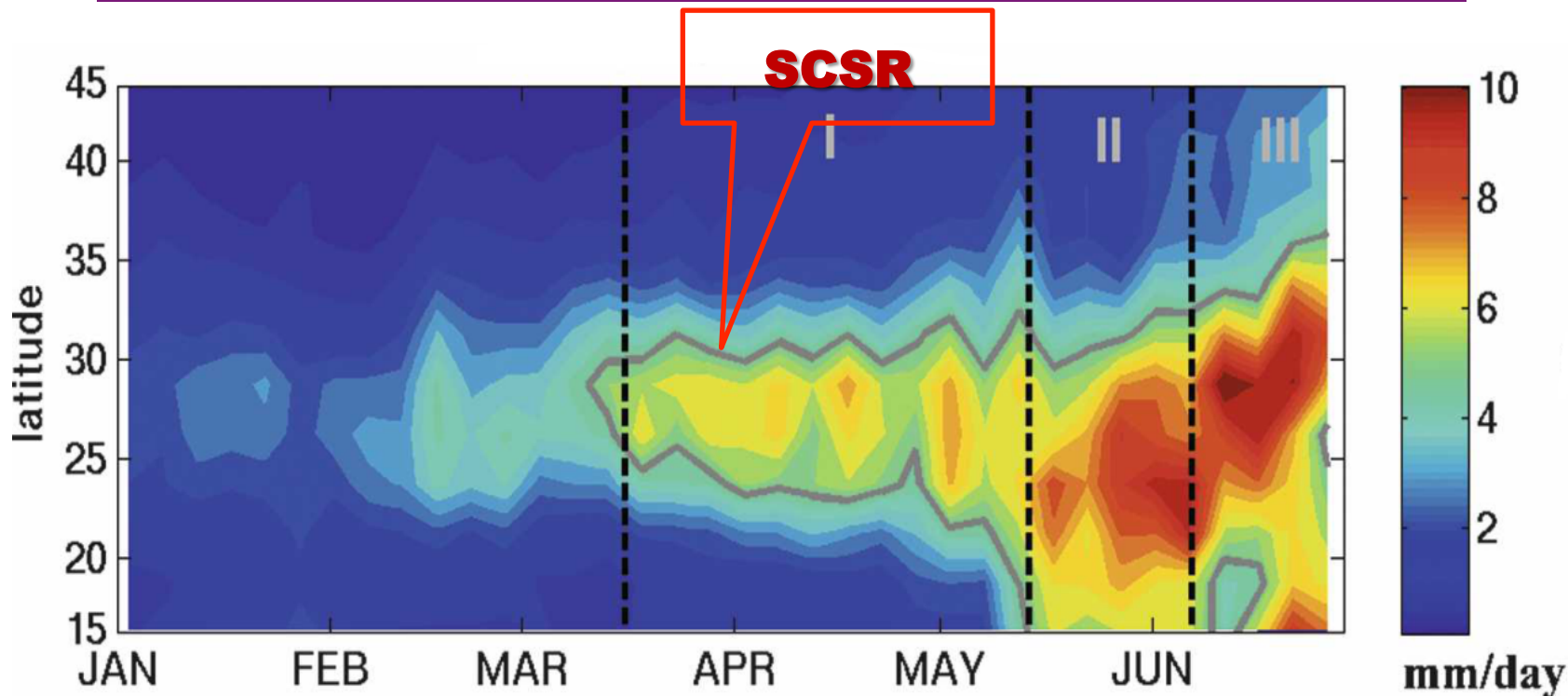
# Outline



- 1 Introduction- general circulation**
- 2 Dynamics of ASM onset**
- 3 Evolution of the ASM onset**
- 4 Maintenance of the ASM**
- 5 Variability of the ASM**
- 6 Conclusion**



# 110°-130°E averaged precipitation



LinHo等(2008)

降水年际变率大，致使旱涝灾害频繁

春季连阴雨天气是华南地区常见的一种灾害性天气

季节内振荡是全球大气多时间尺度振荡现象的重要组成部分，是联系天气与气候的直接纽带，对阶段性、持续性极端事件的发生具有重要影响

□ 理解**季节内振荡**如何影响**华南春季气候**

□ 提高华南春季延伸期以及月季降水趋势预测能力

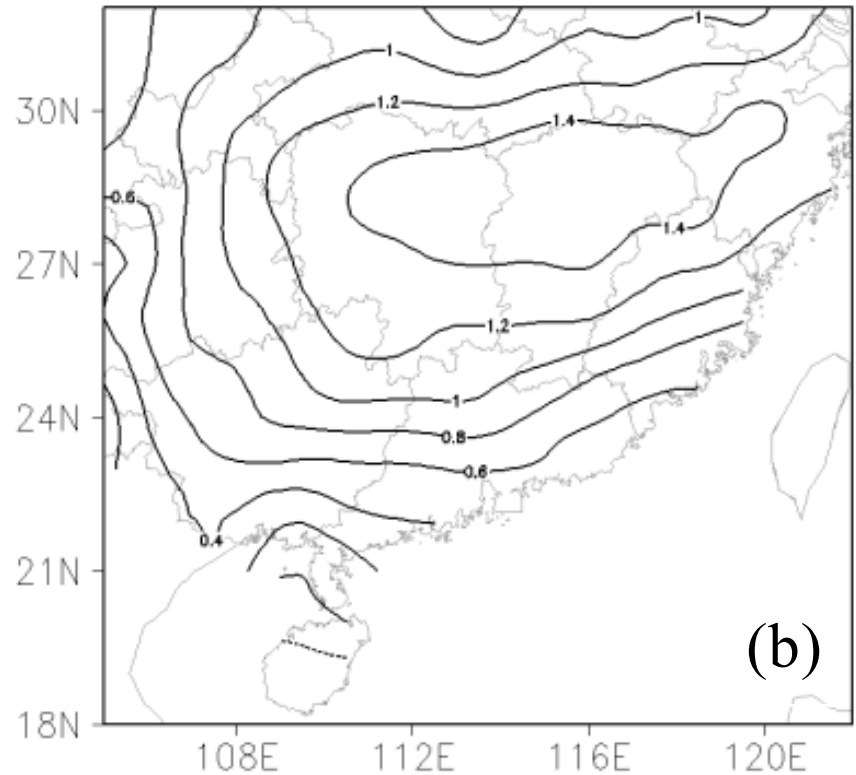
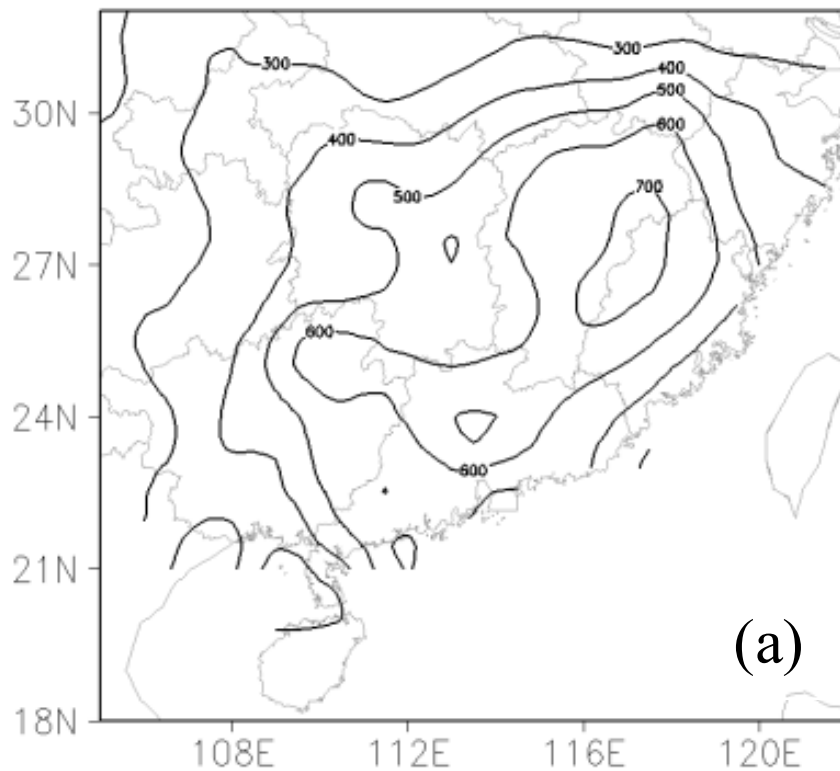


Figure 1. (a) Spatial distribution of the climatological spring (March–May) **precipitation (mm)** over Southern China for the period 1980–2008. (b) Spatial pattern of the first EOF mode (**EOF1**) for daily spring precipitation anomalies over Southern China.

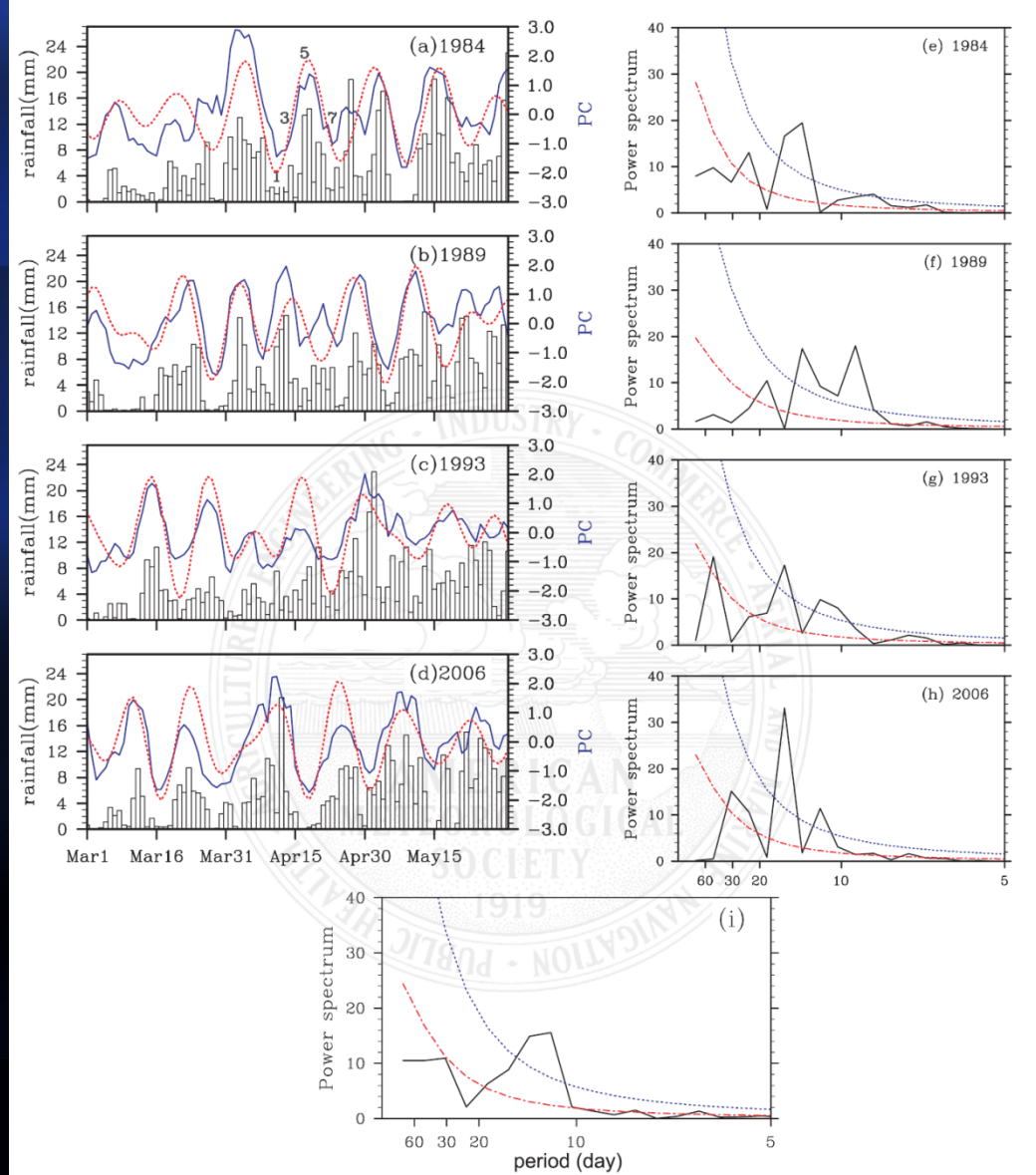


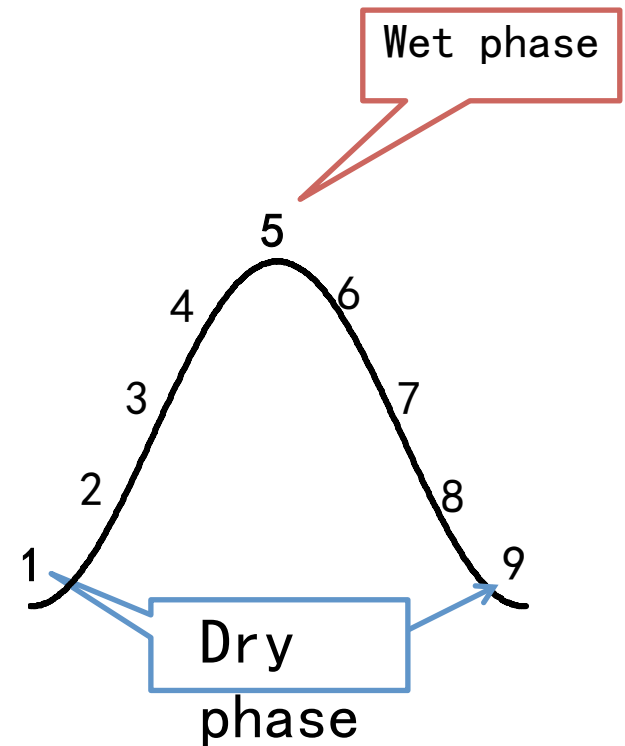
FIG. 2. Time series of daily rainfall (histogram; mm day<sup>-1</sup>) averaged over southern China (18–32°N, 105°–120°E), the corresponding unfiltered PC1 (blue solid curve), and the 10–20-day filtered PC1 (red dotted curve) for the typical years of (a) 1984, (b) 1989, (c) 1993, and (d) 2006. (e)–(h) The corresponding power spectrum of the unfiltered PC1 (black curve), together with the Markov red noise spectrum (red dot-dashed curve) and a posterior 95% confidence level (blue dotted curve) for the selected years and (i) the 29-yr average from 1980 to 2008. The numbers 1, 3, 5, and 7 in (a) indicate the phase of the 10–20-day oscillation.

# Phase definition for the ISO/SCSR

## 位相合成分析方法

Lanczos滤波提取10 - 20天周期分量  
作为降水ISO 指数

- 挑选标准 强ISO个例。
- 10—20天周期：46个
- 20—30天周期：38个



ISO振荡位相示意图

# 850hPa- divergence and streamfield

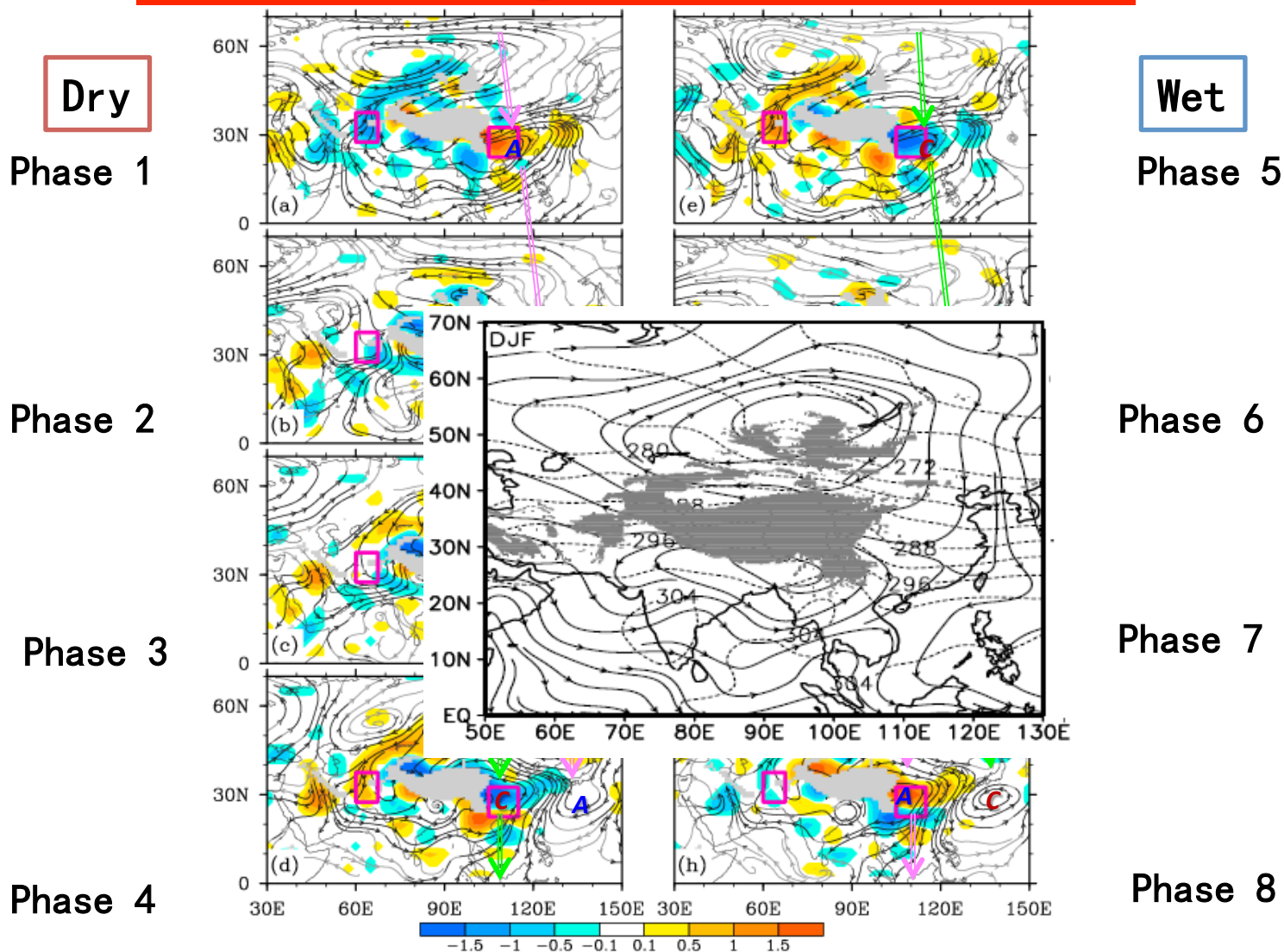
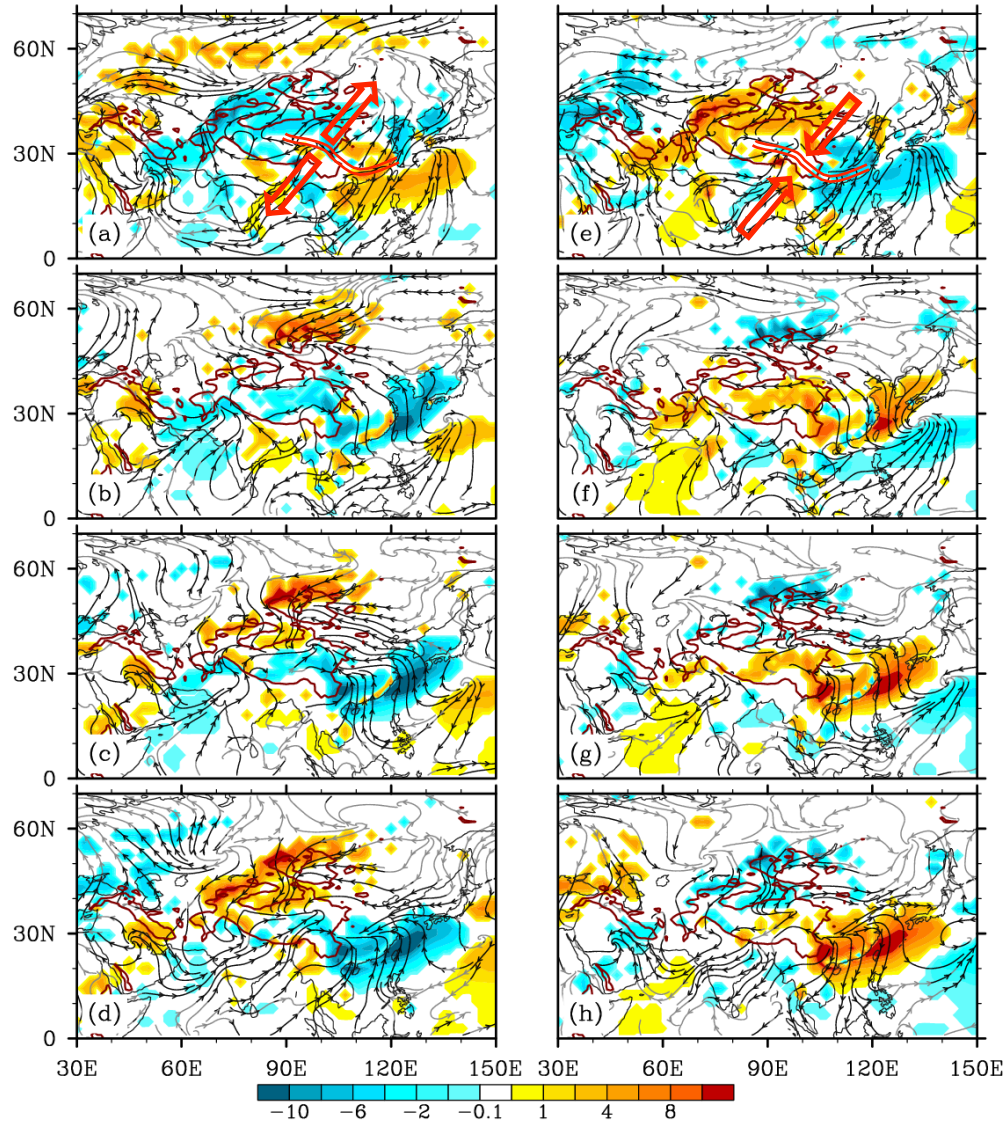


Figure 3. Composite evolution of the 10–20-day filtered 850 hPa streamline (dark streamline indicates where at least one wind component is statistically significant at the 95% confidence level) and divergence (shading, unit is  $10^{-6} \text{ s}^{-1}$ ; only shown if statistically significant at the 95% confidence level) during an ISO cycle. Phases 1–8 are shown from (a) to (h). The Tibetan Plateau with terrain above 1500 m is shaded grey. Western rectangle area ( $60^{\circ}$ – $67.5^{\circ}\text{E}$ ,  $27.5^{\circ}$ – $37.5^{\circ}\text{N}$ ) to the west of the TP and eastern rectangle area ( $105^{\circ}$ – $115^{\circ}\text{E}$ ,  $22.5^{\circ}$ – $32.5^{\circ}\text{N}$ ) to the east of the TP indicate the locations of the two divergence poles of the Spring Dipole Mode Index (SDMI). “A” and “C” denote, respectively, the anticyclone and cyclone centers, and arrows denote the propagation routes of the anticyclone and cyclone.

# 10-m streamfield and surface sensible heat flux

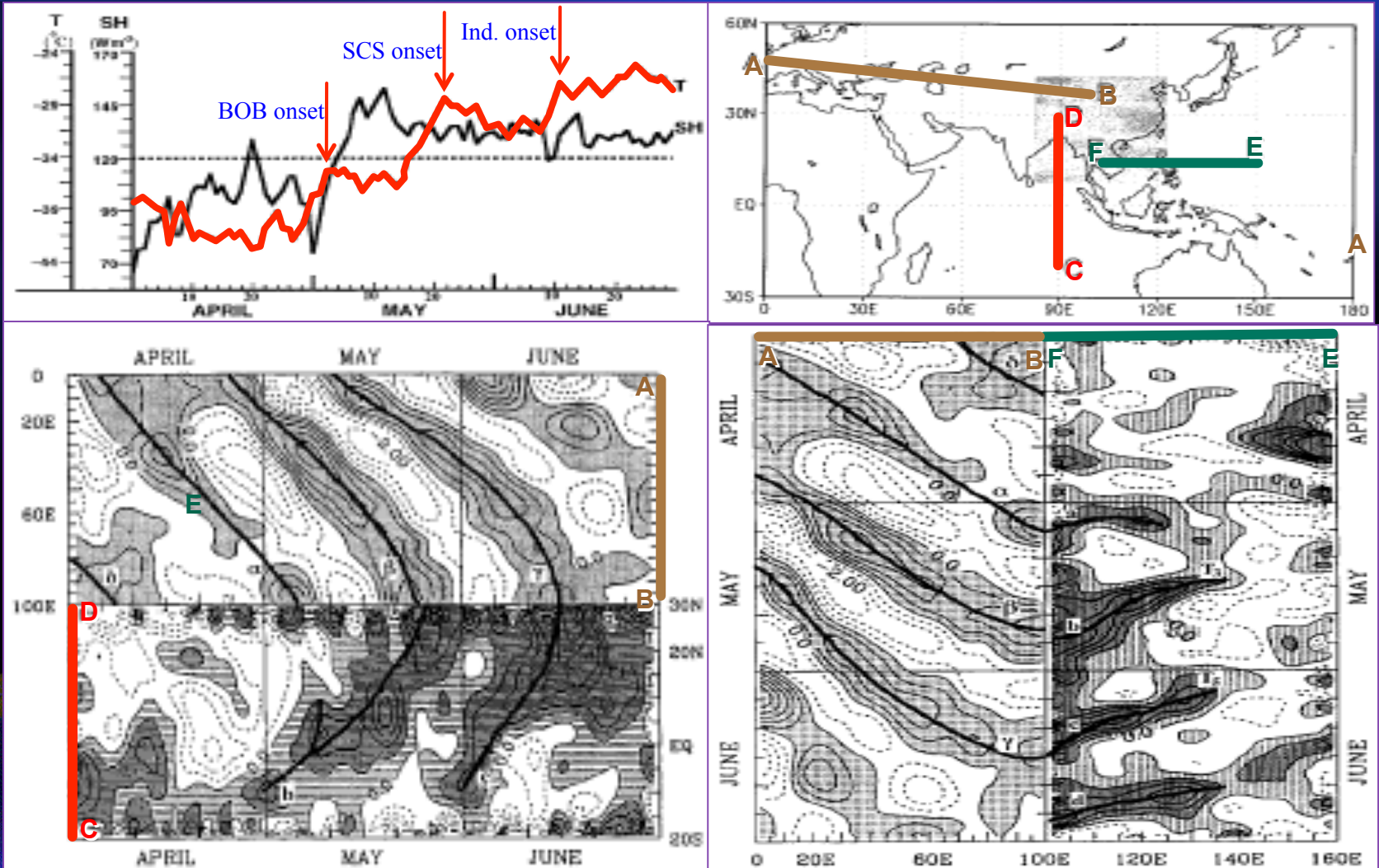
Dry



Wet

Figure 4. Same as Fig. 3, but for the 10–20-day filtered 10 m wind (vectors,  $\text{m s}^{-1}$ ) and surface sensible heating flux ( $\text{W m}^{-2}$ , with shading denoting statistical significance at the 95% confidence level). The Tibetan Plateau with terrain above 1500 m is outlined by a solid curve

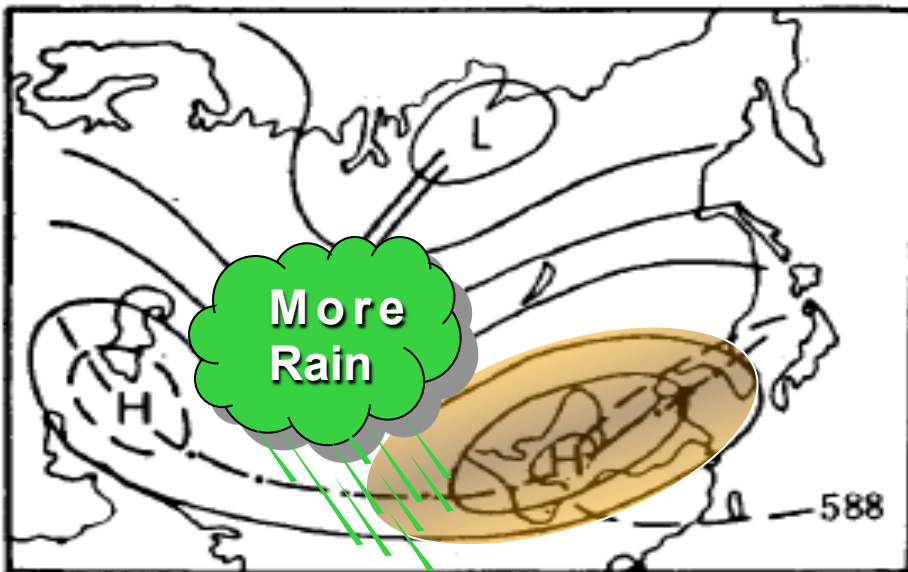
# ISV: TP heating and the three – stage ASM onset



(Wu and Zhang, MWR, 1998)

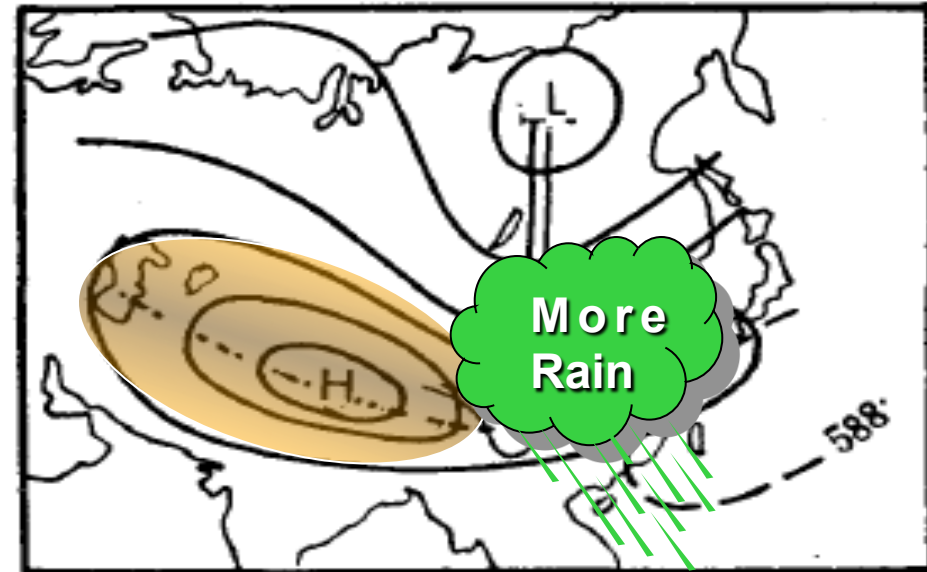
# 夏季高原天气影响：南亚高压准双周振荡

W- mode



a

E- mode



b

FIG. 6. Two major patterns of the Tibetan high at (a) 200 mb; and (b) 100 mb.

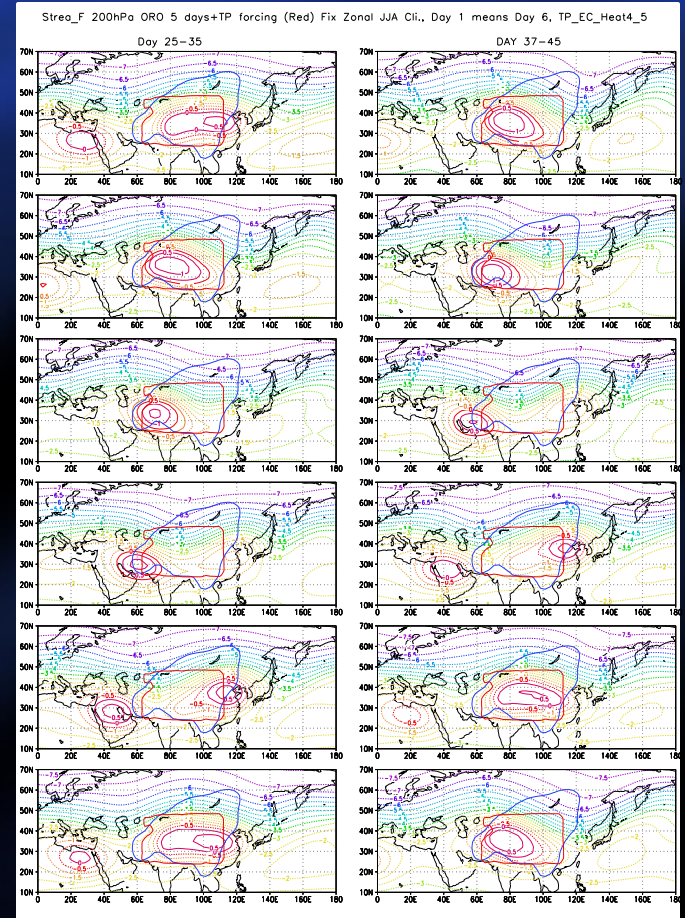
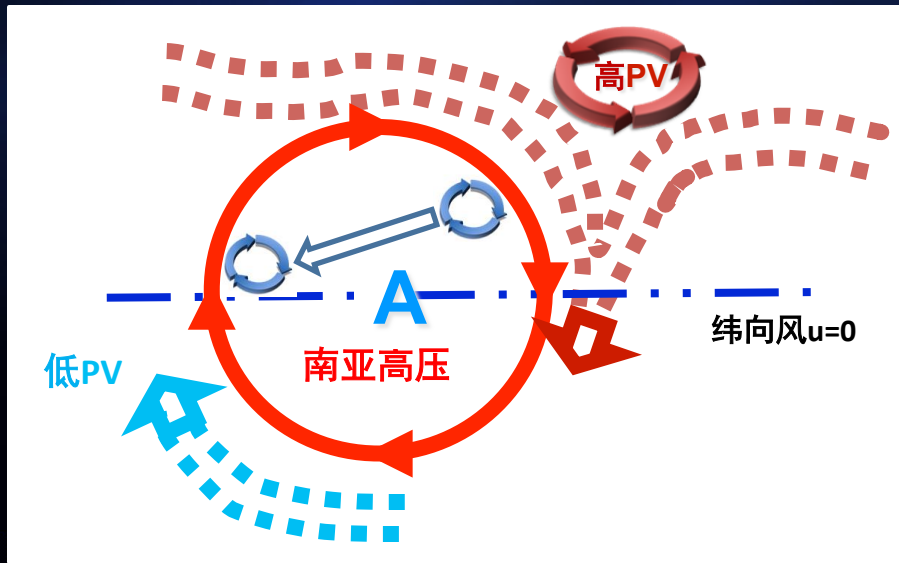
陶诗言和朱福康, 1964

加热弱: 南亚高压稳定; 加热强: 不稳定  
Due to PV asymmetric instability

Liu等, 2007

# ISV: TP summer heating and SAH oscillation

夏季青藏高原强加热能够产生准双周振荡



(Liu, Hoskins, Blackman, 2007 JMSJ)

**Fig. 10 Decadal changes in JJA mean climate between the periods (1991–2000) and (1981–1990) of (a) precipitation based on the PREC/L dataset (unit:  $\text{mmd}^{-1}$ ), (b) 200-hPa geopotential height (unit: gpm) and (c) the 200–400hPa mass-weighted temperature (unit: K) based on ERA40 reanalysis. The solid and dashed curves in (b) and (c) denote, respectively, the 1981–1990 and 1991–2000 means.**

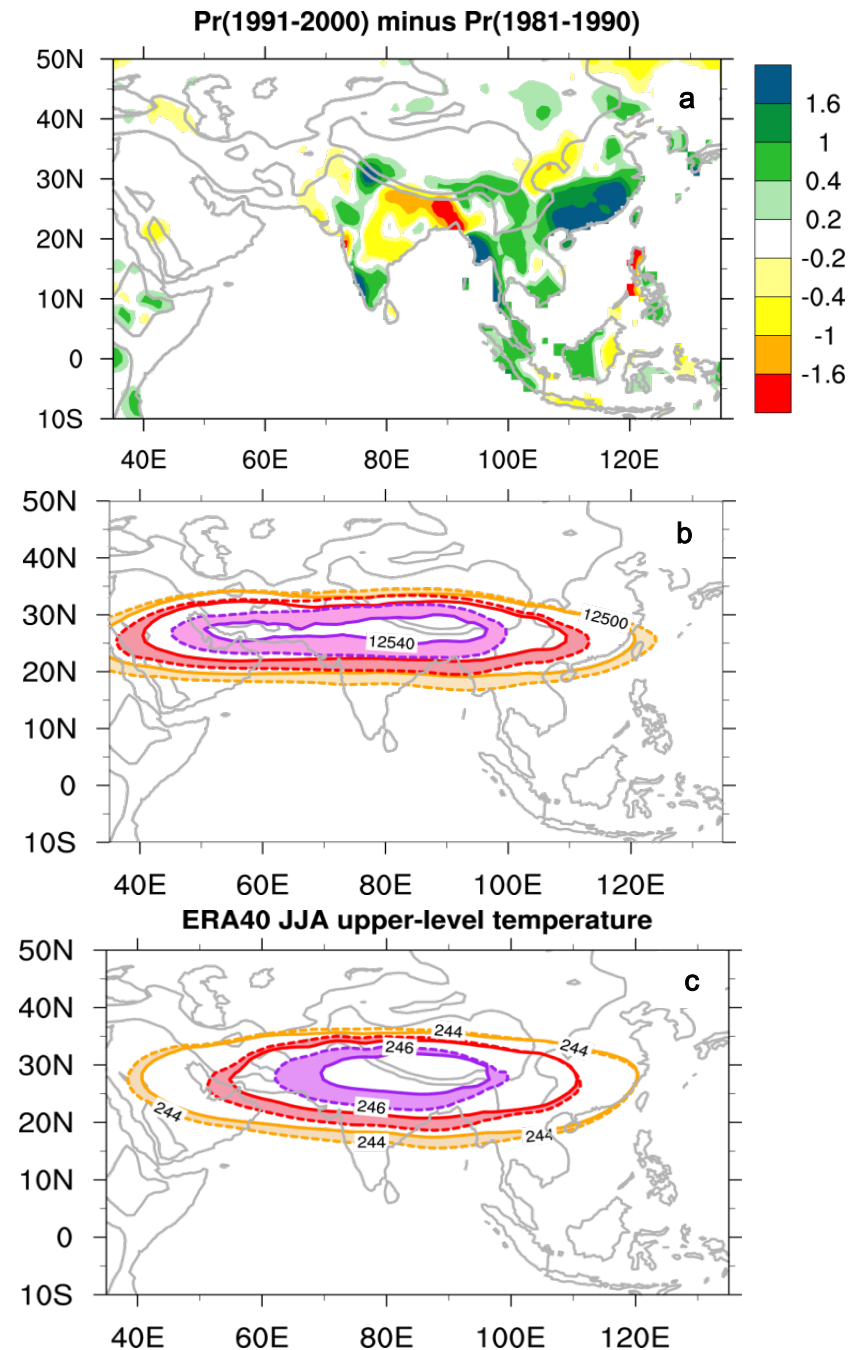
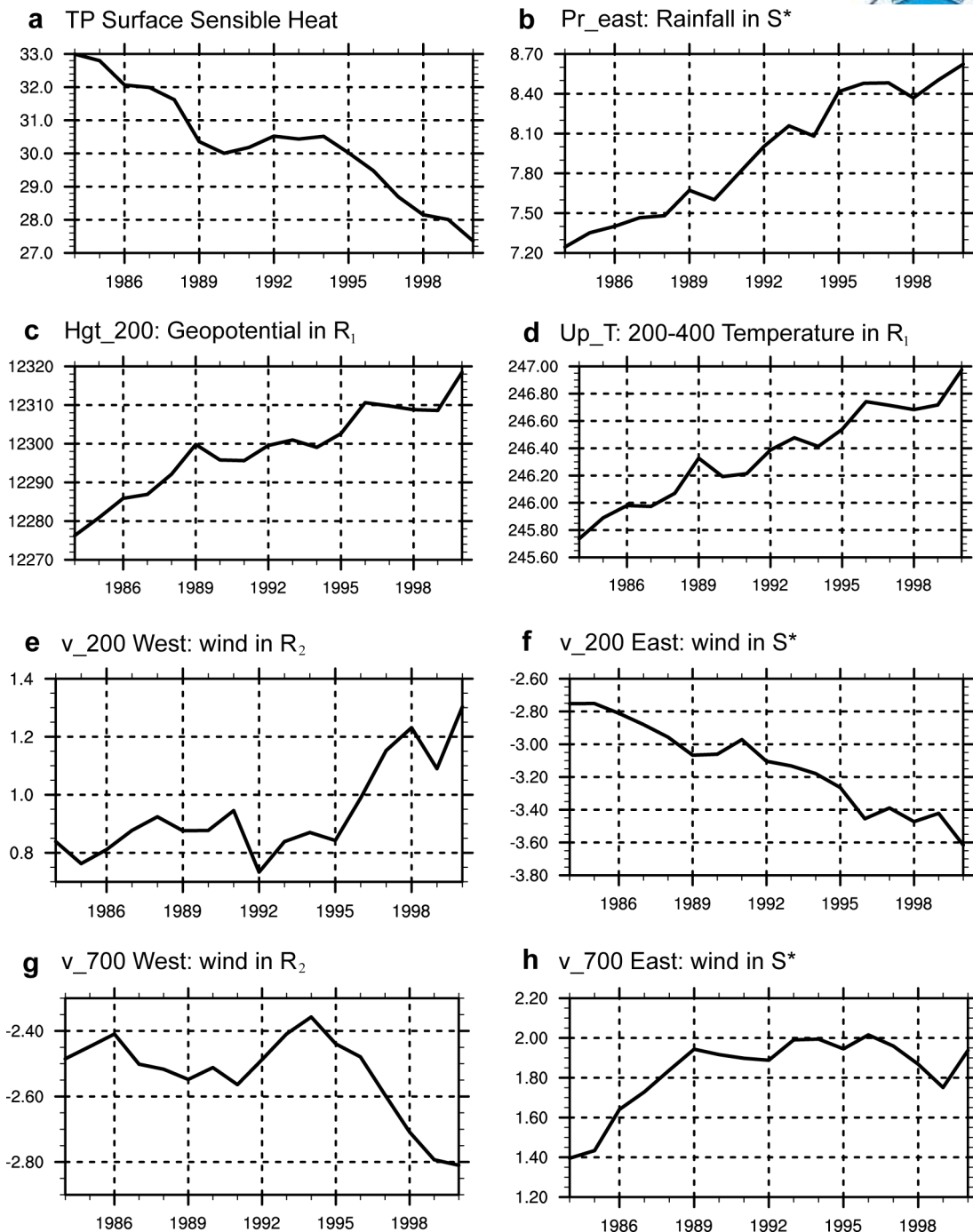
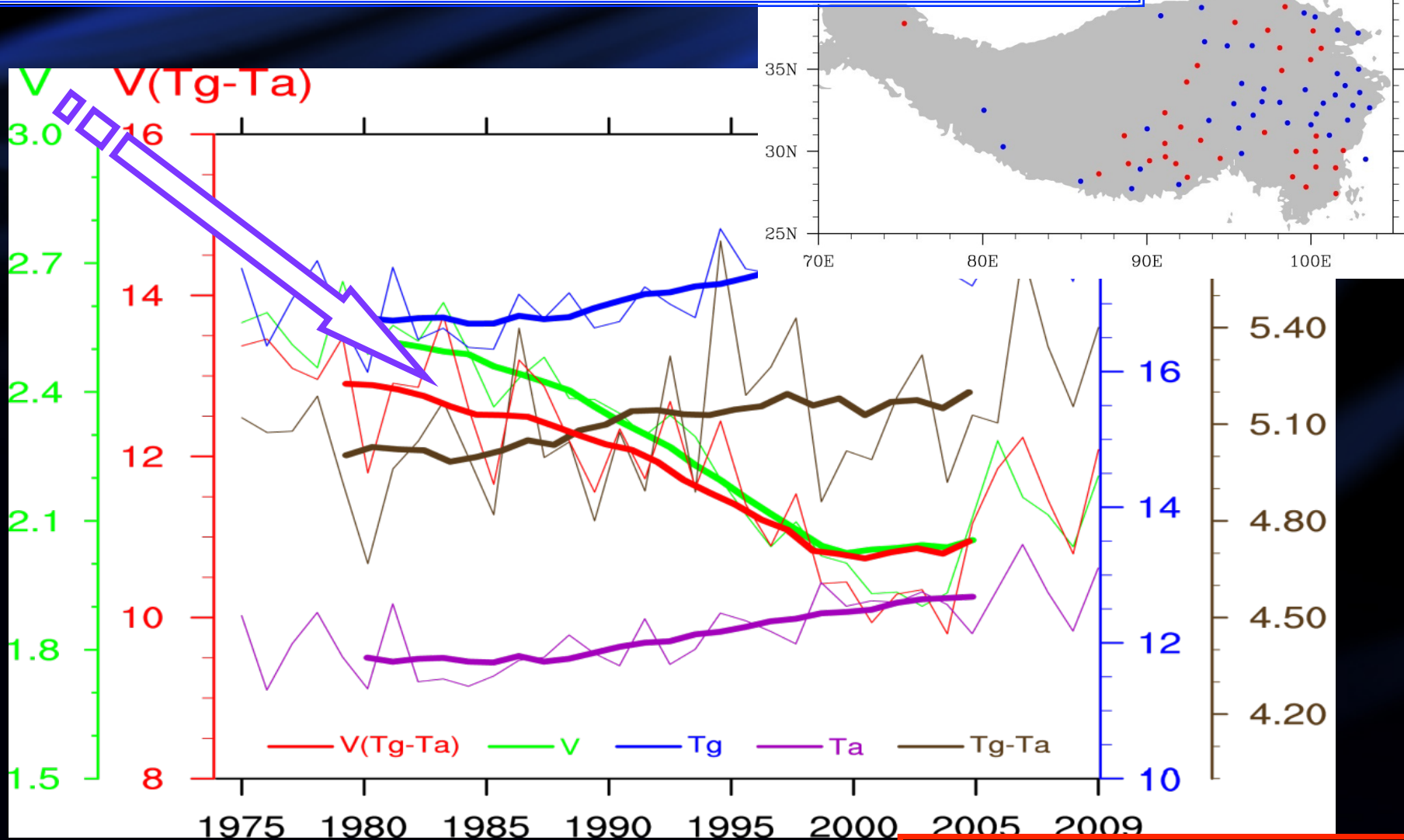


**Fig. 11 Evolution from 1984 to 2000 of the JJA mean based on the ERA40 reanalysis of (a) surface sensible heat flux on the Tibetan Plateau region ( $80^{\circ}$ – $100^{\circ}$ E,  $26^{\circ}$ – $36^{\circ}$ N unit:  $Wm^{-2}$ ), (b) precipitation in the forcing source region  $S^*$  (Pr<sub>east</sub>:  $90^{\circ}$ – $120^{\circ}$ E,  $24^{\circ}$ – $28^{\circ}$ N, unit:  $mmd^{-1}$ ), (c) 200 hPa geopotential height in the response region  $R_1$  (hgt<sub>200</sub>:  $70^{\circ}$ – $90^{\circ}$ E,  $24^{\circ}$ – $28^{\circ}$ N unit: dgpm), (d) 200–400 hPa mass-weighted temperature in  $R_1$  (Up<sub>T</sub>, unit: K), 200 hPa meridional wind (e) in the response region  $R_2$  (v<sub>200</sub> West:  $50^{\circ}$ – $80^{\circ}$ E,  $24^{\circ}$ – $28^{\circ}$ N) and (f) in  $S^*$  (v<sub>200</sub> East, unit:  $ms^{-1}$ ), and 700 hPa meridional wind (g) in  $R_2$  (v<sub>700</sub> West) and (h) in  $S^*$  (v<sub>700</sub> East, unit:  $ms^{-1}$ ).**



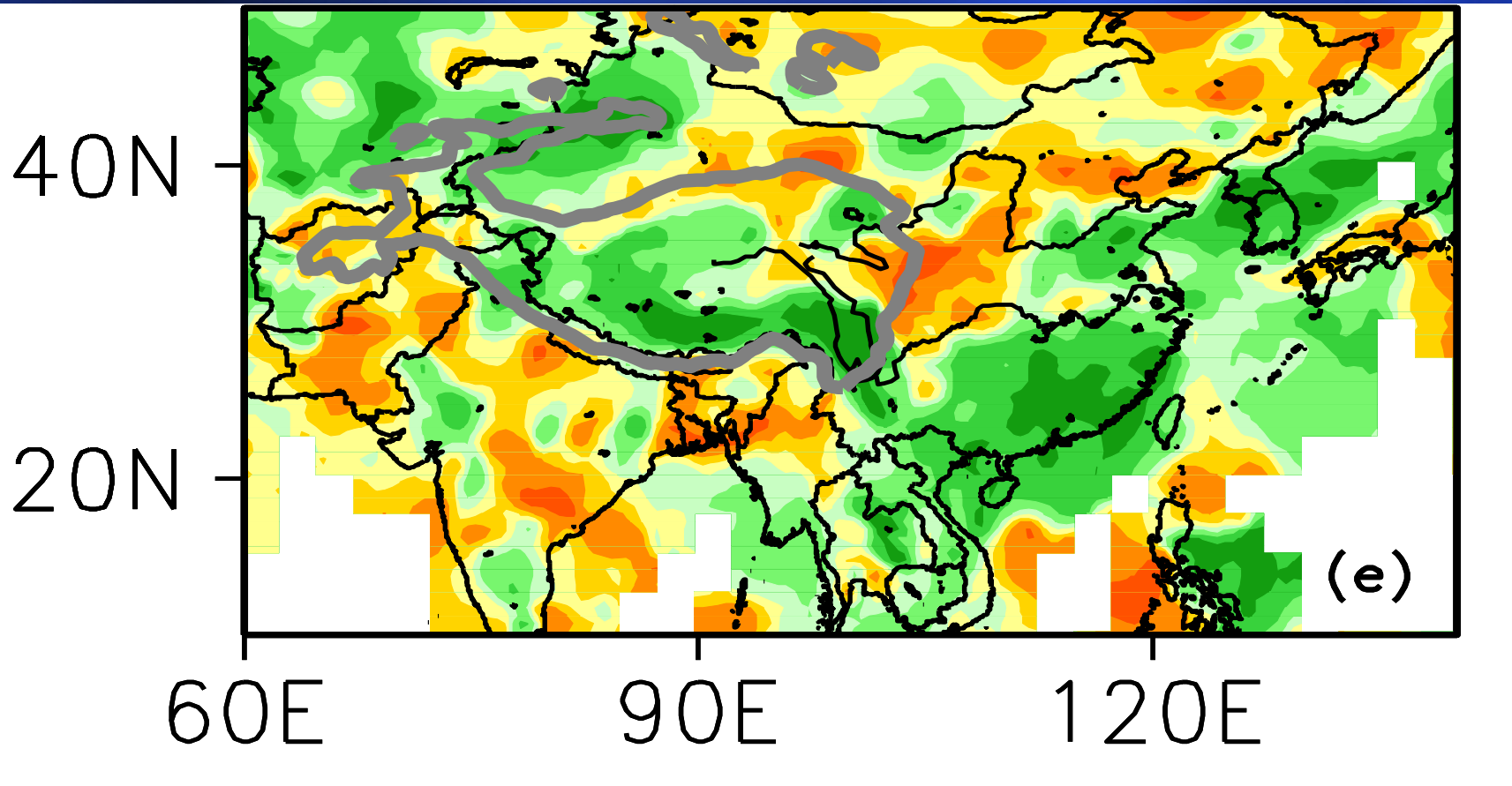
**(1) A weakening trend in the TP forcing in spring and summer from station data**



**Mean over the TP, JJA**

Liu et al. Cli. Dyn 2012

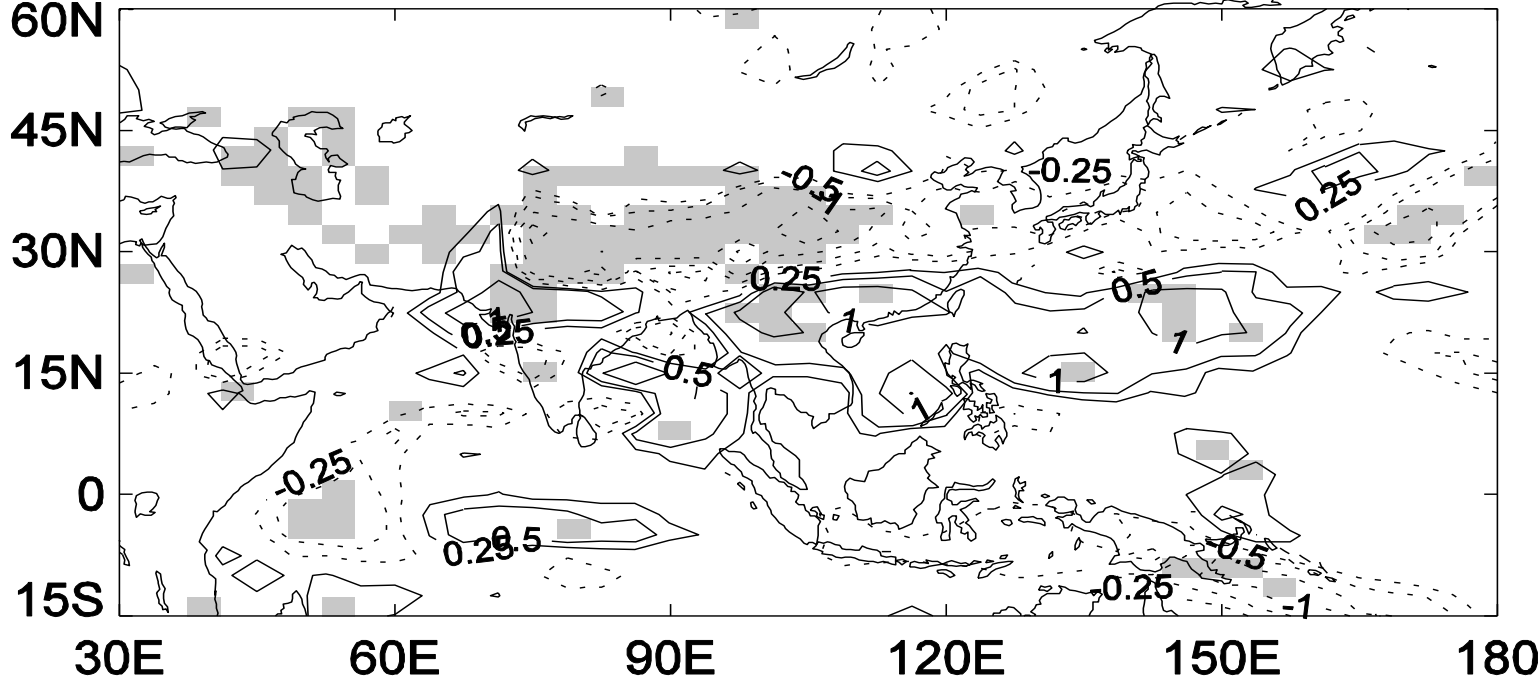
$$\frac{\Delta SH}{SH} = \frac{\Delta V}{V} + \frac{\Delta(T_g - T_a)}{T_g - T_a} \approx \frac{\Delta V}{V}$$



**Correlation: weaker TP heating corresponds to more rain (green) in Southern China and less rain (brown) in Northern China**

# Response

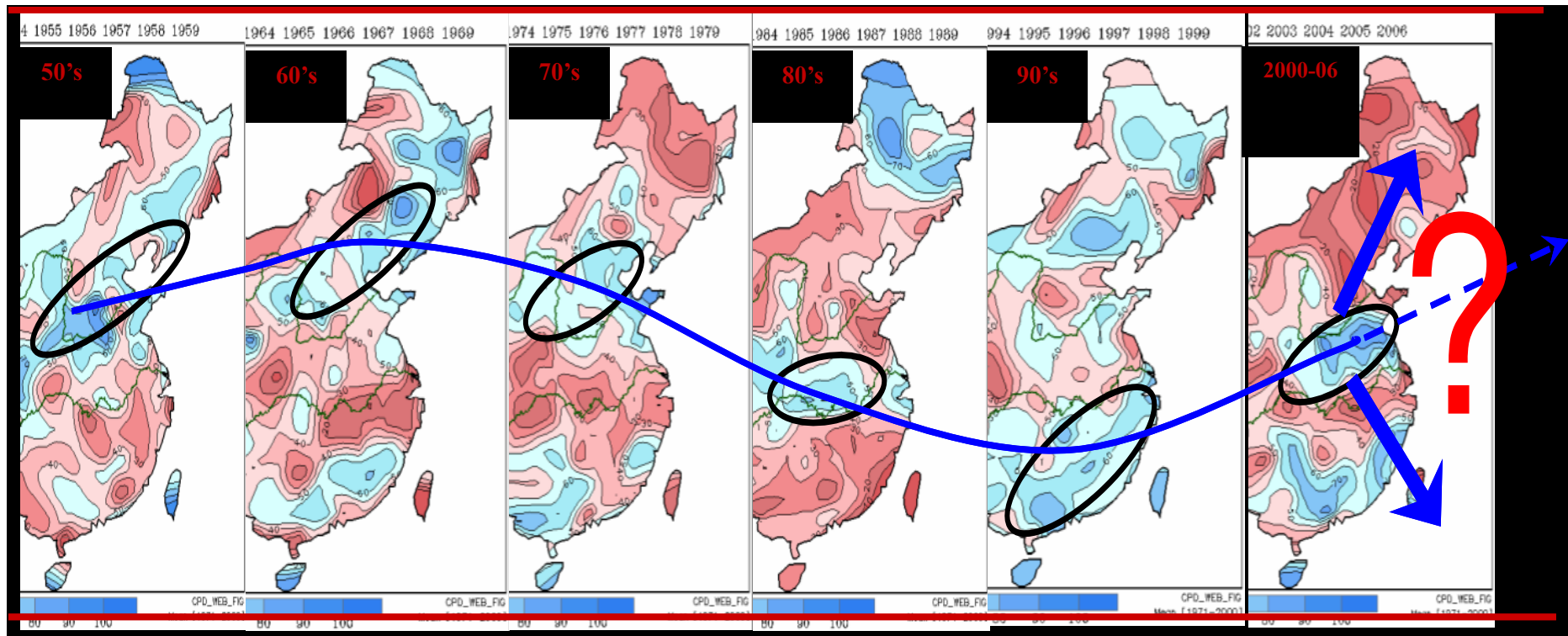
(a) Precipitation (Albedo-I - Albedo-D)



**Less rain in north**  
**More rain in South**

Fig. 5

# 中国未来极端降水事件？

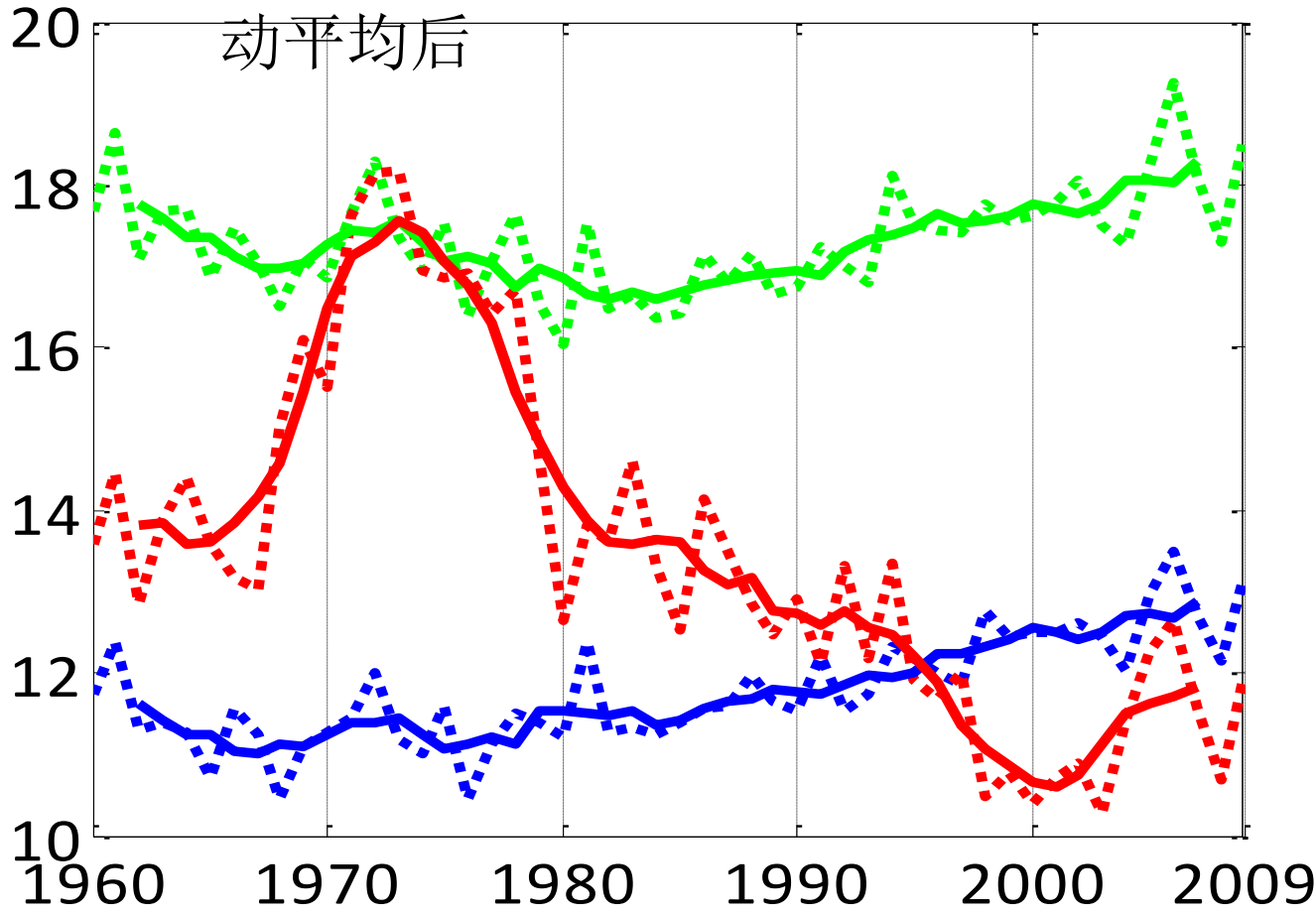


**Inter-decadal variation of summertime rainfall anomaly over E China**

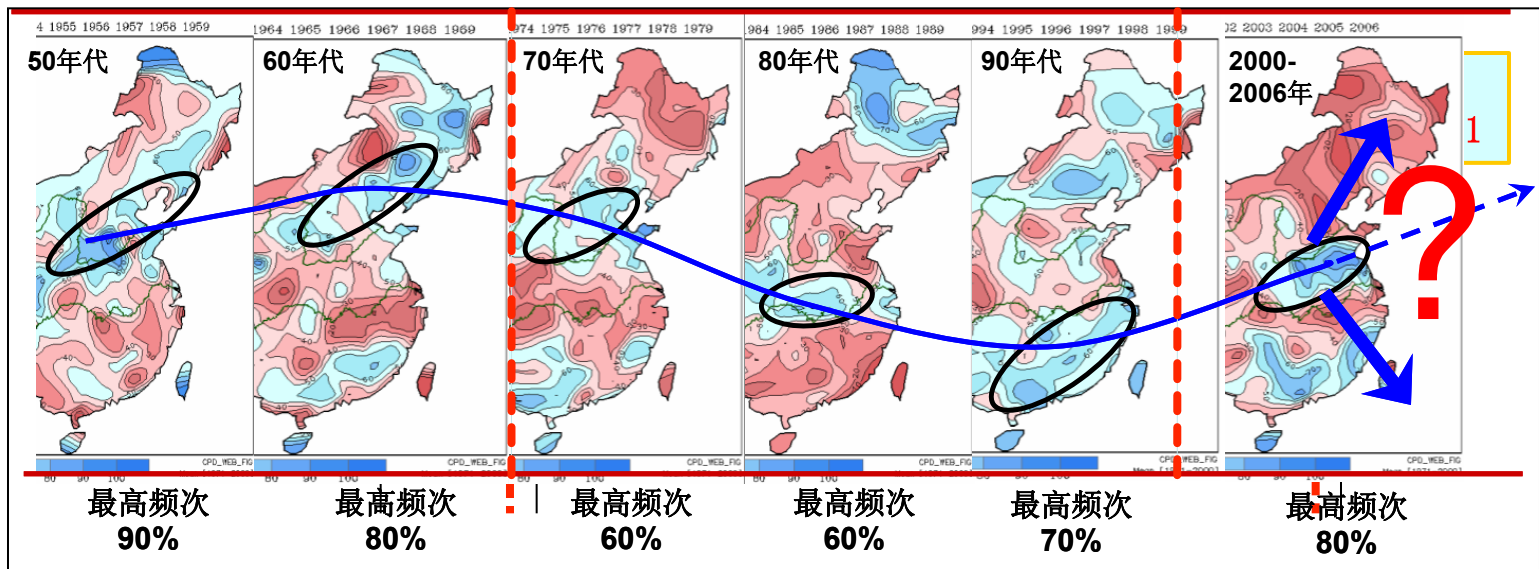
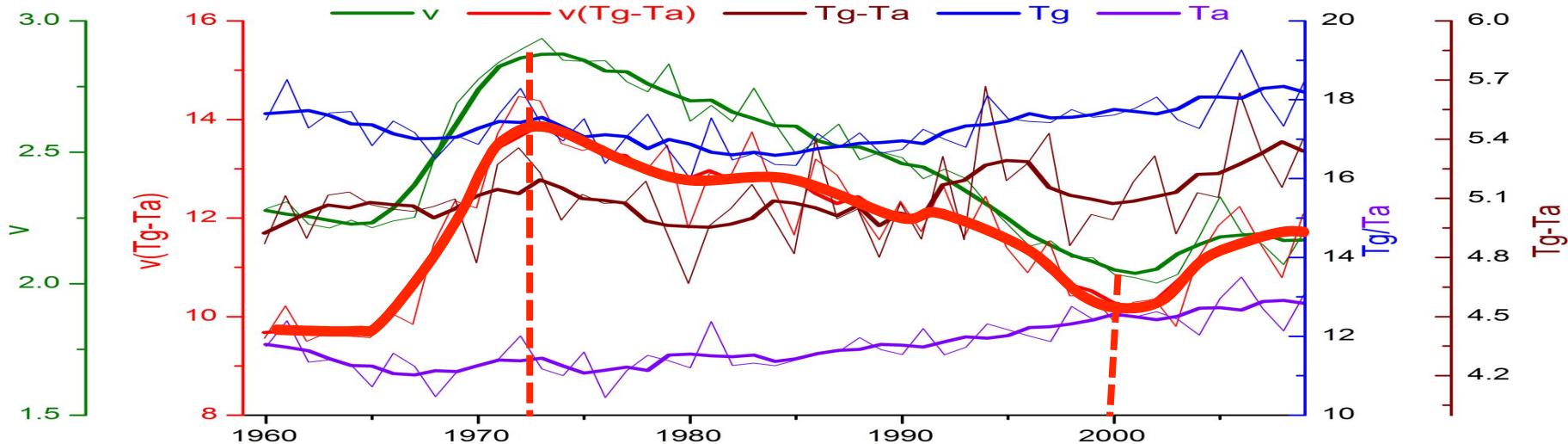
From Dong et al. 2009

虚线：原始数据  
动平均后

实线：5点滑



绿色:  $T_g$     蓝色:  $T_a$     红色:  $(T_g - T_a)V$



$$PSH = V(Tg - Ta)$$

# Summary- III

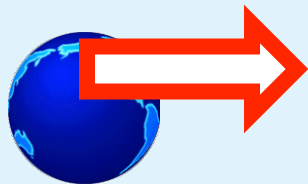
**Weakening of sensible heating over the TP results in weakening of near-surface cyclonic circulation. Consequently, the convergence of water vapor transport is confined to South China, contributes to “wet in south and dry in north.”**



# Outline



- 1 Introduction- general circulation**
- 2 Dynamics of ASM onset**
- 3 Evolution of the ASM onset**
- 4 Maintenance of the ASM**
- 5 Variability of the ASM**
- 6 Conclusion**



# Conclusion

- **The thermal forcing of the Tibetan-Iranian Plateau has strong impacts on the onset, evolution and maintenance of the ASM, and world climate.**
- **Protecting the ecosystem over the TIP and its thermal status not only can improve the local environment, but also can significantly influence the global climate, particularly the Asian monsoon!**

# Related Publications

- Wu, Guoxiong and Yimin Liu, 2003: Summertime quadruplet heating pattern in the subtropics and the associated atmospheric circulation. *Geophys. Res. Lett.*, **30(5)**, 1201,
- YIMIN LIU, GUOXIONG WU, AND RONGCAI REN, 2004: Relationship between the Subtropical Anticyclone and Diabatic Heating. *J. Climate*, 2004, **17**: 682-698.
- Xiaoyun Liang, Yimin Liu, and Guoxiong Wu, 2005: The role of land-sea distribution in the formation of the Asian summer monsoon. *Geoph. Res. Lett.* **32**: 10.1029/2004GL021587
- Guoxiong Wu, Yimin Liu, Tongmei Wang, Rijin Wan, ...,2007: The Influence of the Mechanical and Thermal Forcing of the Tibetan Plateau on the Asian Climate. *J. Hydrometeorology*. **8**: 770-789.
- Wu Guoxiong, Yimin Liu, X. Zhu, W. Li, Rongcai Ren, Anmin Duan, and X. Liang, 2009: Multi-scale forcing and the formation of subtropical desert and monsoon. *Ann. Geophys.*, **27**, 3631-3644.
- Wu Guoxiong, Yimin Liu, Bian He, Qing Bao, Anmin Duan, and Fei-Fei Jin, 2012: Thermal Controls on the Asian Summer Monsoon. *Nature Sci. Rep.*, **2**, 404, 1-7;
- He, B., Guoxiong Wu\*, Yimin Liu\*, Qing Bao. Astronomical and Hydrological Perspective of Mountain Impacts on the Asian Summer Monsoon. *Sci. Rep.* **5**, 17586; doi: 10.1038/srep17586 (2015).



**Thanks for your attention!**

